A Review of Phase Change Materials for the Thermal Management and Isothermalisation of Lithium-Ion Cells

A Review of Phase Change Materials for the Thermal Management and Isothermalisation of Lithium-Ion Cells.

S. Landini[a,*], J. Leworthy[b], T.S. O'Donovan[a]

[a] *Heriot Watt University, School of Engineering and Physical Sciences, Institute of Mechanical, Process and Energy Engineering, Riccarton, EH11 1HA Edinburgh, United Kingdom*

[b] *Dukosi Ltd., Quantum Court Research Avenue South, Heriot Watt University Research Park, Riccarton Campus, Edinburgh EH14 4AP, United Kingdom*

Abstract

Li-Ion batteries will play an important role in reaching emission targets by sustaining the further integration of renewable energy technologies and Electric Vehicles (EVs) in society. Their performance however is quite sensitive to temperature, leading to capacity fade, acceleration of ageing effect and possible thermal runaway. A Thermal Management System (TMS) should maintain a battery at an operating temperature within an optimal range and maximise temperature uniformity, i.e. approaching an isothermal condition. Many studies have experimentally investigated the electrical performance of Li-Ion batteries under controlled environmental temperatures. Notably however, these controlled conditions do not impose a uniform temperature or a controlled rate of cooling, as a TMS would. From a review of the relevant literature a ratio of the heat generation to the power production is proposed, i.e. quantifying an equivalent electro-chemical efficiency to advance research in this technological area and as additional TMS design metric. Overall, there is enough evidence that 25-30 ^oC is the best temperature range to minimise the ageing effect while 25-40 ^oC is typically reported as the general Li-Ion cells operating range. No specific temperature is identified to optimise the cycle electro-chemical efficiency and minimise the ageing effect. Therefore, a TMS should keep Li-Ion batteries within a specific temperature range according to the need for either higher electro-chemical efficiencies (i.e. higher powers and lower heat generation rates) or higher operating life. There are four main thermal management approaches of Li-Ion batteries: air-cooling, liquid-cooling, boiling and Phase Change Materials (PCM). Air cooling is preferred for safety reasons but is less efficient as the rate of heat transfer achievable is relatively low. Forced air cooling can effectively keep the temperature at a preferred level but fails to guarantee a uniform temperature. Liquid cooling is better in terms of heat transfer performance, but it is less safe and can still result in significant thermal gradients within the pack. Boiling effectively keeps Li-Ion cells temperature constant and uniform but can be quite complex to operate and control. Phase Change Materials (PCMs) as a passive cooling approach are proposed as an effective and low-cost isothermalisation technique. However, when Li-Ion batteries are operated under extreme conditions (high ambient temperature, high discharge rates), PCM are not able to recover all latent energy potential during solidification and this leads to possible thermal runaway. Overall, it is clear that no TMS alone is holistically better than others and the choice between air cooling, liquid cooling, boiling and latent heat PCM systems is entirely linked to the specific combination of temperatures, heat rates, cells capacity and geometry. Active PCM systems however, mainly a combination of liquid cooling and passive PCM, show promising results towards an ideal isothermal condition. Also, they introduce the potential to store the thermal energy and use it as needed, converting a Li-Ion cell from an Electrical Energy Storage System (EESS) to a Combined Heat and Power (CHP) system.

Keywords: Li-Ion batteries, thermal management, air-cooling, liquid-cooling, phase change materials, electro-chemical efficiency

*Corresponding author
Email address: sl30@hw.ac.uk (S. Landini)

Contents

Acronyms

R^2 Coefficient of Determination 28

ANN Artificial Neural Network 29

CAES Compressed Air Energy Storage 6, 24

CENG Compressed Expanded Natural Graphite 55, 56

CFD Computational Fluid Dymamics 20, 21, 33, 36, 47, 55

CHP Combined Heat and Power 1, 59, 60

CR Charge Rate 24–26, 30, 37–39, 58, 60

CTES Cascaded Thermal Energy Storage 46

DOD Depth Of Discharge 17–20, 22–24, 27, 29, 30, 72, 78

DR Discharge Rate 13, 17–39, 53, 55, 56, 58, 60, 74, 76, 77, 80

DSM Demand-Side Management 6

EESS Electrical Energy Storage System 1, 6, 24, 32, 59, 60

EG Expanded Graphite 47, 48, 56–58

EOL End Of Life 23, 24

ESS Energy Storage System 6

EV Electric Vehicle 1, 6–8, 14, 15, 29, 36, 53

HEV Hybrid Electric Vehicle 7

HEV Plug-in Hybrid Electric Vehicle 7

HEX Heat Exchanger 40, 46, 52

HPS Heat Pipe System 6, 32–34, 46, 52, 57

HR Heat Ratio 18–22, 76, 77

HTF Heat Transfer Fluid 30, 40, 43, 45, 46, 49–52

LCO Lithium Cobalt Oxide 13, 14

LCOE Levelised Cost Of Electricity 14

LCOS Levelised Cost Of Storage 24

LFP Lithium Iron Phosphate 13, 14

LH Latent Heat 40, 52, 57

LMO Lithium Manganese Oxide 14

MPCM Multiple/Cascaded Phase Change Material 52

NCA Lithium Nickel Cobalt Aluminium 14

NMC Lithium Nickel Manganese Cobalt 14

O&M Operation & Maintenance 32, 53, 56

PCM Phase Change Material 1, 3, 7, 31, 32, 40–60

PHS Pump Hydro Storage 6, 24

PV Photo-Voltaic 6

RET Renewable Energy Technologies 6

RMSE Root Mean Squared Error 28

S&T Shell & Tube 47, 51, 52

SEI Solid-Electrolyte Interface 24, 25, 53

SH Sensible Heat 40

SOC State Of Charge 10, 16, 29

SOH State Of Health 23–26

TCE Thermal Conductivity Enhancement 7, 32, 33, 44–49, 51, 54

TESS Thermal Energy Storage System 40, 45, 47, 52

TMS Thermal Management System 1, 7, 15, 17, 20, 21, 23, 30–39, 41, 53–58, 60

1. Introduction

A significant reduction in energy-related CO_2 emissions is required to meet the binding commitments of COP21/22 to keep the global temperature rise within 2°C of pre-industrial levels. The development and deployed of renewable energy technology and systems can make a significant contribution to the low-carbon energy mix, exploiting local energy sources and displacing high carbon fossil fuels. The world primary energy demand has grown by 1.8% since 2011 [1, 2]. Renewable energy sources accounted for 19.3% of the total final energy consumption in 2015; biomass/geothermal/solar heat accounted for 4.2% and wind/solar/biomass/geothermal electricity contributed 1.6%. In terms of global electricity production, renewable energy technologies contributed a total of 24.5% [1, 2]; this consisted of hydro-power (16.6%), wind (4%), biomass (2%) and solar PV (1.5%). In some cases, ratios of RET electricity production and demand reached values in the range of 106-140 % (e.g. Denmark, Scotland). The most developed technologies in this sector were wind (both onshore and offshore) and solar PV (in the EU 86% of new power additions were from wind and solar PV) [1, 2].

Renewable energy sources such as wind and solar are inherently intermittent however and have limited predictability, therefore any energy systems, irrespective of its scale (domestic, micro-grid, grid level) requires storage to realise the full potential to match demand with supply [3]. Typically Energy Storage Systems (ESS) are chosen for the specific application in terms of capacity, discharge period, response time and power rating for electrical storage and output temperature and capacity for thermal storage [3]. As reported by REN21 [1], the development of electrical RETs is strictly linked to three main areas of R&D: end-use technologies (e.g. EVs and HPSs), electrical energy storage systems (EESS) and Demand-Side Management (DSM). Among these, EESS are considered essential to balance the mismatch between RET electricity production and customers demand (i.e. grid management), permit the exploitation of local RET sources in off-grid systems, avoid further infrastructure spreading and provide backup in case of power outages [1]. The basic idea is capturing electrical energy during off-peak or RET overproduction periods and releasing it during high peak and/or high energy price periods. Today, the most developed EESS are PHS, electro-chemical batteries (mainly Lead Acid, NiCd, NiMH and Li-Ion), flywheels and CAES [1]. The global grid-connected and stationary storage power by 2016 was 156 GW_e, with 96% being PHS [1, 4]. In 2016, "advanced" EESS (not PHS) increased by 0.8 GW_e (+14%), totalling 6.4 GW_e [1, 4]. Of this, 1.7 GW_e (27%) is related to electro-chemical batteries (mainly Li-Ion), which saw a growth of 50% compared to 2015 [1]; this is attributed to the increase in EV battery production in the period 2010-2015, which saw manufacturing costs decrease by 65%. According to IEA [3], 310 GW_e new grid-connected electrical storage power is needed in USA, EU, China and India to sustain future de-carbonised scenarios.

The operating temperature of a Li-Ion battery has a significant influence on its overall electrical performance [5]; batteries performance is sensitive to both high and low temperatures [5]. At low temperatures, they lose storage capacity and charge acceptability [5]. At high operating temperatures the round trip efficiency decreases; the charge acceptance, power and energy capacity, reliability and cycle life are all compromised. All of these factors contribute to the higher capital and operation and maintenance costs when integrated as part of a low carbon energy system and consequently lead to higher unit price of energy on a full life cycle analysis [5, 6].

The effective thermal management of Li-Ion batteries which are exothermic during charge and discharge and subjected to very different environmental conditions depending on their application is therefore essential to reducing the cost of renewable energy [5]. As presented later in this review, the aims of an effective thermal management system (TMS) is twofold: to maintain a battery at an operating temperature within a certain optimal range and minimise temperature variation within the battery. This isothermal condition helps to avoid localised cell deterioration which in turn increases the performance defect throughout all the batteries pack [6].

Many studies [7, 8, 9, 10, 11, 12, 13, 14, 15, 16, 17, 18, 19, 20] have experimentally investigated the electrical performance of Li-Ion batteries under controlled environmental temperatures. Importantly however, these controlled conditions do not impose a uniform temperature or a controlled rate of cooling, as a Thermal Management System would. The review of the relevant literature also proposes that the ratio between the heat generation and the power production, i.e. quantifying an equivalent electro-chemical efficiency would help to advance research and development in this important technological area.

This literature review is composed of four sections. Section 2 gives an overview of Li-Ion batteries benefits, costs, geometries, chemistries, electro-chemical properties. This section is essential to understand the geometries and the main components of a Li-Ion cell, which will be constantly referred in all the following sections. Section 3 focuses on Li-Ion batteries thermal behaviour, thermo-physical properties, electro-chemical efficiencies (based on a complete review of Li-Ion batteries heat generation data available in previous literature), ageing effect and batteries thermal models. This section is crucial to understand how the heat generation rates that the TMS proposed in Section 4 need to dissipate changes with the operating conditions of a Li-Ion cell. Section 4, based on the outcomes of Section 2 and 3, covers the topic of Li-Ion batteries thermal management systems (TMS) based on air-cooling, liquid-cooling, boiling and phase change materials. A detailed subsection on Phase Change Materials (PCM) classification, thermo-physical properties, thermal conductivity enhancement (TCE) methods and their effectiveness as isothermalisation systems is also proposed. Finally, Section 5 draws the main conclusions of the review and propose prospects for future research.

2. Lithium-Ion Batteries

2.1. Overview

There are few types of Li-Ion batteries: cylindrical, coins, prismatic and pouch [7]. Typically, prismatic and pouch geometries are used for high capacity applications, such as EV, HEV and HEV. Similarly to other chemistries, Li-Ion batteries are composed of 6 components: positive current collector, cathode, negative current collector, anode, electrolyte and separator [7]. The cathode (positive electrode) is typically a lithium oxide while the anode (negative electrode) is a compound made with carbon (e.g. graphite) and/or silicon. The electrolyte is a lithium salt dissolved in organic solvents (e.g. ethylene carbonate, diethyl carbonate, dimethyl carbonate) [7]. Typical properties of Li-Ion batteries are reported in Table 1.

In terms of costs, there are different values (mainly derived from EV market) available in literature (Figure 1) even if the most widely accepted range is 200-384 $/kWh [24] with an average in 2016 of 227 $/kWh (-77% compared to

Table 1: Properties of Li-Ion Batteries [6, 21, 22, 23]

Property	Value	Unit
Energy volumetric density	200-630	Wh/L
Energy specific density	90-235	Wh/kg
Power density	1500	W/kg
Operating Life*	500-1000	Number of cycles
Overcharge tolerance	Low	-
Self-discharge	> 10	%/month
Temperature Tolerance	-20-60	°C
Operating Temperature Range	25-40	°C
Temperature difference within cells pack	< 5	°C

** Operating Life: 20 % reduction of battery capacity compared to initial condition*

2010) [6]. Moreover, Cairn Energy Research Advisors and Tesla claim values of respectively 139 $/kWh and lower than 190 $/kWh [6, 24].

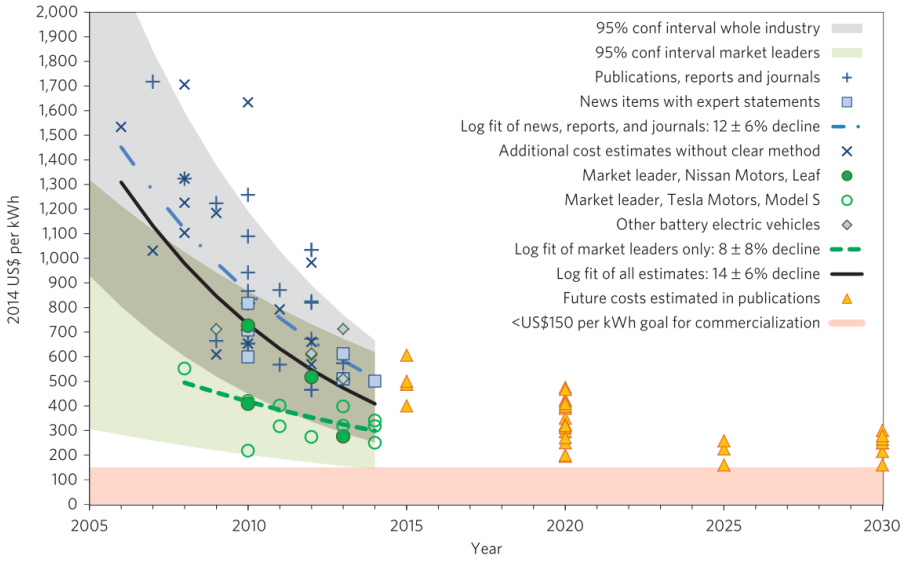

Figure 1: Li-Ion Battery pack cost used in EVs [25]

2.2. Cell Types

2.2.1. Cylindrical Cells

The cylindrical cell is one of the most widely used packaging types for Li-Ion cells, mainly due to their good mechanical stability and ease of manufacture [27]. Cylindrical cells possess high energy densities; however, they have a low packing efficiency due to the unavoidable space left between the cells when they are stacked together, resulting in a lower energy density at a pack level. Figure 2 shows the structure of a typical cylindrical Li-Ion cell, where the electrodes are layered and spirally wound into a "jelly roll" which is then inserted into a steel can. Most cylindrical cells benefit from having built in safety devices such as positive thermal coefficient (PTC) switches that,

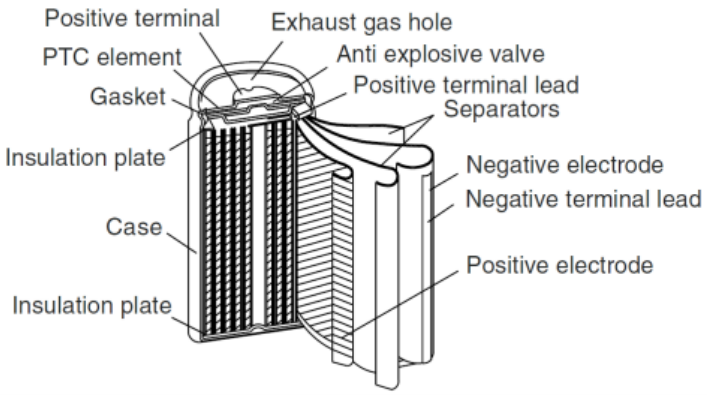

Figure 2: Schematic to show the structure of a cylindrical Li-Ion cell [26].

when exposed to excessive current, heat up and become resistive, stopping the flow of current in the cell. As well as this, cylindrical cells also feature pressure relief mechanisms which are designed to release excessive pressure build up from the formation of gases inside the cell. Gasses inside the cell are usually generated due to abusive use of the cell, i.e. overcharging, physical damage or excessive temperature rises [28]. One great advantage of the cylindrical cell is its mechanical stability; unlike prismatic and pouch cells, cylindrical cells exhibit minimal or no "swelling" due to build ups of internal gases and do not require any externally applied compression.

The cylindrical cell is available in a wide variety of standard formats; for Li-Ion cells, the most common formats are 14500, 18650 and 26650. The first two digits identify the diameter of the cell in millimetres, and the last three digits are the length of the cell in tenths of millimetres; therefore, an 18650 cell measures 18mm in diameter and 65mm in length. The 18650 cell has been the cell of choice for Tesla, using the same cell format in both their electric vehicles and energy storage batteries mainly due to the manufacturability, availability and cost of production. In 2015 Tesla, Panasonic and Samsung have begun manufacturing a new 21700 cell, claiming that this new cell format has 35% more energy capacity per unit volume than the 18650 cell [29]. On this regard, Quinn et al. [30] compared the energy density of the 21700 cell against an 18650 cell and found that the energy content can be as much as 50% greater than an 18650 cell. Table 2 summarises the different sizes of cylindrical cells and their associated volumes and surface areas.

Table 2: Cylindrical Cell Geometries

Cell Format	Cell Height (mm)	Cell Diameter (mm)	A (m^2)	Vol (m^3)	A/Vol (m^{-1})
14500	50	14	2.51x10-3	7.70x10-6	325
18650	65	18	4.18x10-3	1.65x10-5	253
26650	65	26	6.37x10-3	3.45x10-5	184
21700	70	21	5.31x10-3	2.42x10-5	219

A = Surface Area, Vol=Volume

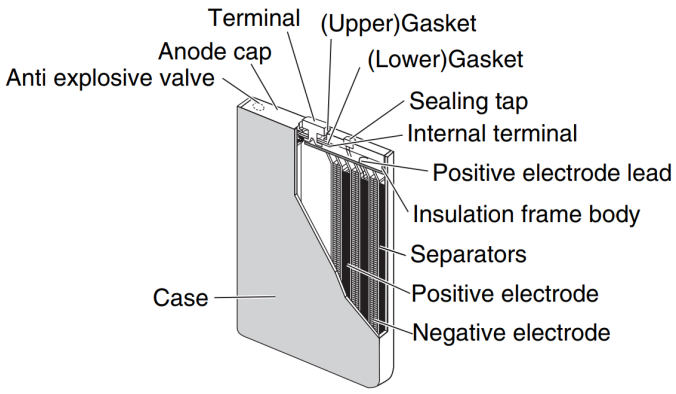

Figure 3: Schematic to show the structure of a prismatic Li-Ion cell [26].

2.2.2. Prismatic Cells

The internal assembly of a prismatic cell is much the same as a cylindrical cell, however in this case the cells "jelly roll" is inserted into a prismatic can as shown by Figure 3. In some prismatic cells, the jelly roll is replaced by a laminated stack of anode-separator-cathode assemblies. Prismatic cells are slightly less energy dense than cylindrical cells due to a thicker can wall; however, they make up for the lost energy density by having a much better packing efficiency due to their cuboid format. Like cylindrical cells, prismatic cells also have in-built safety features such as thermal fuses and gas vent ports. There is currently a lack in standard formats of prismatic cells, as usually they are redesigned to make best use of the available space in each application; however, some standard cell geometries do exist and are listed in Table 3. It can be seen that prismatic cells range of surface area to volume ratios are lower than that of cylindrical cells. From a thermal management perspective, this means that any proposed thermal management system would have to remove heat at a faster rate than for the equivalent cylindrical cell. Unlike cylindrical cells, prismatic cells are prone to "swelling" due to a build of gasses within the cell and are required to be assembled into rigid enclosures that applies compression to the two broad faces of the cell [31], further complicating the battery pack mechanical design. The cells expansion can be seen as a disadvantage from a thermal management perspective as the cells swelling can result in de-lamination of layers within then cell, which in turn would decrease its through-plane thermal conductivity and thus the rate at which heat can be dissipated from the cell [32]. Studies carried out by A123 Energy Solutions found that a typical prismatic cell can expand up to 1% of their initial thickness under normal cycling from 100% to 0% SOC; in addition, over their life cycles they can grow to be 3-5% greater than their initial thickness [31].

Table 3: Verband der Automobilindustrie (VDA) standard prismatic cell formats [33].

Cell Format	Length (mm)	Height (mm)	Width (mm)	Vol (m^3)	A (m^2)	A/Vol (m^{-1})
HEV	120	85	12.5	1.27x10-4	25.52x10-3	200
PHEV1	173	85	21	3.08x10-4	40.24x10-3	130
PHEV2	148	91	26.5	3.56x10-4	39.60x10-3	104
PHEV2+	148	125	26.5	4.90x10-4	51.47x10-3	105
EV1	173	115	32	6.36x10-4	58.21x10-3	91
EV2	173	115	45	8.95x10-4	65.71x10-3	73

A = Surface Area, Vol=Volume

2.2.3. Pouch Cells

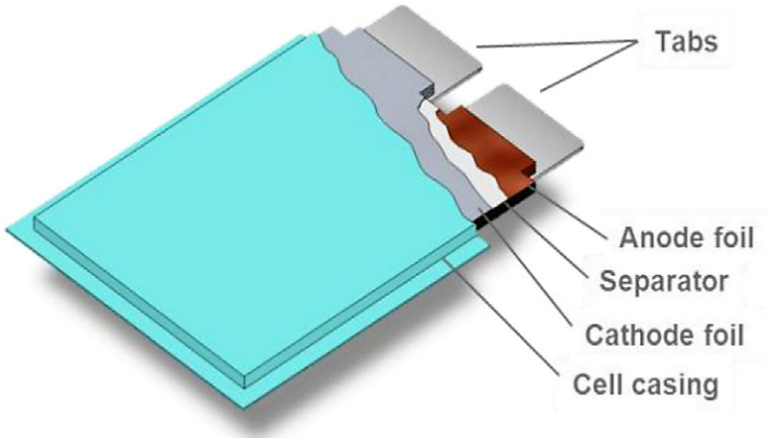

Figure 4: Schematic to show the structure of a Li-Ion pouch cell [34].

Pouch cells are constructed by stacking multiple layered sheets of anode-separator-cathode assemblies which are then inserted into a pouch, the pouch is then filled with electrolyte and sealed leaving the positive and negative terminals outside of the pouch, as shown by Figure 4. The material used for the pouch is a laminated aluminium film with a layer of polyamide on the outside and polyethylene on the inside to electrically insulate the casing material and prevent corrosion from the electrolyte. The elimination of the rigid metal enclosure saves weight and means the pouch cell is capable of high energy densities and packing efficiencies.

A disadvantage of having no rigid case however is that the cells are extremely vulnerable to external mechanical damage and swelling from internal gasses. Because of this, battery packs utilising pouch cells must extensively protect the cells from external damage and provide compression whilst still allowing for small expansions in the cells thickness, the pressure applied to the cell directly effects the cells life [35]. In this regard, Wunsch et al [36] showed that the way in which cells are compressed effects their cycle life. Their experiments compared various methods of compression; no compression, fixed displacement and fixed force using springs. The cell with fixed force performed the best, achieving 3000 cycles until 80% SOH, whereas fixed displacement achieved 1300 cycles and the un-compressed cell achieved 300 cycles. The un-compressed cell degraded rapidly due to electrolyte degradation and

active layer delamination. In the fixed displacement set up, the expansion of the cell is limited and thus larger forces build up in the cell which damage and crack the active materials over time, resulting in an increase of the ohmic resistance of the cell. The best results were achieved when a constant force was applied to the cell whilst allowing for some expansion of the cell.

It is also important to note that pouch cells lack in built safety features such as PTC switches and mechanical gas vents; instead, when gases are formed and pressure within the cell increases above a certain threshold, the gases will vent through an intentional weak spot in the cells pouch which is usually located in one corner of the cell.

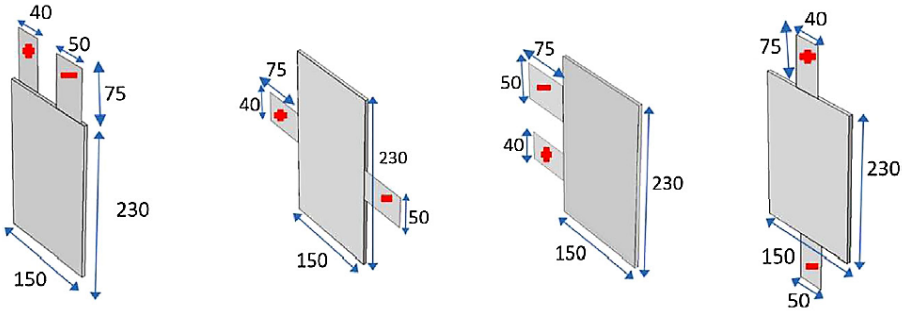

Figure 5: Pouch cells with varying tab locations. All sizes are in mm [37].

Currently there are no standards sizes of pouch cells as they are still a relatively immature technology in comparison to cylindrical cells and are easily manufactured to bespoke sizes. However, like prismatic cells, efforts have been made to standardise the dimensions of pouch cells by organisations such as the Association of German Automobile Manufacturers (VDA), examples of the proposed cell formats are shown in Table 4.

Table 4: Verband der Automobilindustrie (VDA) standard pouch cell formats.

Cell Format	Length (mm)	Height (mm)	Width (mm)	Vol (m^3)	A (m^2)	A/Vol (m^{-1})
HEV	243	121	X (4 – 12)	1.2 – 3.5 x10-4	5.88 x 10-2	500 – 166
PHEV	227	165	X (4 – 12)	1.5 – 4.5 x10-4	7.49 x 10-2	500 – 166
BEV	330	162	X (4 – 12)	2.1 – 6.4 x10-4	1.07 x 10-1	500 – 166

A = Surface Area, Vol=Volume

It can be seen in Table 4 that pouch cells are capable of high surface area to volume ratios when the cell width is small, this is beneficial for thermal management as heat can be dissipated via the two large faces of the cell. The placement of the tabs on pouch cells is also variable. Figure 5 shows examples of the two main formats available; in some cases the tabs are located on the same side of the cell, whereas some pouch cells have tabs at either end of the cell. Investigations have been carried out to find the effect of the tab locations [38] on pouch cells, showing that cells with tabs at either end exhibit a much more uniform potential and current density distribution across the cell, which leads to a more uniform temperature gradient across the cell, which in turn prolongs the life of the cell.

2.3. Chemistries and Electro-chemical Properties

A diagram of the charging process for a Lithium-ion cell is shown in Figure 6. The batteries are typically tested at different constant discharge currents, whose values are reported by using a parameter called Discharge Rate (DR) [7, 8, 9]. This is defined as the constant current which discharges the entire nominal capacity of the battery in one hour [1]. The Lithium-ion cell is composed of a positive electrode (Cathode), negative electrode (Anode) and electrolyte. The two electrodes are separated by a separator sheet to prevent a short circuit from occurring [39].

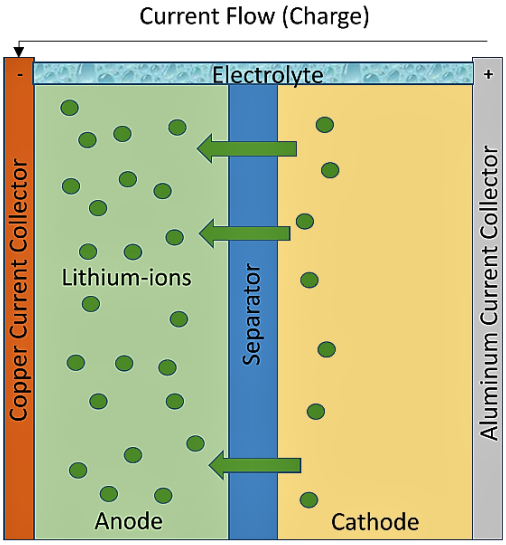

Figure 6: Electrochemical charging process in a Lithium-ion cell [39]

When the cell is connected to a power supply and charged, lithium ions de-intercalate from the positive electrode, flow through the electrolyte and the separator sheet, then intercalate into the negative electrode [39]. Electrons flow in the opposite direction to the ions, flowing from the positive electrode through the external circuit and back to the negative electrode. This process is reversed when the cell is discharged from an external load [39]. The anode material of a lithium-ion battery typically consists of carbon, usually graphite [39]. The cathode of a lithium-ion cell can be made of a variety of different lithium metal oxides. Table 5 below summarises the typical performance characteristics of some of the most common Lithium-ion cathode chemistries. Many more cell chemistries exist as manufactures use combinations of these to exploit the benefits of each chemistry to develop the optimum for a given application [39].

Lithium Iron Phosphate (LFP) batteries have a $LiFePO_4$ cathode and typically a graphite anode. LFP was commonplace in automotive applications where high charge and discharge rates are required for fast acceleration and regenerative braking [39]. Its high power capabilities were well suited to this application as well as having a relatively low cost compared to other chemistries that make use of rare elements [39]. LFP is considered as one of the safer chemistries, especially when compared to LCO, because they start to decompose at higher temperatures.

[1] For instance: Capacity=20Ah, DR=1C, 2C, 3C, 4C : Current 20, 40, 60, 80 A) [7]

Table 5: Summary of common Lithium-ion Chemistries [39]

Cathode Chemistry	LFP	LMO	LCO	NCA	NMC
Specific Energy (Wh/kg)	80-130	105-120	120 – 150	80 – 220	140 – 180
Energy Density (Wh/L)	220-250	250 – 265	250 – 450	210 – 600	325
Specific Power (W/kg)	1400-2400	1000	600	1500 – 1900	500 – 3000
Power Density (W/L)	4500	2000	1200 – 3000	4000 – 5000	6500
Voltage (V)	3.2 - 3.3	3.8	3.6 – 3.8	3.6	3.6 – 3.7
Operating Life ($Cycles$)	1000 – 2000	>500	>700	>1000	1000 – 4000
Operating Temperature Range (^oC)	-20 to 60	-20 to 60	-20 to 60	-20 to 60	-20 to 55

Legend: Lithium Iron Phosphate (LFP), Lithium Manganese Oxide (LMO), Lithium Cobalt Oxide (LCO), Lithium Nickel Cobalt Aluminium (NCA), Lithium Nickel Manganese Cobalt (NMC)

EV's are now moving towards the use of NMC and NCA as they have superior energy and power densities to LFP. NCA batteries have a $LiNiCoAlO_2$ cathode and graphite anodes while NMC batteries have a $LiNiMnCoO_2$ cathode and a graphite anode. For instance, Tesla uses NCA chemistry in the EV models S and X and NMC in their Power Wall battery banks [21]. The higher voltages of NMC and NCA compared to LFP allows battery packs to be smaller, as they require less cells to achieve the specific voltage for a given application, resulting in more compact EVs [21]. LFP is still used in automotive applications but mostly in larger vehicle (e.g. buses) where battery volume is less of a concern [21].

LCO cells are typically found in portable electronic devices such as mobile phones, laptops and cameras [40]. The anodes of LCO cells are made of $LiCoO_2$ and the cathodes are graphite. Its high energy density results in smaller cells and ultimately smaller devices [40]. The disadvantages of LCO are its relatively high cost and low thermal stability. It is one of the most reactive chemistries and can enter a thermal runaway event at lower temperature than other chemistries; for these reasons, it is rarely used in large applications such as EVs [40].

LMO chemistry cells are typically found in power tools and e-bikes, where its high voltage and energy density results in small battery packs; however, this chemistry suffers from a lower cycle life than most chemistries. These batteries are formed of $LiMn_2O_4$ cathodes; the anodes can be graphite or LCO. LMO cells are one of the safest lithium cell chemistries. Thermal runaway occurs at approximately 250^oC compared to 150^oC for LCO cells [21].

3. Li-Ion Batteries Thermal Behaviour

3.1. Overview

The performance of Li-Ion batteries is typically influenced by design, materials and operating temperatures [5]. These batteries suffer both high and low temperatures [5]. At low temperatures, they lose storage capacity and charge acceptability [5]. In general, an increase in the operating temperature leads to lower reliability, risk of thermal runaway, higher capacity fading (i.e. lower cycle life) and consequently higher costs (LCOE) [6, 5].

Therefore, the development of proper thermal management systems (TMS) is essential [5]. The aims are keeping the batteries at an operating temperature within a certain optimal range and keeping the temperature variation within the battery as low as possible. A uniform temperature helps to avoid localised cell deterioration which in turn increases the performance defect throughout all the batteries pack [6]. On this regards, Infra-Red techniques have been proposed in literature to evaluate the detailed temperature distribution of Li-Ion cells during discharge processes. As reported in two studies by Panchal et al. [41, 42] and shown in Figure 7, when Li-Ion cells (in this case pouch geometry) are not conditioned with proper TMS (i.e. air passive cooling), the temperature disuniformity can be as high as 45 ^oC.

Moreover, it must be mentioned that in the case of EV batteries, considering the necessity of more autonomy (i.e. more energy storage), the number of batteries per volume within the pack keeps growing together with the market expansion [6]. Therefore, this will create serious thermal problems within the cells located in the centre of the pack, with more and more probability of thermal runaways and failures [6, 8].

3.2. Thermal Properties

The two thermal transport properties that primarily govern temperature rise in Li-Ion cells are thermal conductivity and heat capacity. As shown in Section 2, cylindrical cells are constructed of a spirally wound electrode assembly (jelly roll) which is then inserted into a metal can usually made of stainless steel ($k_{steel} = 16 - 19\,W/mK$, $c_{p,steel} = 500\,J/kg\,K$). The spiral electrode assembly illustrated by Figure 8 and Figure 2 (Section 2) results in anisotropic thermal conductivity between the radial and axial direction of the cell [43] due to the large number of interfaces between the electrode layers in the radial conduction path, which are absent in the axial direction.

Experimental studies carried out by Drake et al. [43] on cylindrical cells found that the radial thermal conductivity is two orders of magnitude lower than the axial direction. The results of the tests carried out on $LiFePO_4$ 18650 and 26650 cells are summarised in Table 6. The values for thermal conductivity in the radial direction are somewhat lower than those recorded in previous work that reported radial thermal conductivities of around 1-3 $W/m\,K$ [45] and 0.3-1.6 $W/m\,K$ [46]. This is possibly due to the fact that Drake et al.'s work considers thermal contact resistances that exist in an actual cell whereas the other stated values are calculated from individual cell components such as the electrode-separator assembly; hence, the values reported in Drake et al.'s work [43] are expected to be more accurate.

Table 6: Measured thermo-physical properties of 26650 and 18650 $LiFePO_4$ cells [43]

Cell Format	$k_r(W/m\,K)$	$k_z(W/m\,K)$	$c_p(J/kg\,K)$
26650	0.15 ± 0.01	32.0 ± 1.6	1605 ± 80
18650	0.20 ± 0.01	30.4 ± 1.5	1720 ± 86

k_r=radial thermal conductivity

k_z=axial thermal conductivity

c_p=specific heat capacity

The strong anisotropy of thermal conductivity within the cylindrical cell results in a temperature distribution shown

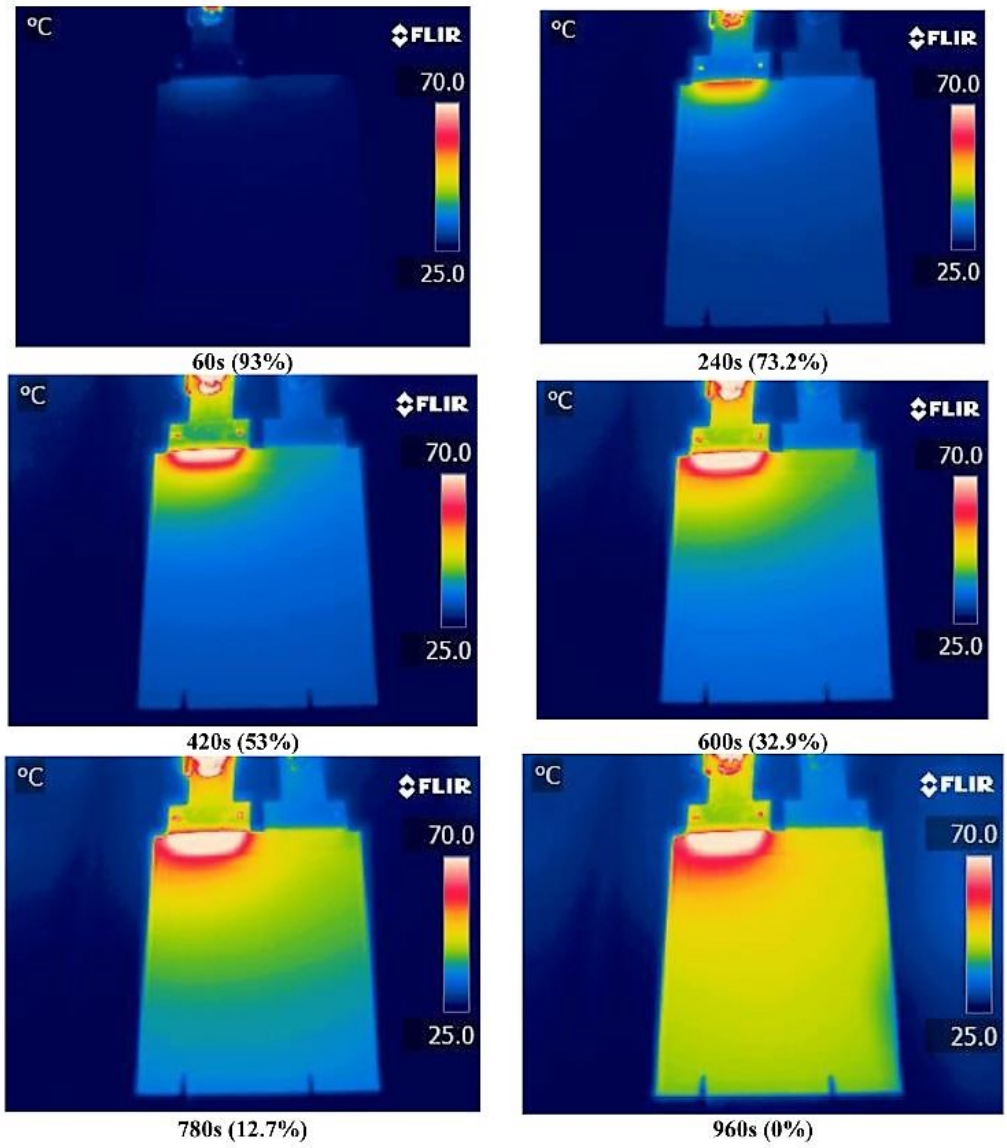

Figure 7: Infra-Red images of 4C discharge with passive cooling. Time after start of discharge and estimated SOC are given below each image[41].

by Figure 9. This knowledge is critical when designing thermal management solutions as this identifies the best thermal pathways for removing heat; in this case, heat is transferred much better in the axial direction of the cell.

Further work carried out by S.J Drake [47] on pouch cells also showed strong anisotropy in in-plane and through-plane thermal conductivity, mainly due to their structure as shown in Figure 4. His experiments were carried out on a range of pouch cells, finding in-plane thermal conductivities of 40-45 $W/m\,K$ and through plane thermal conductivities of 0.3-0.65 $W/m\,K$; however, the exact specifications of the cells were not given [47]. Similar investigations carried out on a range of $LiCoO_2$ pouch cells also showed a large anisotropy in thermal conductivity, finding thermal conductivities through-plane ranging from 0.84–1.63 $W/m\,K$ and in-plane thermal conductivities of 29.99–36.96 $W/m\,K$ [32]; again, however, the exact cell specifications were not published. The same study also showed that the

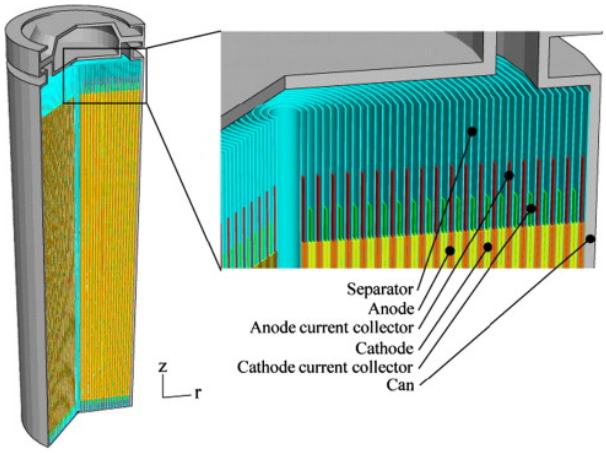

Figure 8: Schematic illustration of cylindrical Li-Ion cell [44]

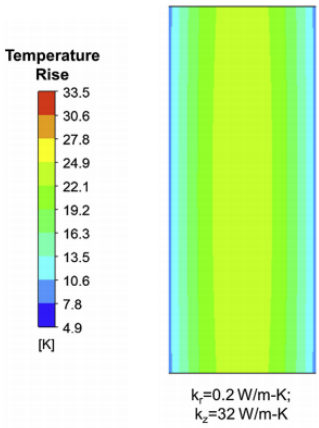

Figure 9: Temperature profile of cylindrical cell with anisotropic thermal conductivity [43]. A constant volumetric heat generation rate within the cell body and a constant convective heat transfer coefficient on the cell surfaces were assumed.

through-plane thermal conductivity of pouch cells can reduce over the cells life cycle due to the pouch cell swelling and layers within the cell becoming de-laminated. They showed that a cells through-plane thermal conductivity can be reduced by up to 30% when cycled at 45°C for 500 cycles. The aluminium foil casing material for pouch cells also has anisotropic thermal conductivity properties as it is a laminated structure, an investigation found through-plane and in-plane thermal conductivities of 0.28 $W/m\,K$ and 90.8 $W/m\,K$ respectively, a volumetric heat capacity of 2096 $kJ/m^3\,K$ and an inter-facial thermal conductance between the battery core (jelly roll) and the aluminium foil case of 1300 $W/m^2\,K$ [48]. All the information found in literature on thermal conductivity and thermal capacity of Li-Ion cells has been summarised in Table 7; some values are left empty as this has not been supplied by the referenced material.

3.3. Electro-chemical Efficiency

Several papers deal with the Thermal Behaviour of Li-Ion batteries without implementing any TMS in order to evaluate their heat generation. The heat generation rates are evaluated at different operating conditions (i.e. DR, DOD, ambient temperature), for both cylindrical [53, 54, 55, 56] and pouch geometries [7, 8, 57, 58, 9, 59, 60, 61, 62].

Table 7: Summary of Thermophysical cell properties found in open literature.

Cell Format	$K_{(x,y)}\,(W/m\,K)$	$K_z\,(W/m\,K)$	$K_r\,(W/m\,K)$	$c_p\,(kJ/kg\,K)$
SONY US-18650 $LiCoO_2$ [49]	-	N/A	0.35	1.04 ± 0.02
Cylindrical $LiFePO_4$ cell [50]	-	N/A	0.33 – 0.66	1.02
$LiCoO_2$ Pouch Cell [51]	24.840	1.035	N/A	-
LCO Pouch Cell [32]	36.96	1.63	N/A	-
LCO Pouch Cell [32]	32.31	1.35	N/A	-
6 Ah Li-Ion cell [52]	-	-	-	0.795
4 Ah Li-Ion cell [52]	-	-	-	1.0118
Li-Ion Polymer Pouch cell [32]	-	-	-	1.028
$LiFePO_4$ 18650 Cell [43]	30.4 ± 1.5	N/A	0.20 ± 0.01	1.720
$LiFePO_4$ 26650 Cell [43]	32.0 ± 1.6	N/A	0.15 ± 0.01	1.605

$K_{(x,y)}\,(W/m\,K)$ = In-plane Thermal Conductivity

$K_z\,(W/m\,K)$ = Through-plane Thermal Conductivity

$K_r\,(W/m\,K)$ = Radial Thermal Conductivity

$c_p\,(kJ/kg\,K)$ = Specific Heat Capacity

At time of writing, no studies reporting heat generation rates for prismatic geometries have been found. However, some of the fundamental principles discussed and concluded in this section apply more generally to all Li-ion cells geometries.

However, all the mentioned papers fail in evaluating the ratio between the heat generation and the power production, i.e. quantifying an equivalent electro-chemical efficiency. Therefore, data were collected from all the studies mentioned (raw data when provided by the authors or extrapolated from graph) and systematically analysed to evaluate two meaningful factors defined in Equation 1:

$$\eta = \frac{P}{P+\dot{Q}} = \frac{1}{1+HR} = \frac{P}{P_{tot}} \tag{1a}$$

$$HR = \frac{\dot{Q}}{P} = \frac{1-\eta}{\eta} \tag{1b}$$

where P [W] is the electrical power, $\dot{Q}$ [W] is the heat generation rate, P_{tot} [W] is the total power discharged by the battery (i.e. chemical power, defined as $P_{tot} = P + \dot{Q}$), η is the battery electro-chemical efficiency and HR is the heat ratio. These two parameters are instantly determined (i.e. based on power), i.e. for each operating condition (DR, ambient temperature) and specific DOD. The equivalent total discharge performance (i.e. based on energy) can be evaluated by the overall factors determined by Equation 2:

Table 8: Pouch cell datasets for Efficiency and HR.

Reference	Chemistry	Mass [kg]	Volume [L]	ρ $[kg/m^3]$	A $[m^2]$	L_c* [mm]	Capacity [Ah]
[8]	$LiFePO_4$	0.496	0.2633	1884	0.0783	3.365	20
[9]	$LiFePO_4$	0.496	0.2633	1884	0.0783	3.365	20
[15]	$LiFePO_4$	1.138	0.576	1976	0.0539	10.68	40
[59]	$LiFePO_4$	0.2596	0.138	1881	0.0282	4.9	10
[60]	$LiFePO_4$	0.261	0.127	2054	0.029	4.38	10
[61]	$LiMnNiCoO_2$	0.99	0.5061	1956	0.1039	4.87	40
[62]	$LiFePO_4$	0.2698	0.164	1645	0.0853	1.92	6

* L_c=Characteristic Length=$Volume/Area$

$$\eta_{overall} = \frac{E}{E+Q} = \frac{1}{1+HR_{overall}} = \frac{E}{E_{tot}} \tag{2a}$$

$$HR_{overall} = \frac{Q}{E} = \frac{1-\eta_{overall}}{\eta_{overall}} \tag{2b}$$

$$E = \int_{t=0}^{t=\tau} P(t)\,dt, \quad Q = \int_{t=0}^{t=\tau} \dot{Q}(t)\,dt, \quad \tau = \frac{1}{DR} \tag{2c}$$

where E [Wh] is the total electrical energy discharged, Q [Wh] is the total heat generated, $\eta_{overall}$ is the overall electro-chemical efficiency and $HR_{overall}$ is the overall heat ratio.

It must be pointed out that, due to its definition (Equation 1), the instant electro-chemical efficiency can be equal or even higher than 100% when the heat generation rate [W] is zero or negative (i.e. endothermic Li-Ion cell absorbing heat from the surroundings). This behaviour is observed typically for low DR, high temperatures and/or low DOD, as experimentally verified by the previous studies and shown in the following sections 3.3.1. and 3.3.2. In addition, when evaluating the overall performance (Equation 2), the overall efficiency, based on total energy discharged and total heat generation, is typically lower than 100% as reported in the following sections 3.3.1. and 3.3.2.

3.3.1. Pouch Cells

Table 8 reports the information regarding the dataset analysed for pouch geometry [7, 8, 57, 58, 9, 59, 60, 61, 62] while Table 9 gives details on tests condition. The dataset is characterised by different nominal capacities (from 6 to 40 Ah) and consequently different geometric sizes and weights. It must be pointed out that the main chemistry presented in the literature is the $LiFePO_4$ (Lithium Iron Phosphate) due to its low cost, reduced toxicity and chemical stability (i.e. long operating life) as extensively shown in Section 2.3.

Figure Appendix A.1 gives an overview on the efficiency η, HR, volumetric heat generation Q_{vol} $[W/L]$ and specific power $[W/kg]$. It can be claimed that $LiFePO_4$ cells have η higher than 75%, Q_{vol} up to 150 W/L, specific power reaching maximum values of 900 W/kg and HR lower than 30%. In addition, the heat flux q $[W/m^2]$ is found to increase with the DR, as reported in Figure Appendix A.5, with its median growing quadratically from 2.5 W/m^2 at

Table 9: Pouch cell datasets for Efficiency and HR. Specifics on experimental test

Reference	DR	T_a [°C]	Cooling Fluid	TMS	Regime
[8]	1,2,3,4	5-35	Water	Dual cold plate	Forced Convection
[9]	0.25,0.5,1,2,3	-10-40	50-50 Water-EG	Thermal Bath Calorimeter	Forced Convection
[15]	0.33,1,2	23-24	Air	Accellerated Rate Calorimeter	Natural Convection
[59]	1,3,5	24-25	Air	CFD	Natural Convection
[60]	1,2,3,5	25	Air	Thermal Chamber	Natural Convection
[61]	1,2	22	Air	Adiabatic Calorimeter	Natural Convection
[62]	10	25	Air	CFD	Natural Convection

Legend: T_a=Ambient Temperature [^oC], EG=Ethylene Glycol

0.25C to 642 W/m^2 at 5C.

Moreover, η can be plotted in function of DOD (Figure Appendix A.2), DR, ambient and battery temperatures, nominal capacity (Figure Appendix A.3) and characteristic length L_c (i.e. $Volume/Area$, Figure Appendix A.4). The following observations can be highlight from these figures (Figure Appendix A.2, Figure Appendix A.3, Figure Appendix A.4):

- η decreases non-linearly with DOD from a median of 97% for DOD=0-0.1 to a median of 92% for DOD=0.9-1; also, the dispersion of data is more prominent for high DOD, where the effect of heat generation due to internal resistance are quantitatively important.
- η increases with the ambient temperature in range 15-45 °C. For temperatures in range -5-5 °C, few data were found in literature [8, 9] and therefore are not deemed to be completely reliable. This suggests the necessity to collect more experimental data for low ambient temperatures (down to -20 °C), to better evaluate the efficiencies at this extreme working conditions.
- η generally increases with the cell temperature from 15 to 35 °C. A sharp decrease is found for temperature higher than 45°C. Similarly, few data are reported for temperature lower than 15°C, therefore, the apparent beneficial cold cell temperature must not be taken as trustworthy. This suggests the necessity to collect more experimental data for low cell temperatures (down to -20 °C), to better evaluate the predictive poor efficiencies at this extreme working conditions. In addition, it is not completely clear what is the best cell temperature in terms of instant efficiency optimisation.
- There is a strong correlation between η and DR, with a non-linear decrease between 0.25C and 4C. Again, due to few data reported in literature for DR higher than 5, the unexpected increase of efficiency for DR higher than 4 must be carefully considered. This suggests the necessity to collect more experimental data for high DR, to better evaluate the poor efficiencies at this extreme working conditions.
- η increases with the nominal capacity from 10 Ah to 40 Ah. This could be taken into consideration for the development of an η predictive model. Also, this suggests the necessity to collect more experimental data for several nominal capacities, from hundreds of mAh up to 40 Ah.

- The characteristic length L_c doesn't have a strong correlation with η and therefore can be neglected for efficiency prediction.

When evaluating the overall performance of each discharge process (based on total energies discharged), Li-Ion pouch cells provide integral average electrical powers and heat generation rates up to respectively 250 W and 35 W (Figure Appendix A.6). The median overall efficiency $\eta_{overall}$ and $HR_{overall}$ are 93% and 7.5%, in range of respectively 81-99 % and 1-24%. Moreover, as reported in Table Appendix A.1, Table Appendix A.2 and Figure Appendix A.7, the overall efficiency typically decreases with an increase in DR (from 96% at 0.25C to 86% at 4C) and a decrease of the nominal capacity (from 89% at 10 Ah to 97% at 40 Ah). The effect of the ambient temperature is not completely clear. However, the overall efficiency seems to be strictly dependent on the cell temperature, with the median value reaching its maximum at 25°C while the interquartile range improves for higher temperatures in range 35-45°C. Therefore, it is not completely clear what is the best cell temperature in terms of overall energy optimisation and if this differs from the instant efficiency optimisation one.

3.3.2. Cylindrical Cells

Table 10 reports the information regarding the dataset analysed for cylindrical geometry [53, 54, 55, 56] while Table 11 gives details on tests condition. The dataset is characterised by different nominal capacities (from 0.675 to 4.4 Ah) and consequently different geometric sizes and weights. Contrarily to pouch cells, cylindrical cells tested in previous literature are characterised by many chemistries, from the over-known $LiFePO_4$ to Manganese ($LiMnO$, $Li_yMn_2O_4$) and Nickel-Cobalt-Aluminium ($LiNiCoAlO_2$), whose main properties and performance indices are reported in Table 5 in Section 2.3.

Table 10: Cylindrical cell datasets for Efficiency and HR.

Reference	Chemistry	Mass [gr]	Volume [ml]	ρ $[kg/m^3]$	A $[cm^2]$	L_c* [mm]	Capacity [Ah]
[53]	$LiMnO$	92	44.8	2056	86	5.19	4.4
[54]	$Li_yMn_2O_4$	48.5	16.5	2932	37	4.5	0.675
[55]	$LiNiCoAlO_2$	48.5	17.6	2763	38	4.63	3.25
[56]	$LiFePO_4$	40.5	17	2388	37	4.55	1.25

* L_c=Characteristic Length=$Volume/Area$

Table 11: Cylindrical cell datasets for Efficiency and HR. Specifics on experimental test

Reference	DR	T_a [°C]	Cooling Fluid	TMS	Regime
[53]	1	-10-40	Air	Ventilated Thermal Chamber	Forced Convection
[54]	1, 3	24	Air	CFD	Natural Convection
[55]	0.2, 1, 1.5	25	Air	CFD	Natural Convection
[56]	0.2, 0.4, 0.8, 1.6, 2.4, 4	15-55	Air	Wind Tunnel	Forced Convection

Legend: T_a=Ambient Temperature $[^oC]$

Figure Appendix A.8 gives an overview on η, HR, Q_{vol} and specific power for the four different chemistries. It can

be claimed with 99% of confidence (box-plots whiskers) that $LiFePO_4$ and $LiNiCoAlO_2$ cells have the highest performances, with respectively η higher than 88% and 83%, Q_{vol} up to 50 W/L and 120 W/L, specific power reaching maximum values of 450 W/kg and 380 W/kg and HR lower than 13% and 18%. In addition, q is found to increase with the DR for both chemistries, as reported in Figure Appendix A.12 and Figure Appendix A.13, with its median growing quadratically from 2.5 W/m^2 at 0.25C to 460 W/m^2 at 4C for $LiFePO_4$ and from 80 W/m^2 at 0.5C to 540 W/m^2 at 1.5C for $LiNiCoAlO_2$.

Moreover, η can be plotted in function of DOD (Figure Appendix A.9), DR, ambient and battery temperatures, nominal capacity (Figure Appendix A.10) and characteristic length L_c (i.e. $Volume/Area$, Figure Appendix A.11). The following observations can be highlight from these figures (Figure Appendix A.9, Figure Appendix A.10, Figure Appendix A.11):

- In opposition to pouch cells, η seems to oscillate around a median of 93% for DOD 0-0.7 and then sharply decrease down to 87% for DOD=1; also, the dispersion of data is more prominent for DOD higher than 0.5, where the effect of heat generation due to internal resistance are quantitatively important.
- Similarly to pouch cells, η increases with the ambient temperature in range 25-55 °C. For temperatures in range -5-15 °C, few data were found in literature [53] and therefore are not deemed to be completely reliable. This suggests the necessity to collect more experimental data for low ambient temperatures (down to -10 °C), to better evaluate the efficiencies at this extreme working conditions.
- η has a different behaviour with the cell temperature compared to pouch cell. In fact, median efficiencies are quite stable in range 15-55 °C while the interquartile range worsen with higher temperatures. This might suggest a best cell temperature range of 15-25 °C. Similarly, few data are reported for temperature lower than 15°C. This suggests the necessity to collect more experimental data for low cell temperatures (down to -10 °C), to better evaluate the efficiencies at this extreme working conditions.
- Even if more scattered than pouch cells, there is still a strong correlation between η and DR, with a non-linear decrease between 0.2C and 4C. Again, due to few data reported in literature for DR higher than 1, more experimental data must be collected for high DR, to better evaluate the poor efficiencies at this extreme working conditions.
- Compared to pouch cells, no evident η dependence to nominal capacity (in range 0.675-4.4 Ah) is evaluated. This could suggest that this factor is less valuable for the development of an η predictive model for cylindrical cells. However, more experimental data must be collected for several nominal capacities to evaluate this point.
- Similarly to pouch cells, the characteristic length L_c doesn't have a strong correlation with η and therefore shouldn't be considered as a potential independent variable for efficiency prediction.

When evaluating the overall performance of each discharge process (based on total energies discharged), Li-Ion cylindrical cells provide integral average electrical powers and heat generation rates up to respectively 11 W and 1.2 W (Figure Appendix A.14). The median $\eta_{overall}$ and HR are 93% and 7.5%, in range of respectively 85-98 % and 1-17%. Moreover, as reported in Table Appendix A.3 and Figure Appendix A.15, $\eta_{overall}$ typically decreases with an increase in DR (from 99% at 0.2C to 81% at 3C) and a decrease of the nominal capacity (from 90% at 675 mAh

to 96% at 4.4 Ah). Likewise pouch cells, the effect of the ambient temperature is not completely clear. However, $\eta_{overall}$ seems to be dependent on the cell temperature, with the median value reaching its maximum at 25°C while the interquartile range improves for higher temperatures in range 35-65°C. Therefore, likewise pouch geometries, it is not completely clear what is the best cell temperature in terms of overall energy optimisation and if this differs from the instant efficiency optimisation one.

3.3.3. Statistical Analysis Summary

The electro-chemical efficiency η was analysed for both pouch and cylindrical cells. The main chemistry present in literature for pouch cells is the $LiFePO_4$ while also $LiMnO$, $Li_yMn_2O_4$ and $LiNiCoAlO_2$ are found for cylindrical cells. This precluded any statistical evaluation of the effect of chemistry and geometry on the electro-chemical efficiency. Strong correlations were found with DOD, Li-Ion cell surface temperature and DR while a mild dependency with the nominal capacity for the only pouch geometry was indicated. No clear effect of the characteristic length on η was found.

As will be shown in Figure Figure 13, the internal resistance typically increases with DOD and decreases with the Li-Ion cell temperature. The latter effect is mainly due to higher kinetic reaction rates of the active material and higher diffusivity of the solid and solution phase of the Li-Ion cell. Therefore, this is the main reason why from the statistical analysis proposed in this review, there is enough evidence to claim that η decreases with DOD and increases with Li-Ion cell surface temperature.

In terms of the effect of DR, it is expected that η should decrease with increasing DR due to the quadratic increase of the irreversible heat generation by joule effect. However, in some particular cases, due to a combination of high heat generation and accumulation due to poor TMS, the Li-Ion cell temperature may increase faster with high DR, leading to lower internal resistances and higher η. Also, it must be pointed out that the DR typically depends on the specific case, leading to increasing DR from static to automotive applications.

Moreover, η could be dependent to the capacity (i.e. size) of the Li-Ion cell due to the relative weight of factors such as tab design, electrodes and current collector thicknesses on the overall internal resistance of the cell and therefore the higher importance of joule irreversible losses.

3.4. Ageing Effect

The ageing effect is defined as the phenomena for which the capacity and discharged energy of a Li-Ion battery decreases with the number of cycles [63]. This is typically measured by the State Of Health (SOH), which is defined as the ratio of the actual capacity compared to its nominal value (i.e. starting un-aged cell) [63]. Moreover, SOH equal to 80% is considered to be the so-called End-Of-Life (EOL) of a battery [63]. However, it must be mentioned that typical warranty contracts consider SOH equal to 70% as preferred value [64].

The ageing rate r_a is the rate of change of the SOH. Previous literature shows that r_a is mainly dependent on the Li-Ion cell operating temperature. However, studies have shown that in case of pouch geometries a higher external compressive load on the cell (i.e. pressure) can decrease the ageing rate up to 24% [65]. Typically, one measures r_a for different operating temperatures and then plots its logarithm as a function of $1/T$. Therefore, by means of linear

regression techniques, one can fit an Arrhenius coefficient A (pre-exponential factor) and E_{act} (activation energy) [63], as reported in Equation 3:

$$r_a = A \cdot \exp\left(-\frac{E_{act}}{k_b T}\right) \tag{3a}$$

$$\ln r_a = \ln A - \left(\frac{E_{act}}{k_b T}\right) \tag{3b}$$

where k_b is the Boltzmann constant, equal to $1.38 \cdot 10^{-23} \frac{J}{K}$ or $8.618 \cdot 10^{-5} \frac{eV}{K}$ ($1\,eV = 1.602 \cdot 10^{-19} J$).

The main ageing effects presented and evaluated in previous literature are [63, 66]:

- Mn dissolution from the cathode
- Mn deposition on the anode
- Mn re-deposition on the cathode
- Particle cracks
- Loss of cyclable Lithium (also called Lithium inventory)
- Li plating
- Solid-Electrolyte Interface (SEI) growth and decomposition.
- Corrosion of current collectors

These degradation processes increase the internal resistance of the Li-Ion cell, leading to higher heat generation rate, lower capacity and lower electro-chemical efficiency.

In terms of life cycle analysis, the acceleration of ageing effect leads to typical operating life of up to 1000 cycles, leading to LCOS [£/kWh] for a short-term EESS (i.e. 365 cycles per year, 100 MW, 400 MWh, DOD=80%, calendar life 20 years) three times higher than PHS and CAES. This means that Li-Ion cells are nowadays not economically competitive with traditional EESS. In addition, it has been predicted that with a cycle durability of 10000 cycles at DOD=100%, Li-Ion cells LCOS would still be 60% higher than PHS. These figures explain the strong necessity to either decrease Li-Ion cells capital costs or minimise the ageing effect by implementing sound Thermal Management Systems.

Waldman et al. [63] analysed the ageing effect on a cylindrical 18650-type Li-Ion battery, focussing on operating temperatures in the range of -20-70 °C, CR 0.5C and DR 1C. Therefore, each charge/discharge cycle took 3 hours in total. The authors claim that this procedure has been done before in literature but just for limited temperature ranges. The initial capacity of all batteries was 1.5 Ah. All cells were charged and discharged in potential range 2-4.2 V. The criteria of EOL was 80% of SOH. Ageing rates r_a are considered as the gradient (tangential slope) of the SOH plotted against time (expressed in number of charge-discharge cycle). From the results of SOH plotted with number of cycles for different operating temperatures (Figure 10), it can be seen that the relation is quite linear in range of SOH (90-100%) except for 25 °C. For increased operating temperatures from 25 to 70 °C, the ageing rate is higher and therefore it takes less cycles to reach 80% SOH (EOL). Similarly, this effect is noted for temperatures lower than 25 °C. In this case the effect is even worse. In fact, we have an equal degradation history for temperature of 0 °C (-25 °C from optimum) and 70 °C (+45 °C from optimum). This can be seen also in the Arrhenius plot in

Figure 11. The slopes in this plot are different for the two temperature ranges. Therefore, from theory, one can claim that the degradation mechanism is different and the one for the low temperatures seems stronger. In fact, the activation energy E_a for the cold conditions is 0.43 eV compared to 0.18 eV of the hot conditions. The authors claim that the high temperature depleting effect is due to Li plating phenomena while the worst condition at low temperatures is due to Mn dissolution and SEI thickness increase. Overall, as shown in Figure 10, the optimal operating temperature (i.e. minimum ageing rate) is deemed to be 25 °C.

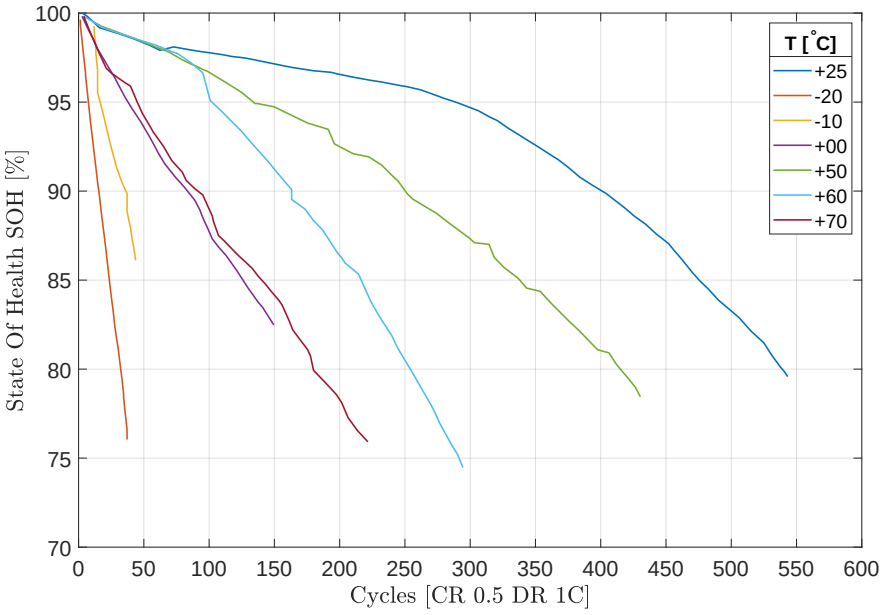

Figure 10: Ageing effect at different operating temperatures. Data have been elaborated from [63]. Specifically, the x-axis has been converted from time [day] into number of cycles considering that cycles were conducted by Waldmann et al. continuously and each cycle lasted 3 hours in total, i.e. 8 cycles per day.

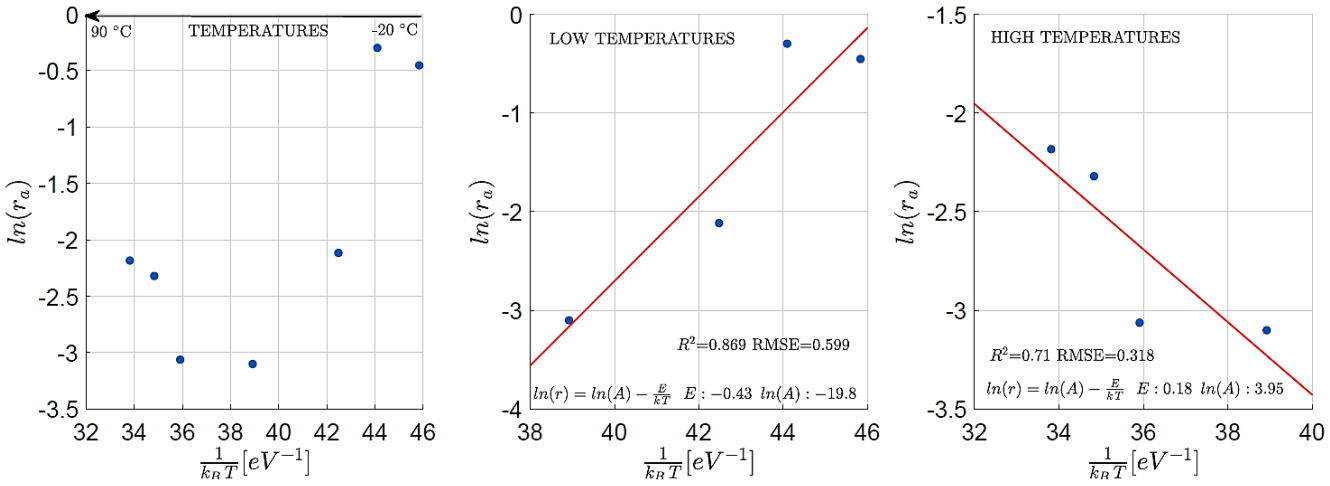

Figure 11: Arrhenius plot for the ageing effect at CR 0.5C and DR 1 C. The solid lines correspond to linear fits (drawn from [63]).

Similarly, Rao et al. [6] report ageing effect on Li-Ion batteries for a different number of cycles and operating temperatures, as reported in Table 12. It can be inferred that with the same operating temperature, 200 more cycles lead to an absolute 10% more capacity loss. Moreover, similar levels of SOH are obtained with 100 cycles more but

at 5 °C lower temperature.

Table 12: Li-Ion batteries ageing effect for different number of cycles and operating temperatures [6]

Number of cycles	800	600	500
Operating Temperature [°C]	50	50	55
SOH [%]	60	70	70

Finally, Shabani et al. [5] claim that Li-Ion batteries have a safe temperature range of -10-50 °C and the ideal operating range is 20-30 °C. Also, the battery operating life decreases by roughly 2 months every 1 °C of temperature increase when considering a range 30-40°C. Moreover, the authors suggest that in order to maximise the batteries pack life time, each cell should be operated at a uniform and equal temperature, guaranteeing pack temperature gradients lower than 5 °C.

Overall, there is evidence (Table 13) that the best temperature to minimise the ageing effect is around 25-30 ^oC. However, previous literature focuses on low CR/DR (or don't specify their value) and cylindrical geometry. Therefore, further research is needed on this matter for prismatic/pouch cells tested at broad temperature ranges (including extreme conditions) and high CR/DR.

Table 13: Ageing Effect

Reference	CR	DR	Temperature Range [°C]	Ageing Rate r_a $[\frac{\%}{cycle}]$	Optimal Temperature [°C]
[63]	0.5	1	-20, 70	0.04 - 0.12	25
[6]	-	-	50,55	0.05 - 0.06	-
[5]	-	-	-10, 50	-	20 - 30

3.5. Batteries Thermal Models

There are numerous methods for modelling the heat generation rates (reported in Appendix and commented in Section 3.3) and thermal management systems in a Lithium-ion battery system, ranging from simplified lumped parameter models [67, 5, 7] to computationally intense 3-dimensional numerical models [68, 69]. In terms of equivalent thermal circuits, previous studies proposed 3 main alternatives [7]: internal resistances, single RC, double RC circuit. The internal resistances (R_i) model uses different values for charging and discharging processes and is based on evaluating an ohmic resistance and a polarization resistance to compute the open circuit voltage of the cell. The single RC model introduces a resistive-capacitance component to the simple Ri model. In this case, the total equivalent resistance of the battery is determined by a combination of charge transfer resistance, ohmic resistance and diffusion capacitance. The double RC circuit is just a development of the single RC, taking into account two types of polarisation mechanism, concentration and activation.

3.5.1. Lumped Capacitance

The lumped parameter approach relies on the assumption that the temperature of the battery is spatially uniform and varies only with time. This approximation can be used to model Lithium ion cells, but only if internal temperature

gradients are small, i.e. the Biot number [2] is lower than 0.1 and the maximum relative error is equal to 5%.

One study by S. Al Hallaj et al. [67] used such a method to create a 1-dimensional thermal model with lumped parameters to simulate the temperature rise of a small 1.35 Ah 18650 cylindrical Li-Ion cell. The model developed treats the cell as a thermally homogeneous body with effective thermo-physical properties which are assumed to be independent of temperature over the cell's operating temperature range. Heat generation within the cell is assumed to be generated uniformly, subsequently assuming that the current distribution within the cell is also uniform. The heat generated within the cell was calculated based on the reversible heat due to electrochemical reactions and irreversible losses due to joule heating. The heat generated was calculated using Equation 4.

$$\dot{Q}_t = \dot{Q}_j + \dot{Q}_{rev} \tag{4a}$$

$$\dot{Q}_j = I\,(V_{oc} - V) = R_i\,I^2 \tag{4b}$$

$$\dot{Q}_{rev} = -\,I\,T\,\frac{\partial V_{oc}}{\partial T} = -\,I\,T\,\frac{\Delta S}{n\,F} \tag{4c}$$

where:

- $\dot{Q}_t$ is the total heat generation [W]
- $\dot{Q}_j$ is the irreversible Joule/ohmic heat generation [W]
- $\dot{Q}_r$ is the reversible heat generation due to chemical reactions [W] (positive for exothermic and negative for endothermic reactions respectively for discharging and charging phases)
- I is the current [A] (positive for exothermic and negative for endothermic reactions respectively for discharging and charging phases), which is linearly dependent on DR
- V_{oc} is the open circuit voltage [V]
- ΔS is the reaction entropy variation [J/K]
- V is the cell voltage [V]
- n is the number of electrons
- F is the Faraday constant equal to 96485 $\frac{C}{mol}$.

The term $\dot{Q}_j = I\,(V_{oc} - V)$, referred to as the over-potential, is the irreversible heat generation due to Joule heating and the term $\dot{Q}_r = -I\,T\left(\frac{\partial V_{oc}}{\partial T}\right)$ is the reversible heat due to entropy change. $\frac{\partial V_{oc}}{\partial T} = \frac{\Delta S}{n\,F}$, often referred to as the entropy coefficient, is the measure of the cell's open circuit voltage dependency on temperature. Both terms are dependant of DOD and temperature, as suggested in Section 3.3.3. The current I is positive during discharge and negative during charge. Both the over-potential and entropy coefficient were measured experimentally at 35 ^oC and DR of C/1, C/2, C/3 and C/6. The calculated heat generation profiles for the cells were then used as input to a general energy balance equation with proper boundary conditions to calculate the temperature rise of the cell, as

[2] The Biot number Bi is defined as the ratio of the heat transfer resistances inside of and at the surface of a body: $Bi = \frac{h_c\,L_c}{k}$

reported in Equation 5 [70].

$$\frac{\partial^2 T}{\partial r^2} + \frac{1}{r}\frac{\partial T}{\partial r} + \frac{q_{vol}}{k_{cell}} = \frac{1}{\alpha}\frac{\partial T}{\partial t} \tag{5a}$$

$$\left(\frac{\partial T}{\partial r}\right)_{r=0} = 0 \tag{5b}$$

$$-k_{cell}\left(\frac{\partial T}{\partial r}\right)_{r=R} = h_c\,(T - T_a) \tag{5c}$$

$$(T)_{t=t_0,r} = T_a \tag{5d}$$

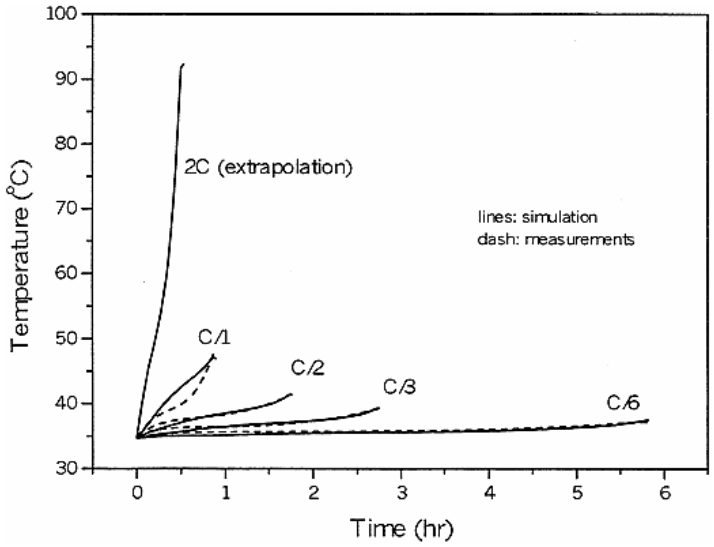

Figure 12: Simulation results against temperature measurements for Sony 18650 cell at all DR, T_a=35^oC, h_c = 10 $W/m^2\,K$ [67].

Figure 12 shows the results of the simulated cell temperature rise plotted together with the experimental measurements. Using this model, the simulated results for DRs C/2, C/3 and C/6 are in good agreement with the measured results, with relative RMSE lower than 1%. However, at a DR of C/1, the simulated results deviate from the measured ones, leading to relative RMSE and R^2 of 3.55% and 87%. S. Al Hallaj et al. [67] stated that the discrepancy between the simulation and measurement at C/1 is likely due to the assumption that heat is generated uniformly in the cell. This assumption is inaccurate as shown in Figure 7 in Section 3.1, where a local peak of the Li-Ion cell surface temperature due to the heat generation close to the anode (negative electrode) during discharge phase is clearly visible. At high DRs, temperate gradients are likely to increase within the cell as the temperature at the core builds up. This subsequently causes heat to be generated at different rates throughout the cell which could explain the error in both heat generation and temperature rise estimations.

Similarly, Shabani et al. [5] and Panchal et al. [8] proposed a simple model considering just ohmic losses and reversible entropic heat generation, as reported in Equation 4. Moreover, Panchal et al. [8] claimed that a lumped capacitance model seems to be accurate enough for most of the cases. In fact, whenever the Biot number is lower than 0.1 (with errors lower than 5%), it seems more convenient to use this kind of model to minimise the computational time. In addition, the authors observed that the heat dissipation is mainly due to external surface convection, considering that the Biot number is low and so the temperature uniformity of the battery leads to an absence

of internal conduction. Typically, the internal resistance R_i is a function of both SOC (or DOD) and operating temperature (Figure 13) while the entropy coefficient ΔS is only a function of the SOC.

Panchal et al. [7] developed a Simulink model based on experimental data to evaluate the thermal behaviour of a Li-Ion ion battery. The subsystems used were voltage, internal resistance, heat generation and temperature calculation. The heat generation was divided in two main arguments: the reversible entropy variation due to chemical reactions and the irreversible ohmic/Joule heating losses, following a lumped capacitance modelling technique. Interestingly, the authors point out that the heat generated by reversible entropy change is lower than the one generated by ohmic losses for high DR (e.g. EV batteries) [7]. From the results of the simulations shown in Figure Figure 13, the internal resistance seems to remain constant for the most part of the discharge period (until 85% of DOD) and then increases at high DOD [7]. The value of the internal resistance and its sharp increase at the end is higher for lower DR (1C) [7].

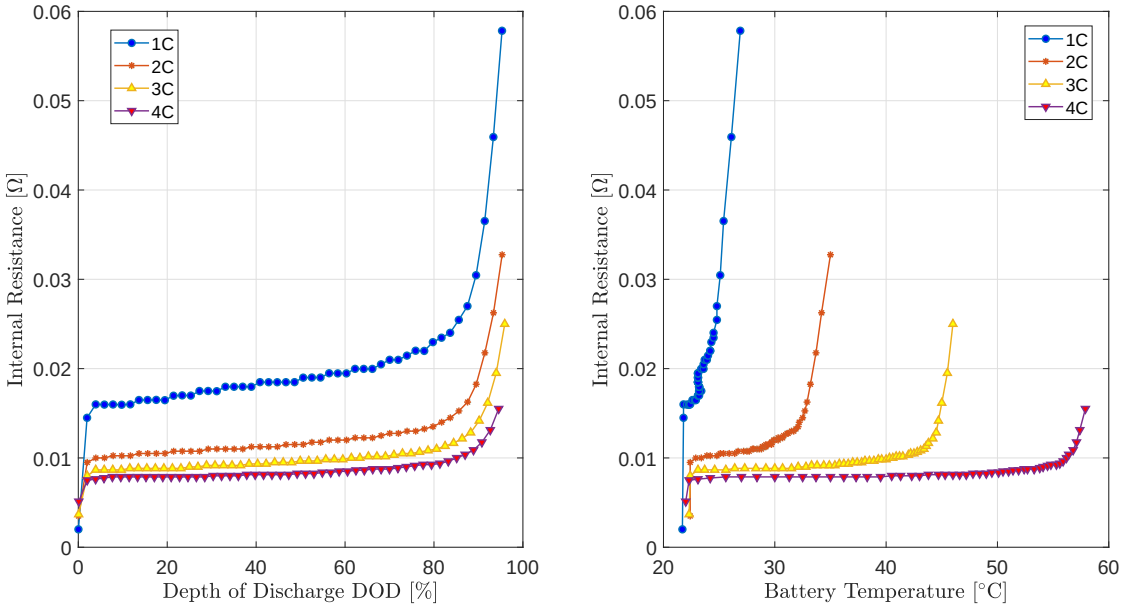

Figure 13: Li-Ion batteries Internal Resistance R_i at different DR (drawn from [7]).

The same authors [8] proposed an Artificial Neural Network (ANN)) method based on three input parameters: cooling plate water inlet temperature, discharging current (i.e. DR) and battery capacity. The only output is the heat generation and the model is validated by experimental data, leading to good agreements.

3.5.2. Electro-chemical models

Other researchers have achieved more accurate results at higher DRs using electrochemical-thermal modelling methods. Hosseinzadeh et al [71] developed an electrochemical-thermal model of a large format lithium-ion pouch cell and validated their model over an ambient temperature range of 5-45^oC and DR in the range of 0.5-5C, including various drive cycles for EVs . They used a combination of a pseudo 2D electrochemical-thermal model to model a single electrode pair within the pouch cell and coupled this to a 3D thermal model to simulate the temperature distribution within the cell. Using an electrochemical-thermal model also allowed them to predict the cells available

capacity and power under different temperature and DRs. Their model was able to predict the cell voltage and temperature rise with peak errors of 6.4% and 6% respectively.

In conclusion, choosing a numerical model is always a trade-off between accuracy and complexity (i.e. computation time) [5]. Most of the time, a lumped capacitance method results more than appropriate. However, there could be problems in applying this simple method in case of HTF with low heat transfer coefficient (high Biot number), high DR (more than 1C) and "abnormal" operating conditions (high ambient temperature).

3.6. Summary

Overall, there is enough evidence to claim that at time of writing 25-30 ^oC seems the best temperature range to minimise the ageing effect. However, the electro-chemical efficiency is typically maximised for higher temperatures in range 35-45 ^oC. Therefore, no specific temperature is indicated in literature which can optimise the cycle electro-chemical efficiency and minimise the ageing effect. Depending on the specific application, the selected TMS should focus on keeping the Li-Ion cells at a specific temperature range according to the need for either higher electro-chemical efficiencies (i.e. higher powers and lower heat generation rates to be dissipated by the TMS) or higher operating life.. Moreover, from the author's literature data elaboration, it seems that optimising a Li-Ion cell for a specific DOD level can lead to non-optimal condition for the overall cycle. Moreover, even if different geometries can use same chemistries (as shown in Section 2), different efficiency behaviours are observed for pouch and cylindrical cells, with the former having a smooth decrease of η with DOD and the latter a more oscillating behaviour. In conclusion, more experimental data are necessary for "extreme" operating conditions, i.e. high CR-DR and high-low ambient temperatures to acquire a more robust data set to evaluate the best operating temperature which must be guaranteed by the TMS.

4. Thermal Management Systems (TMS)

4.1. Overview

There are four main techniques to cool batteries as proposed in previous literature [6, 8, 72, 73]:

- Air-cooling
- Liquid-cooling (e.g. water, glycol, oil, acetone, refrigerants)
- Boiling
- PCM systems.

Previous reviews [74, 75] and Section 3 showed that the aim of a TMS is to keep the Li-Ion cell average temperature within a certain range and minimise the temperature disuniformity by acting on heat transfer coefficients, thermal contact resistances and, in case of active cooling, flow configurations and heat vectors chemistries.

Air cooling is preferred in terms of electrical safety but it is reported to be less efficient due to low heat transfer coefficients [8]. In addition, forced air cooling is effective to keep the temperature at a preferred level but fails in guaranteeing a constant and uniform temperature within the cells (in-cell) and the cells pack (cell-to-cell) [72]. Water cooling is better in terms of heat transfer quality but it is intuitively considered to be less safe [8]. Boiling guarantees a better surface temperature uniformity [76] but it is intrinsically complex to operate and control. PCM are capable of reducing both maximum temperature and cell-to-cell temperature gradients, leading to a reduction in capacity loss rate up to 50% [72]. However, when Li-Ion batteries are operated under extreme or "abuse" conditions (high ambient temperature, high DR), PCM, considered more a buffer than a heat sink system, are not able to recover all latent energy potential during solidification and this leads to possible thermal runaway (Figure 14) after a certain number of charge/discharge cycles of the batteries [72].

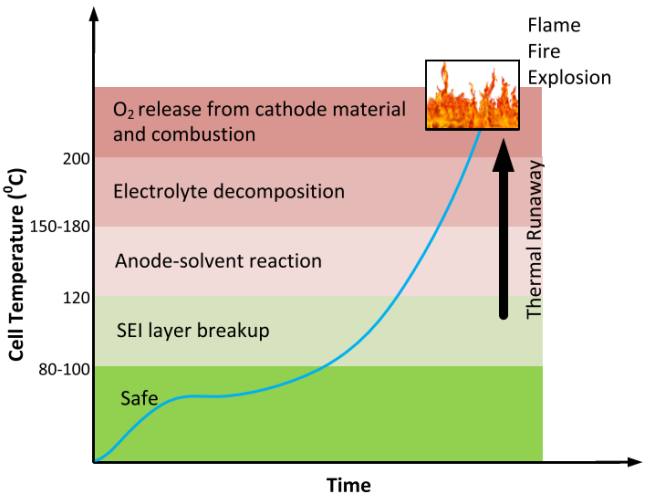

Figure 14: Thermal runaway process with respect to cell temperature [24]

Table 14 reports an overview of all TMS already mentioned. It seems clear that PCM is a promising method and deserve further R&D [24]. In fact, it has several good properties compared to other TMS, e.g. long operating life,

moderate use and integration complexity, moderate maintenance, high efficiency, low capital and O&M costs, large Li-Ion cell average surface temperature decrease potential and temperature uniformity capability [24].

Table 14: Thermal Management Systems TMS for Li-Ion cells: advantages and disadvantages [73]

	Advantages	**Disadvantages**
Air cooling	Low cost	Low h (i.e. low η and high volumes)
	Simple design	High T gradients
	Highly commercialised	Noise issues
Liquid cooling	Good h (i.e. high η and low volumes)	Safety issues (leakages)
	Medium T gradients	Complex design
	Highly commercialised	High costs, weights and maintenance
HPS	High h (i.e. high η and low volumes)	High costs
	High operating life	Non commercialised
Boiling	High h	Non commercialised
	T uniformity	Complex operation
PCM	High thermal energy density	Low thermal conductivity (low powers)
	T uniformity	Potential liquid leakage due to volume expansion

Legend: h=heat transfer coefficients [$\frac{W}{m^2\,K}$], T=Li-Ion cell surface temperature [K], η=thermal efficiency

4.2. Air-cooling

Air-cooling is the most wide-spread TMS technique and is characterised by low costs, simple design but also low thermal performances due to air thermo-physical properties at operating conditions and high cell temperature dis-uniformity [12]. Therefore, there are several ways to improve it proposed in literature [77, 12, 78, 73]:

- Increase air flow rates: higher Reynolds number, higher heat transfer coefficients, but uneven temperature distribution, higher parasitic consumption. Chen et al. [79] report that air cooling has from two to three times the energy consumption compared to liquid cooling.
- Battery layout optimisation: use of wide spaces between cells and staggered configuration can improve the air flow turbulence and therefore Nusselt number values, but this leads to lower energy/power EESS densities
- Air flow path: possible better temperature uniformity with so called reciprocating air flow (i.e. alternate air-flow inlet-outlet), leading to 72% drop in temperature gradients, or Z-type configuration, but this requests higher complexity and control systems.
- TCE: Integration of metal/high conductive foam/matrices/honeycomb/fins/pins structures to improve the equivalent heat conductivity of air-flow [73, 80].
- Mist cooling: mixture of air and water droplets to improve the equivalent heat transfer coefficient [81].

Giuliano et al. [16] claim that air cooling can be as effective as liquid cooling. This results can be obtained by adding aluminium foams within the air flow duct to improve the heat transfer coefficient, leading to battery temperature increase lower than 10 °C even at DR of 4C. Chen et al. [82] studied finned and/or pinned direct/indirect systems to improve the air flow heat transfer coefficients and decrease the average cell temperature. They conclude that

satisfactory cooling rates can be achieved by increasing the air flow rate and inevitably the parasitic consumptions. Shaid et al. [83] showed that a better Li-Ion cells spatial configuration can reduce the cell-to-cell and in-cell temperature gradients of 21.5% and 16% and the in-cell and maximum temperature of 5%. However, this is done with complex system design where multiple vortex generators and jet inlets are added to a normal air channel. Similarly, He et al. [13] showed that air fan consumption can be reduced by up to 84% by sound control strategies. Yu et al. [84] confirmed that air cooling can be improved by imposing different air-flow patterns, like two directional flows, e.g. longitudinal plus transversal jet-cooling systems. This permits to decrease the battery temperature of around 9 °C and reach better isothermalisation.

In regards to TCE based on metals, Saw et al. [80] proposed a combination of aluminium foam and heat spreader as TCE for 20-Ah pouch cell TMS. The authors have shown that the metal foam helps the heat transfer increasing both the heat exchange area (up to 10 times) and, due to the continuous destruction and re-initialisation of the thermal boundary layer, a higher equivalent heat transfer coefficient. By using a CFD model validated with experimental data taken from previous literature, the authors considered a uniform heat generation rate of 30 W, equivalent to a discharge rat of 3C. From the simulation, the authors have shown that the best thermal performance is reached by using a foam of 10 PPI (Particle Per Inch) and 91.9% of porosity. This foam led to the same TMS performance (Li-Ion cell average surface temperature below 40 ^oC, temperature dis-uniformity lower than 5^oC) as for a pure air-cooling system with a third of the air mass flow rate (down from 60 to 20 g/s).

Saw et al. [81] proposed an experimental and numerical study on mist cooling based on a dummy battery test rig whose heat generation profiles are based on discharge tests at DR=1,3,5C made by an accelerating rate calorimeter. The authors showed how water droplets in equilibrium with a mixture of dry air and water vapour can increase the overall heat transfer coefficient due to better thermo-physical properties when compared to dry air. The high heat capacity of the mist keeps the temperature of the cooling vector lower compared to dry air, leading to more uniform Li-Ion cell temperatures. Tests at DR=3,5C showed that the temperature difference on the Li-Ion cell surface was 1.3^oC and 0.4^oC for dry air and mist cooling respectively; the latter accomplished by a 3% mist loading fraction.

4.2.1. Micro-channels

There is evidence in literature of the research interest [85, 86] in micro-channel systems for air-cooling of Li-Ion cells. The basic principle is that decreasing the size of the air-flow channels (or increasing their number per volume) increases the heat transfer area per unit of volume, i.e. improving the heat transfer rates [85]. Moreover, if the mass flow rate can be increased, this leads to higher velocities, higher Reynolds and Nusselt numbers and better thermal performance [85].

4.2.2. Heat Pipes

Compared to micro-channel systems, HPS can improve the temperature uniformity of the Li-Ion cells if properly positioned, thanks to their high equivalent thermal conductivity, which can assume values in the range of $8.225 - 19.169 \cdot 10^3\, W/m\,K$ depending on their size [87]. Shah et al. [88] investigated different combinations of HPS and air cooling in annular channel to avoid cell core thermal run-away, showing a potential decrease of the core temperature

of up to 20 °C with a constant cell heat generation of 1.62 W. It must be mentioned that this study is based on the experimental simulation of a Li-Ion cell by using an electrical cartridge in the shape of a 26650 cell. Similarly, Yuan et al. [89] showed that for a 10Ah pouch cell discharged at DR 2.5C HPS can decrease of around 6 °C the cell temperature and improve the temperature uniformity.

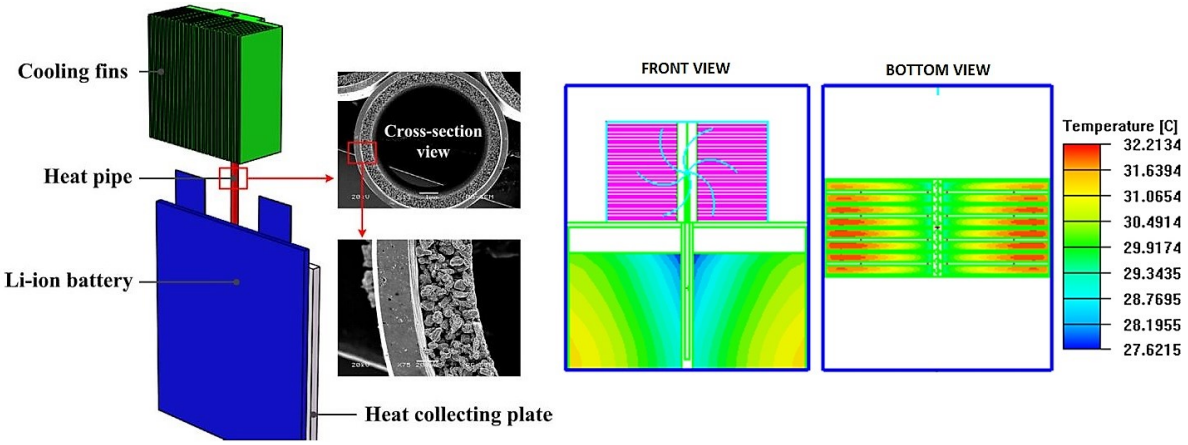

Figure 15: Air-cooling by HPS: configuration and temperature profile [89]

4.3. Liquid-cooling

Several studies [90, 91, 77, 79, 92, 93, 94, 17, 95, 11, 96, 93, 10] report that air cooling fails in case of high DR and large battery packs, leading to a necessary implementation of liquid cooling. Tong et al. [92] claim that liquid cooling can be easily implemented with battery pack of different sizes and, by changing flow rate and channel width, it can handle extreme operating conditions of high DR up to 5C. There are two main categories of liquid cooling [77]: passive and active. However, as passive liquid cooling systems don't guarantee considerable higher performance compared to air force convention, only active liquid cooling is used due to the beneficial effect of higher heat transfer coefficients (350-400 $W/m^2\,K$ compared to 5-25 $W/m^2\,K$ of air cooling [79]). However, this adds complexity and costs (both capital and operational) to the TMS. In fact, liquid cooling TMS comprehends pump, heat exchangers and coolant/refrigerant pipes [79]. Moreover, this leads to extra mass and increased weights (Table 15), from 3 to 7 % depending on the fluid used, which could be a clear drawback for motive applications [79].

Table 15: Extra weight added by cooling system for each 35Ah pouch cell of mass 1.01 kg, elaborated from [79].

Coolant	Extra Mass [kg]	Extra Mass [%]
Air	~ 0	~ 0
Mineral Oil	0.0298	2.95
Water/glycol	0.0723	7.16
Fin	0.394	39

Zhao et al. [77] argue that the optimisation of these systems breaks down into refrigerant selection and fluid flow configuration. For the latter, due to safety reason and compactness, the most used design is the cold plate, where fluid and Li-Ion cells are separated by a thin highly conductive metal plate on which a series of coolant

pipes (serpentine or straight bundles) are mechanically sold. Moreover, in accordance with air forced convection improvement techniques, multi/micro channels are typically applied to achieve higher specific exchange areas and Reynolds numbers. However, this comes with higher pressure drops and parasitic consumptions for the pump [93]. On this regards, Du et al. [97] report that this can be minimised once an hysteresis control technique is implemented in the cooling system, leading to cell operation in safe temperature range conditions and reduced energy consumption. Moreover, Cheng et al. [79] demonstrate that water-glycol cooling has a pumping consumption more than two order of magnitude lower than air cooling for the same average temperature rise (Figure 16). Typical fluids are water, water glycol or silicon/dielectric mineral oils (Table 15).

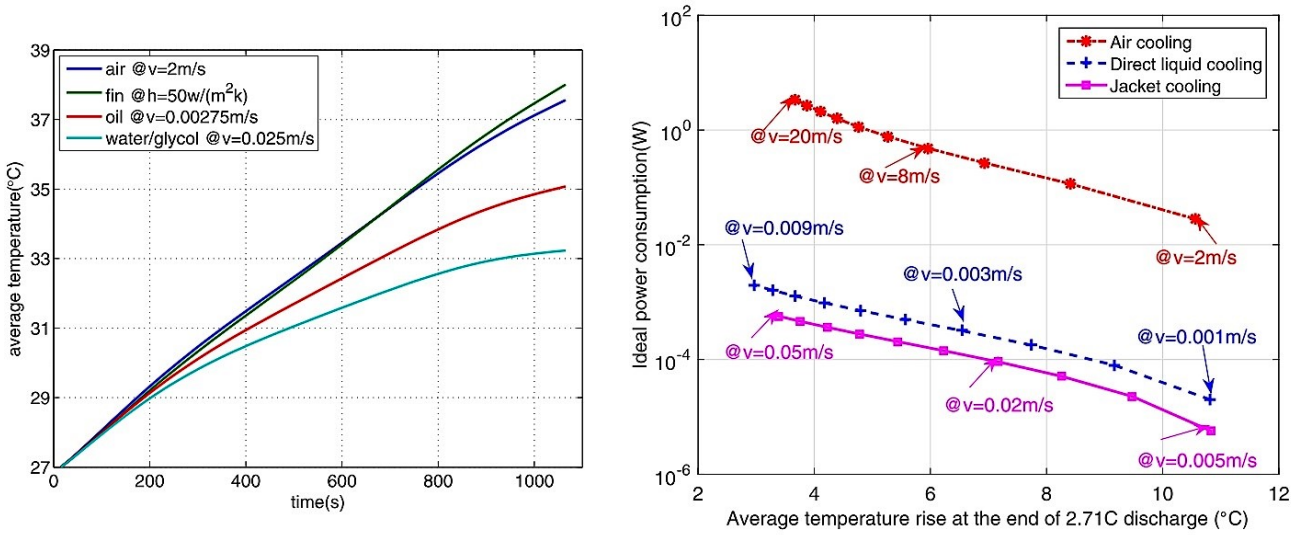

Figure 16: Average cell temperature and ideal fan/pump power consumption for air, fin, direct liquid (i.e. oil) and indirect (i.e. jacket) cooling at DR 2.71C [79]

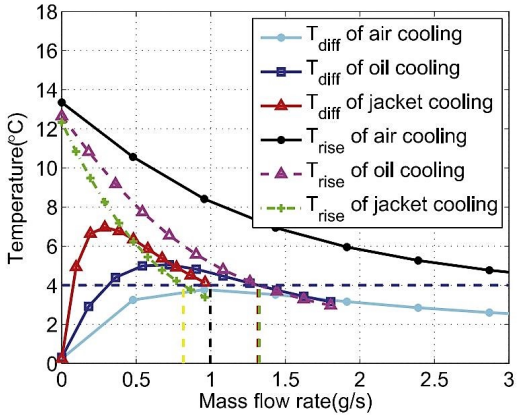

Figure 17: Cell temperature rise and in-cell temperature gradient for air, fin, direct liquid (i.e. oil) and indirect (i.e. jacket) cooling at DR 2.71C [79]

Panchal et al. [19, 20] proposed a water-cooling TMS on a prismatic lithium-ion battery pack with both experimental and numerical approach. Discharge tests at DR of 1C, 2C, 3C, and 4C were proposed with inlet cooling water temperatures of 5, 15, 25 and 35 ^oC. Comparing the water cooling tests at 25^oC with air-cooling at 22^oC,both at

DR=4C, the experimental results showed that water cooling decreased the average/maximum Li-Ion cell surface temperature from 41.38/56.49 ^oC to 28.25/30.66 ^oC (i.e. -32/46 %).

However, several studies [94, 77, 98, 17, 95, 79] report that, although liquid cooling is better than air cooling to reach lower average cell temperature, it is not effective for maintaining a low in-cell thermal gradient which leads to cell degradation. Panchal et al. [94] show that using cold plate with high exchange area as pouch cells TMS decrease the cell maximum temperature but worsen the temperature uniformity. Chen et al. [79] show that liquid cooling (jacket) is not capable of keeping the in-cell temperature gradient lower than the deemed limit of 5 °C unless mass flow rates higher than 1 gr/s are imposed to the system (Figure 17).

Moreover, Huo et al. [86] demonstrated that a cold-plate water cooling TMS can decrease the maximum temperature of Li-Ion cells by up to 13.9 °C (Figure 18) when compared to air-cooling for a discharge rate of DR=5C and subject to a water inlet temperature of 25 ^oC (equal to ambient). This method reduces the in-cell temperature gradient compared to air-cooling from 12.59 ^oC to 9 ^oC (i.e. 28%)

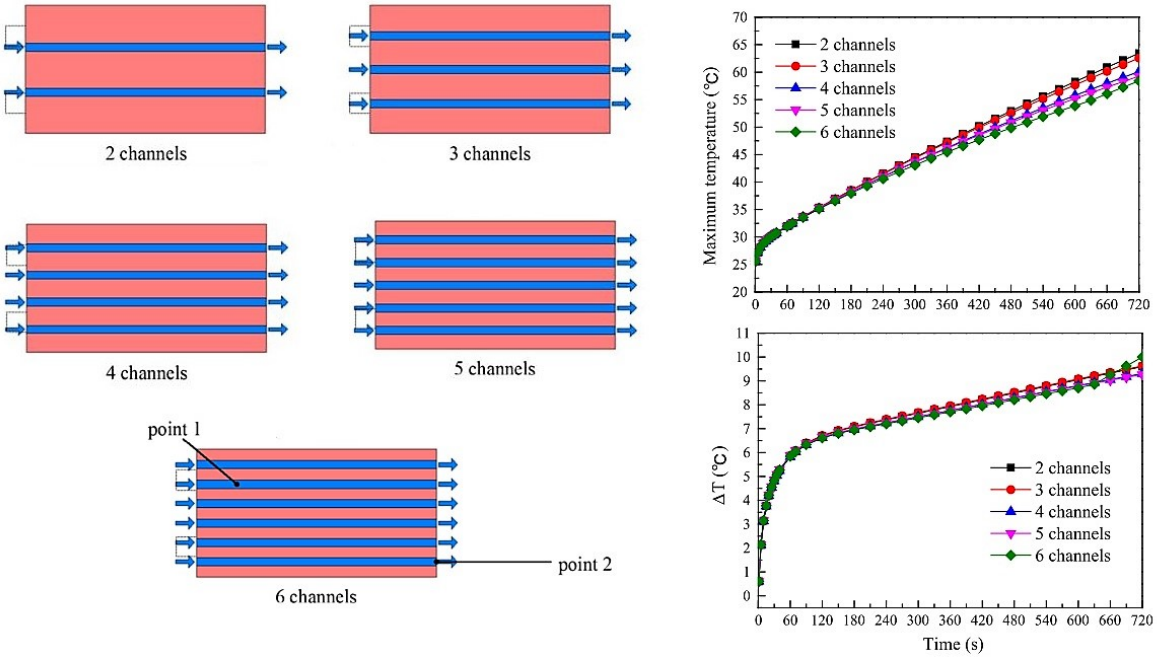

Figure 18: Air-cooling by micro-channels: maximum temperature and in-cell temperature gradients [86]

Similarly, Jarrett et al. [90] investigated the design optimisation of a cold-plate water cooling TMS and the influence of operating conditions on Li-Ion pouch cells for EV applications. In their first study [90], the authors proposed an optimisation of the cold plates design by CFD analysis. The main conclusion was that typically optimised designs for coolant pressure drops and average temperature lead to increased temperature dis-uniformity. Moreover, in their following study [91] the authors demonstrated that the Li-Ion cell temperature uniformity is highly sensitive to dis-uniform heat generation rates (such as the ones present in real Li-Ion pouch cells) and to the specific coolant flow rate.

However, there are several solutions proposed in literature. Zhao et al. [77, 17] suggest to optimise the fluid

flow direction, pattern and increase the mass flow rate. Similarly, Zhang et al. [98] demonstrate that the in-cell temperature difference can be kept lower than 5 °C with water cooling when sound designs are used, such as the application of flat flexible graphite sheets in between cell and cooling tubes. Finally, Yang et al. [95] propose an innovative liquid metal TMS. They claim that liquid cooling is still limited by the low conductivity of coolant such as water or aqueous ethanol. So, they propose liquid metal such as Gallium (melting temperature 29.8 °C) and his alloys with Indium and Tin $Ga^{80}In^{20}$, $Ga^{68}In^{20}Sn^{12}$ (melting temperatures of 16 °C and -10 °C), leading to lower maximum cell temperatures and better temperature uniformity, together with lower pump consumption (due to usage of electromagnetic pump). However, no efforts were done in estimating the costs, weight, maintenance (potentially lower than water due to no moving part in the pumping system), corrosion and leakage problems. Also, liquid metals are incompatible with aluminium [95] so this can't be used for the jacket, restricting the choice to nickel an copper, far more expensive.

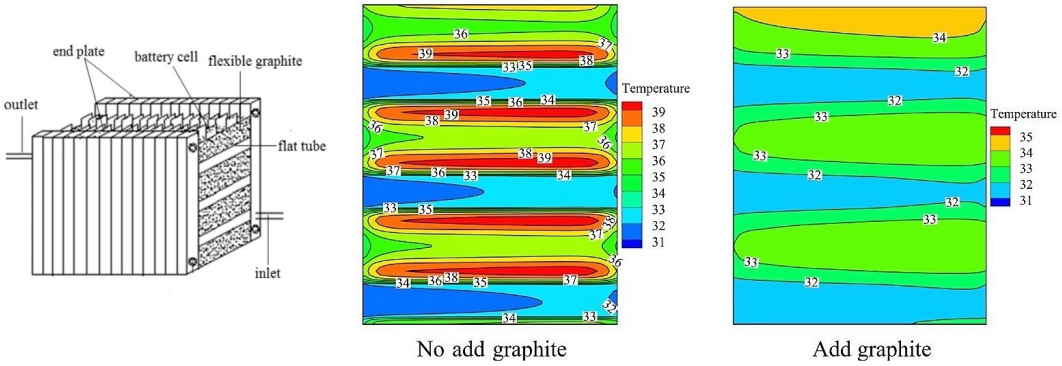

Figure 19: Improvement of temperature uniformity in liquid cooling by adding graphite sheets in between Li-Ion pouch cells and cooling tubes [98]

4.4. Boiling

Li-Ion cell TMS by liquid boiling (pool boiling, flow boiling) has been proposed in previous literature [76, 99, 100, 101, 102]. As shown in Table 16, both pool and flow boiling have been investigated in a relative broad range of CR and DR. The liquid mainly used is Novec7000, an hydrofluoroether with boiling point at ambient pressure of 34 ^oC, latent heat of vaporisation of 142 kJ/kg, specific heat of 1300 J/kg K and thermal conductivity of 0.075 W/m K. Overall, all studies report an effective cooling performance and isothermalisation.

4.4.1. Pool Boiling

Van Gils et al. [76] investigated the effectiveness of pool boiling sing Novec7000 as TMS for a cylindrical Li-Ion cell charge/discharge of 0.5C/5C. From their experimental tests, they found that when pool boiling is activated (mainly fully-developed nucleate boiling, see Figure 20), high heat transfer coefficients are reached (up to 700 $W/m^2\,K$ compared to 350 $W/m^2\,K$ without boiling) and the cell's average surface temperature is kept steady at 34.4 ^oC and the surface temperature gradient is entirely negligible, leading to an ideal iso-thermalised condition even at high DR. This is mainly due to the direct contact of the cooling fluid with the external surface of the cell, including both tabs. Moreover, they proposed a fast regulation technique based on a boiling chamber pressure control as shown in

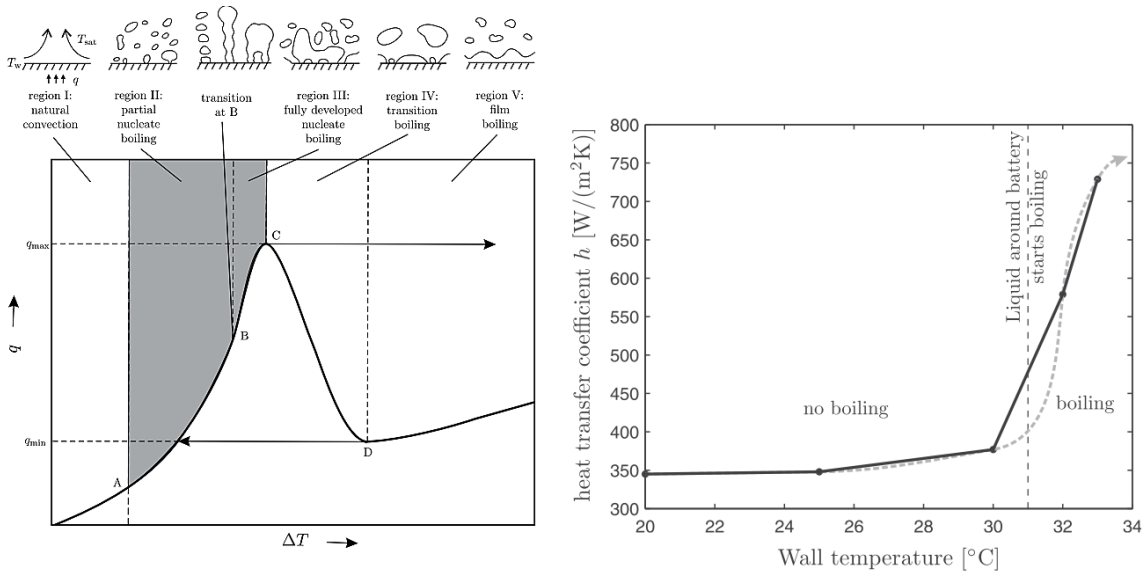

Figure 20: Typical boiling curve, showing qualitatively the dependence of the interface heat flux (q) on the surface superheat (ΔT), defined as the difference between the surface temperature and the boiling temperature of the liquid. The maximum heat transfer coefficients are experienced within the region III (fully developed nucleate boiling) [76].

Figure 21. However, it must be pointed out that the Li-Ion cell core temperature has not been evaluated: therefore, there is no experimental evidence of the Li-Ion cell temperature radial disuniformity.

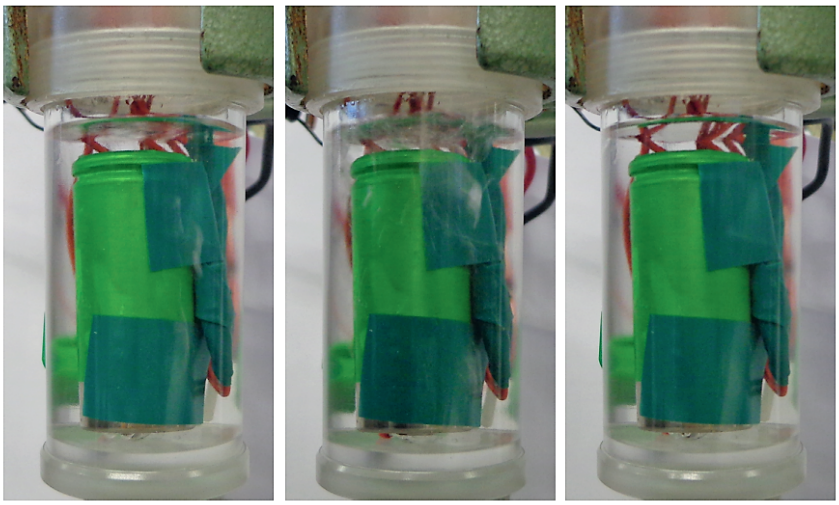

(a) Atmospheric pressure (b) Sub-atmosphericpressure (c) Super-atmospheric pressure

Figure 21: Visualisation of the boiling experiments at atmospheric pressure (a), at sub-atmospheric pressure (b) and at super-atmospheric pressure (c) [76].

Hirano et al. [99] proposed a pool boiling TMS for Li-Ion pouch cells tested at high CR/DR (10C/20C). Similarly to Van Gils et al. [76], they used Novec7000 as liquid. To evaluate the effect of the liquid boiling temperature, they compared Novec7000 (34 ^oC) with Novec649 (49 ^oC).From their results, they inferred that Novec7000 is capable to keep the Li-Ion cell's temperature around 35 $\pm$ 2.5 ^oC at both DR 10C and 20C. Also, comparing a TMS with 100%-wetted porous material and 50%-immersed microfibre cloth, they demonstrated that the two TMS have the same thermal performance, leading to 50% liquid savings in the latter TMS.

Table 16: Overview of literature on liquid boiling as TMS for Li-Ion cells.

Reference	Boiling Mode	Capacity [Ah]	n. Cells	Geometry	CR/DR	Liquid	T_b (1 atm) [^oC]
[76]	Pool	1	1	Cylindrical	0.5/5	Novec7000	34
[99]	Pool	1	10	Pouch	10/20	Novec7000	34
						Novec649	49
[100]	Flow	-	-	Pouch	-	R134a	24 (at 650 kPa)
							29 (at 750 kPa)
							33 (at 850 kPa)
[101]	Flow	20	14	Pouch	2/(1,3,5)	Novec7000	34

T_b= boiling temperature [^oC]

4.4.2. Flow Boiling

An et al. [101] investigated the thermal performance of a Li-Ion cells TMS based on flow boiling in mini-channels (Figure 22). Similarly to Van Gils et al. [76] and Hirano et al. [99], they used Novec7000 as liquid. They tested a Li-Ion battery pack (51 V, 20Ah) composed by 14 20Ah pouch cells connected in series under different DR (1C, 3C, 5C), ambient temperature (0,15,25,35 ^oC) and constant CR (2C). from their results, it could be claimed that the proposed flow boiling TMS was capable to keep the Li-Ion cells temperature around 40 ^oC with a dis-uniformity up to 4 ^oC. Also, the Re number has a strong influence of the triggering of the flow boiling within the mini-channels and therefore the TMScooling effectiveness.

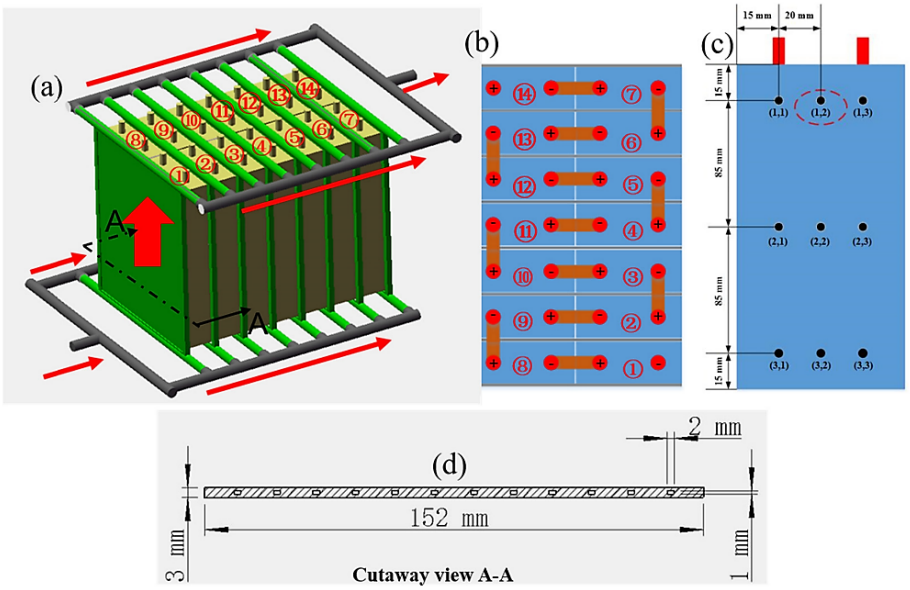

Figure 22: Schematic diagram of battery module. (a) Layout of battery module and coolant flow direction; (b) series type of battery module; (c) thermocouple locations for the temperature measurements of battery module; (d) cutaway view of cold plate [101]

4.5. Phase Change Materials

4.5.1. Overview

TESS are typically divided into thermal and thermo-chemical [103, 104], where the former are also classified as sensible (SH) and latent (LH) heat systems. As shown in Figure 23, LH have been shown to have higher energy densities (5-14 times) for a fixed temperature difference than SH [103, 105] due to the highly-energetic isothermal phase transition.

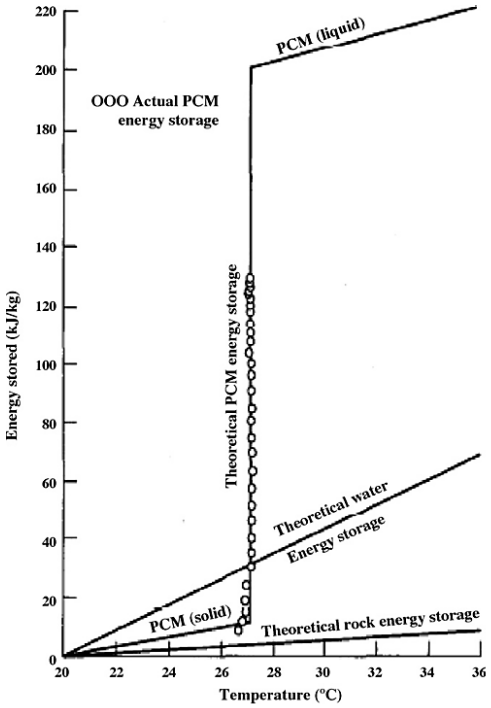

Figure 23: Comparison of Sensible Heat (water, rock) SH and Latent Heat (PCM) LH TESS [103].

Among LH storage, there are three main categories: solid-solid, liquid-gaseous and solid-liquid [103, 104]. The solid-solid systems have small volumetric variation during transition but are characterised by low specific heat. Liquid-gaseous systems have the disadvantage of a non-negligible volume change to the gas phase. Therefore, the solid-liquid phase appears to be the best option, considering its high latent heat, high energy storage density and quasi-isothermal storage process [106, 107, 108, 109, 110, 111, 105, 112, 113, 114, 103, 115]. Moreover, low expansion ratio (lower than 10%) is permitted and consequently low structural stresses are exerted by the PCMs on the HEX walls [106, 108, 109, 103, 115]. In addition, thanks to a great multitude of PCM typologies, e.g. organic (paraffins, fatty acids), inorganic (hydrated salts, metallic) and eutectic mixtures, and related melting temperatures, a good thermal match between heat transfer fluid (HTF) and PCM can always be found, leading to high energy and exergy efficiencies [116, 105, 115, 117, 118].

4.5.2. Classification

PCMs are divided into 3 main groups (Figure 24): organic (paraffin, non-paraffin compounds such as fatty acids), inorganic (salt hydrates, metallics) and their eutectic mixtures [103, 104, 119]. Historically, common PCMs used in

the literature were paraffins, Glauber's salt (Na_2SO_4), waxes, stearic acid and n-octadecane [118].

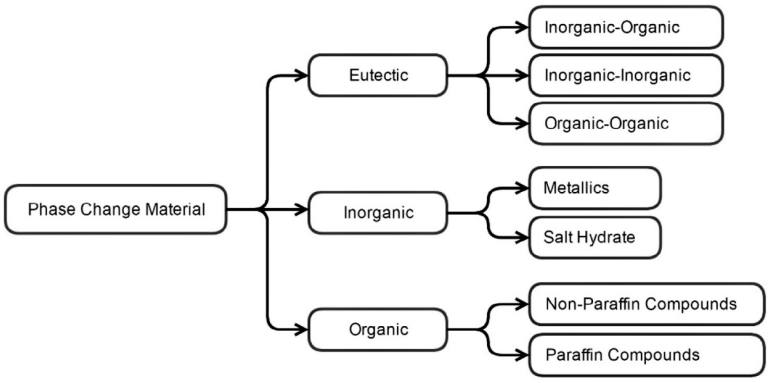

Figure 24: PCM classification considering material composition [119]

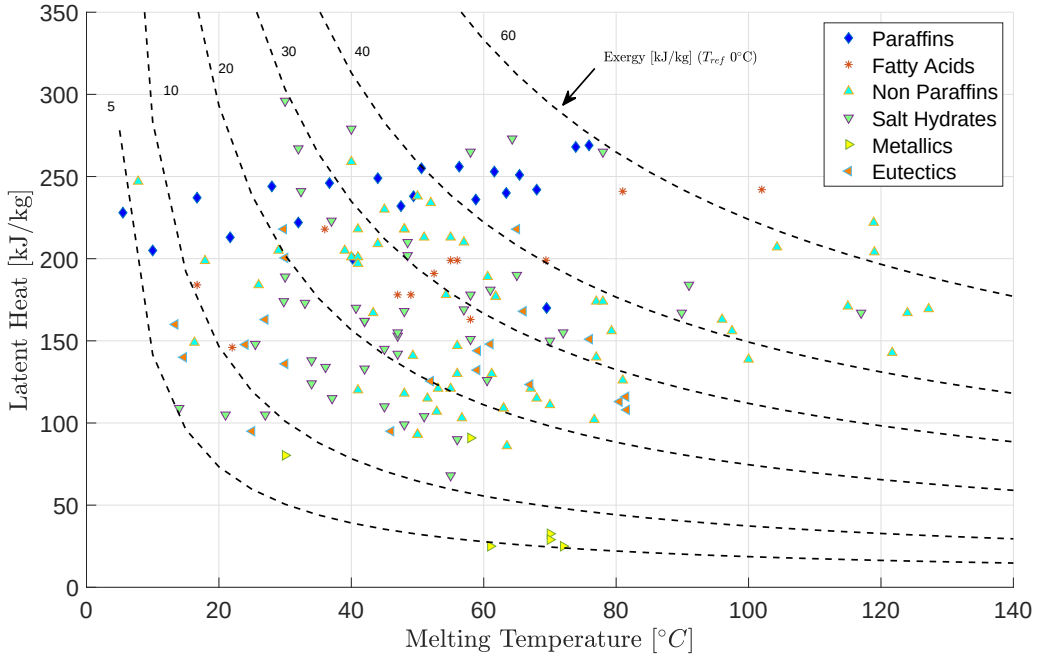

Figure 25: Melting temperature T_m and Latent Heat h_m for different PCM (elaborated from [103]). The equivalent thermal exergy is calculated considering a fictitious reference temperature T_{ref} of 0 °C.

The organic and salt hydrates PCMs are promising for applications with temperatures lower than 100 °C (e.g. TMS of Li-Ion batteries) while eutectic mixtures can be employed for temperatures up to 250°C [105]. Organic materials have typically latent heat in the range 128-200 kJ/kg (Figure 25) while inorganic compounds (e.g. salt hydrates) reach values of 250-400 kJ/kg [103].

Organic PCMs are typically divided into two main subcategories: paraffin and non-paraffin. Paraffins (Table 17) are considered to be safe, reliable, chemically stable, predictable and cheap [103]. Moreover, they have low volumetric expansion during phase transition and have low transition pressure. They are composed of chains of alkanes whose chemical structure and formula are $CH_3\,(CH_2)_m\,CH_3$ and C_nH_{2n+2} [103]. Typically, their melting temperature and their latent heat grow logarithmically with their chain length (i.e. number of C atoms) [103]. Their main drawback

Table 17: Paraffins properties [105, 121, 103]

	C number	ρ	T_m	h_m	E_{vol}	Price (Min)	Price (Max)
n-Tetradecane	14	764	5.5	228	48.39	8.27	10.33
n-Pentadecane	15	769	10	205	43.79	9.13	11.42
n-Hexadecane	16	770	16.7	237.1	50.71	7.89	9.86
n-Heptadecane	17	777	21.7	213	45.97	8.70	10.88
n-Octadecane	18	777	28	244	52.66	7.60	9.49
n-Nonadecane	19	786	32	222	48.47	8.25	10.32
n-Eicosane	20	792	36.7	246	54.12	7.39	9.24
n-Henicosane	21	792	40.2	200	44.00	9.09	11.36
n-Docosane	22	794	44	249	54.92	7.28	9.10
n-Tricosane	23	797	47.5	232	51.36	7.79	9.73
n-Tetracosane	24	799	50.6	255	56.60	7.07	8.83
n-Pentacosane	25	812	49.4	238	53.68	7.45	9.31
n-Hexacosane	26	803	56.3	256	57.10	7.00	8.76
n-Heptacosane	27	802	58.8	236	52.58	7.61	9.51
n-Octacosane	28	807	61.6	253	56.71	7.05	8.82

Units: Melting Temperature $T_m\,(^\circ C)$, Specific Latent Heat $h_m\,(kJ/kg)$, Density $\rho\,(kg/m^3)$, Energy Density $E_{vol}\,(kWh/m^3)$, Price $(£/kWh)$

is a low thermal conductivity in the range 0.15-0.21 $W/m\,K$ [103, 105, 104, 120].

Non-paraffins can be classified as esters, fatty acids, alcohols and glycols [103, 104, 120]. Generally, non-paraffin organic PCMs are characterised by high heat of fusion, non-flammability, low thermal conductivity, mild toxicity and instability at high temperatures [103, 120]. Moreover, fatty acids are the most important subgroup of this kind of PCM. They have high heat of fusion compared to paraffins and have no problems of thermal hysteresis and sub cooling during freezing processes (unlike salt-hydrates) [103, 120]. Their general chemical structure and formula are $CH_3\,(CH_2)_m\,COOH$ and $C_nH_{2n}O_2$ [103, 120]. From Figure 25 and Table 18 it can be appreciated that latent heat and energy density of fatty acids increase with their melting temperature, and are typically in the range 150-200 kJ/kg and 35-51 kWh/m^3 [122, 103, 120]. Their thermal conductivity is quite low, in the range 0.14-0.17 $W/m\,K$, leading to thermal diffusivities in the range 7.5-10 $\cdot 10^{-8}\,m^2/s$. The good properties of fatty acids are: melting point congruency, good chemical stability, non-toxic, small volumetric expansion, compatibility with storage container materials (i.e. no corrosion), high latent heat, high energy density, derivation from common oils, no effect of sub cooling, no phase segregation. The only issue is that they are more expensive than other materials such as salt hydrates and paraffins; for instance, their specific cost is roughly 2-2.5 times that of paraffin and even more compared to salt-hydrates [103, 120].

Inorganic PCMs are divided in salt hydrates and metallics [103, 104]. Salt hydrates are basically alloys or mixture

Table 18: Fatty Acids Properties [122, 105]

Properties	Capric	Lauric	Myristic	Palmitic	Stearic
Number of Carbon atoms	10	12	14	16	18
T_m (°C)	32	44	58	64	69
h_m (kJ/kg)	152.7	177.4	186.6	185.4	202.5
ρ solid (kg/m^3)	1004	1007	990	989	965
ρ liquid (kg/m^3)	878	862	861	850	848
c_p Solid $(kJ/kg\,K)$	1.9	1.7	1.7	1.9	1.6
c_p Liquid $(kJ/kg\,K)$	2.1	2.3	2.4	2.8	2.2
k Liquid $(W/m\,K)$	0.153	0.147	0.15	0.162	0.172
α (m^2/s)	8.13E-08	7.87E-08	7.91E-08	7.50E-08	9.99E-08
α (vs. copper) (%)	7.22E-02	6.99E-02	7.02E-02	6.66E-02	8.87E-02
Energy density (kWh/m^3)	39.91	46.05	47.97	47.35	50.99
Price $(£/m^3)$	-	276	-	354	345
Price $(£/kWh)$	-	6.5	-	8.3	11

of inorganic salts (AB) and water ($n\,H_2O$), to form a compound with equivalent chemical formula $AB \cdot (H_2O)_n$. The process of melting/solidification is basically a dehydration/hydration of the salt [103]. This leads to the first issue of salt hydrates, i.e. non-congruent or sedimentation processes during melting (dehydration) [103]. This is due to the fact that dehydrated salts are heavier than water and tend to sediment at the container base [103]. When solidification (hydration) need to be triggered, the system is characterised by areas of different salt concentration and consequently the complete solidification (hydration) is impossible, i.e. the material can't regenerate properly for the following charging phase [103]. However, solutions to this problem have already been found, such as mechanical stirring, encapsulating the PCM to avoid the separation of dehydrated salt from its released water and adding special thickening materials [103]. Dannemand et al. [123] proposed the utilisation of proper thickening agents, such as carboxy-methyl cellulose (carboxy-methyl groups $-CH_2 - COOH$) or xanthan rubber. The other issue of salt hydrates is supercooling [103, 123], due to poor nucleation properties of the material. This means that generally the nucleation rate of salt hydrates is quite low at transition temperatures and the material needs to be sub-cooled (or supercooled) before nucleation is naturally triggered [103]. This means that the stored thermal energy is released at much lower temperatures, decreasing the exergy efficiency of the heat storage system. However, there is evidence that the addition of nucleation agents or even injection of nuclei trigger the cooling process [103]. An idea proposed by Dannemand et al. [123] could be to provide "seed" crystals or evaporate some liquid CO_2 in a chamber in contact with the PCM container. Moreover, the same authors report that, during the crystallisation or solidification processes, possible cavities can be formed which introduce additional thermal contact resistance [123]. This can be avoided with additional inert HTF within the PCM. Overall, the good properties of salt hydrates (Table 19) are high latent heat, high thermal conductivity (2 times compared to paraffin and comparable to water), low volumetric expansion during melting, low level of toxicity, low level of corrosivity (compatibility with plastics) and low cost

Table 19: Salt Hydrates Properties [105]

	T_m	h_m	$c_{p,s}$	$c_{p,l}$	k_s	k_l	ρ_s	v_{exp}	E_{vol}	Price $(£/m^3)$	Price $(£/kWh)$
Water	0	333	3.30	4.18	1.60	0.61	920	-8.7	109	0	0
CCH	30	125	1.42	2.20	1.09	0.53	1710	11	64	93	2
SSD	32	180	1.93	2.80	0.56	0.45	1485	4	82	48	1
STP	46	210	1.46	2.39	0.76	0.38	1666	6	103	199	3
SAT	58	266	1.68	2.37	0.43	0.34	1450	3	113	233	3

Units: Melting Temperature $T_m\,(^\circ C)$, Specific Latent Heat $h_m\,(kJ/kg)$, Specific Heat Capacity $c_p\,(kJ/kg\,K)$, Thermal Conductivity $k\,(W/m\,K)$, Density $\rho\,(kg/m^3)$, Volumetric Expansion $v_{exp}\,(\%)$, Energy Density $E_{vol}\,(kWh/m^3)$

CCH=Calcium chloride hexahydrate, SSD=Sodium sulphate decahydrate

STP=Sodium thiosulfare pentahydrate, SAT=Sodium acetate trihydrate

Table 20: Thermo-physical properties of selected eutectic compounds [105]

	$\%w$	T_m	h_m	$c_{p,s}$	$c_{p,l}$	k_s	k_l	ρ_s	E_{vol}	Price
$CaCl_2(H_20)_6$										
$MgCl_2(H_20)_6$	67-33	25	127	1620	2270	0.93	0.55	1661	57	80/1.4
$Urea$										
$CH_3COONa(H_2O)_3$	60-40	30	200	1750	2210	0.63	0.48	1370	74	206/2.8
$Mg(N0_3)_2(H_20)_6$										
NH_4N0_3	61-39	52	125	2130	2670	0.59	0.50	1672	58	188/3.3
Urea-Acetamide	38-62	53	224	1920	2660	0.51	0.34	1216	73	924/13
Stearic acid-Acetamide	83-17	65	213	1800	2400	0.30	0.18	972	56	485/8.6
Stearic/palmitic acid	36-64	53	182	1720	2230	0.23	169	0.97	46	351/8
$Mg(N0_3)_2(H_20)_6$										
$MgCl_2(H_20)_6$	59-41	59	132	2290	2810	0.67	0.53	1610	58	99/1.7

Units: Melting Temperature $T_m\,(^\circ C)$, Specific Latent Heat $h_m\,(kJ/kg)$, Specific Heat Capacity $c_p\,(kJ/kg\,K)$, Thermal Conductivity $k\,(W/m\,K)$, Density $\rho\,(kg/m^3)$, Energy Density $E_{vol}\,(kWh/m^3)$, Price $(£/m^3)/(£/kWh)$

(when pure) [103, 105].

The last category of inorganic PCMs is metallics (low temperature melting metals) [103, 104]. They have high volumetric energy density but, due to high density, have low specific energy density. Moreover, they have high thermal conductivity, so TCE methods are not necessary in this case [103]. In addition, eutectic mixtures (from the Greek eu = easy, teksis = melting) are mixtures of 2 or more PCMs which, at specific compositions, melt at a singular temperature [105]. These mixtures are proposed in the literature; their properties are reported in Table 20.

Table 21: Commercial PCM manufacturers in the world. [118]

Manufacturer	Online site	Melting Temperature Range (°C)	Number of PCMs
EPS Ltd	http://epsltd.co.uk	−114/164	61
RUBITHERM	http://www.rubitherm.de	−3/100	29
TEAP	http://www.teappcm.com	−20/78	22
Cristopia	http://www.cristopia.com	−33/27	12
Climator	http://www.climator.com	−18/70	9
Mitsubishi Chemical	http://www.mfc.co.jp	9.5/118	6
Doerken	http://www.doerken.de	−22/28	2

In terms of PCM containers, these are generally divided in compact and encapsulated [105]. Compact system consist of PCM shell-and-tube systems, where the PCM is located typically within the shell and the HTF flows within the tubes. For instance, PCM encapsulated systems consist of an encapsulated packed bed, encapsulated staggered cylinder, PCM bags [105]. When these systems are filled with PCM, a void fraction need to be included to account for the volumetric expansion during melting. Compact systems have better energy density, in terms of m^3 of PCM per m^3 of container [105]. However, they are worse in regards to heat transfer properties due to lower effective thermal diffusion, resulting in a low power rating [105]. Encapsulated systems have higher heat transfer area per unit volume, therefore better heat transfer properties (higher power rating) but have lower ratio of m^3 PCM per m^3 of storage therefore lower energy density [105]. From Table 19, it appears that salt hydrates have the highest energy densities (64-113 kWh/m^3) and the lowest specific costs (1-4 £/kWh) compared to all other PCMs. In fact, organic compounds (Table 17, Table 18) lead to energy densities of 50-70 kWh/m^3 and specific costs 6.5-11 £/kWh. Eutectic mixtures can reach 46-74 kWh/m^3 and costs equal to 1.4-8 £/kWh (Table 20). A list of current PCM producers/suppliers is reported in Table 21.

4.5.3. Thermal Conductivity Enhancement (TCE) Methods

There is plenty of experimental evidence which suggests that PCMs have low thermal conductivities, leading to small heat transfer rates during either charging and discharging [106, 107, 108, 147, 109, 110, 111, 105, 113, 118, 124, 130, 125, 126]. Therefore, thermal conductivity enhancement (TCE) methods are necessary to be implemented in the PCM TESS [131, 109, 110, 111, 105, 118, 108, 106]. As shown in Table 22, these methods include fins, insertion of high conductivity material or particles (e.g. carbon nano-tubes, metallic rings, graphite or carbon matrices, brushes, chips), multi-tube configurations, micro or macro encapsulation [118, 148, 110, 108, 111, 149]. The aim of these methods is either to increase the heat exchange area or increase the effective heat conductivity [118, 148, 110, 108, 106], the latter leading to better overall heat transfer coefficients. In this regards, Tian et al. [142] propose an interesting review of potential heat transfer rate improvement of different TCE methods, claiming that:

- Adding high conductivity elements (e.g. metal fins, beads, powders) leads to 60-150% increase of the overall thermal conductivity

Table 22: PCM Thermal Conductivity Enhancement (TCE) Methods

Type	Reference	Improvement
Fins	[113]	76% reduction in melting time
	[109]	40% reduction in solidification time
		Depletion of natural convection in melting phase
	[124]	24% increase in thermal efficiency
Carbon and Metallic Additives	[110]	500% increase of PCM effective thermal conductivity
	[106]	100 times reduction in melting time
	[109]	7.5 times increase thermal conductivity
		80%/50% decrease in solidification/melting time
Carbon Nano-particles/wires/tubes	[109]	900% increase of thermal conductivity
		85% decrease in solidification time
	[110, 112, 125, 126]	Higher heat transfer rate
Carbon brushes	[127]	233% increase in thermal conductivity
		30% increase of discharge heat rate
Copper/Titanium doping	[128, 129]	38-73% increase in thermal conductivity
PCM HTF direct contact	[108]	Higher heat transfer rate
Slurries	[107]	Higher heat transfer rate
Multi-tubes	[130, 114]	Higher heat transfer rate
HPS	[109]	Higher heat transfer rate
Metal rings and matrices	[111]	Higher heat transfer rate
PCM encapsulation	[107, 131, 132]	Higher heat transfer rate
PCM dynamic systems	[108]	Higher heat transfer rate
PCM foams	[133]	Higher heat transfer rate
Multiple-cascaded PCM	[134]	Decrease of discharge/charge time of 19/12.5%
	[135]	15% increase of heat transfer rate
	[136]	Increase of heat transfer rate
	[137]	2 PCM leads to 15.2% higher melting heat transfer rate
		3 PCM leads to 21.9% higher melting heat transfer rate
	[138]	9% increase of exergy efficiency
	[139]	33/42/47% increase of exergy efficiency using 2/3/5 PCMs
	[140]	25-40% decrease of phase transition time
	[141]	2 PCMs lead to 16% higher energy stored
		3 PCMs lead to 22% higher energy stored
	[142]	30% higher heat transfer rate
	[143]	6% higher exergy efficiency
	[116]	Exergy efficiency up to 87%
	[133]	19% higher HEX effectiveness
	[144]	45% decrease of melting time
	[145, 146]	25/40% decrease of charging/discharging time
		0.1% decrease in exergy efficiency for unsteady conditions

- Using porous media (e.g. carbon fibres, Expanded Graphite EG composites) leads to 81-272% increase of the overall thermal conductivity
- Adopting metal foams with porosity in range 85-97% leads to increase slightly better than EG composites
- Using cascaded thermal energy systems (CTES) with 5 stages (i.e. 5 different PCMs) can increase the

performance by up to 34.7%. Moreover, this method increases the stability of the outlet HTF temperature and leads to higher liquid fractions.

4.5.3.1. Fins. The general idea of fins is to increase the heat exchange area on the side of the low conductivity medium, i.e. PCM. It must however be taken into consideration that during melting processes natural convection of the liquid phase can further improve the heat transfer rate and this phenomenon must be taken into account when designing fins.

Caron-Soupart et al. [113] study the implementation of circular and longitudinal fins as a TCE method to improve the effective thermal conductivity of the PCM and therefore increasing the heat transfer rate (power) of the TESS (6-19.7% increase in max heat rate). This of course tends to decrease the energy density of the system (5.5-6.7% decrease in terms of kWh/m^3), considering that part of PCM is substituted with TCE material. The general energy density of the TCE systems is 46 kWh/m^3 compared to a value of 49 kWh/m^3 of the base case. In order to compare different heat exchangers, a characteristic time is defined as the time necessary to reach 90% of the maximum energy stored. In this way, it is possible to consider 3 configurations: single steel tube, single steel tube with longitudinal steel fins and single steel tube with circular copper fins. From the experimental results, the melting time reduces from 5000 s of the base case to an average of just 1200 s, i.e. a reduction of 76%.

However, Ibrahim et al. [109] report that fins do not give any improvements for the liquefaction (i.e. charging) of the PCM (actually they deplete the natural convection of liquid phase if wrongly positioned) but improve the solidification rate, with discharging time decreased by up to 40%. In regards of fins geometry, longitudinal fins reach the highest thermal powers due to a better natural convection during the melting phase.

Sciacovelli et al. [124] present the optimisation of fin design as a TCE method for a PCM system. A shell-and-tube (S&T) storage system with Y shaped fins with different numbers of branches is optimised with CFD techniques, in order to find the best combination of base length and opening angle of the two branches (Figure 26). By means of optimisation procedures, it is possible to increase the thermal efficiency by 24 %. Moreover, the authors suggest that the optimisation is a function of the operating time considered. For short operating times, the angle of the fins must be bigger than the ones used for long time periods. Therefore, transient operating conditions must be taken into account when proceeding with the optimisation. It must also be noted that typically the discharging process is slower than the charging one, due to the natural convection regime present in the melting phase.

4.5.3.2. Carbon and Metallic Additives. Liu et al. [110] propose the addition of carbon and metallic materials in different shapes to increase the PCM thermal conductivity. From the results of their literature review, there is enough evidence to claim that, among carbon additives, expanded graphite EG, carbon nano-tubes, carbon fibres and graphene aero-gel lead to an increase of more than 500% of PCM effective thermal conductivity with an average optimal fraction of 0.48-30 vol% and 10-30 wt%. Moreover, among metal additives, foams (e.g. copper, nickel) and particles (nickel, aluminium) lead also to an increase of more than 500% of effective thermal conductivity with foam porosities of 88-90 % and particles fractions of 9 wt% or 35 vol%.

Abujas et al. [106] compare carbon foams and fins as TCE techniques. The graphite foam is analysed considering

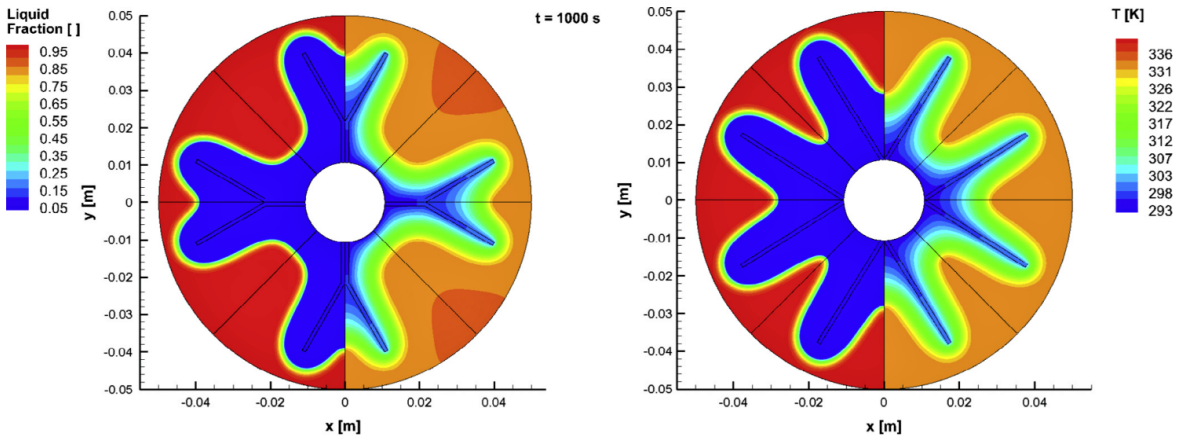

Figure 26: Optimization of Y shaped fins as TCE. Liquid fraction (half left) and Temperature (half right) profiles: initial (left) and optimal design (right). [124]

different grade of foam percentage (22-30%) and the fins are considered with two different materials: carbon steel and aluminium, both with percentage of TCE material in the range of 5-20%. The results show that graphite foams can reduce the charging time up to 100 times while the fins by 3-15 times (aluminium performs better than carbon steel). Moreover, the foams help in keeping the heat flux more constant during the entire charging time (i.e. lower decrease of heat flux compare to single PCM or fins). However, the authors report that there are problems related to TCE. Graphite foams lead to low energy density. Some suggestions for this problem could be to develop new kinds of foams with higher porosity to increase the PCM absorption within the foam pores and increase the energy density of the system.

Thus far, several studies reviewed in [109] have highlighted that porous materials typically increase the thermal conductivity of the system but lead to lower energy densities. Therefore, there is always a trade-off value of material weight or volume percentage [109]. For instance, Ibrahim et al. [109] report that for copper porous foam, the optimal porosity is 95% [109]. In this case, the thermal conductivity can increase from 0.4 to 3 $W/m\,K$ (7.5 times) leading to a decrease of freezing time (-80%) and melting time (-50%) [109]. Generally, both metal foams and expanded graphite (EG) structures are preferred. The average increase of the thermal conductivity is 4.9-6.9 times [109].

Nano powders, nano wires and carbon nano-tubes are proposed to increase the thermal conductivity of PCMs also [109]. It must be pointed out that the ratio of powder must not exceed 5% because of the depleting effect on the natural convection within the liquid phase during charging [109]. The thermal conductivity can be increased up to 900% when using copper nano wires at a volume ratio of 11.9%, reaching a value of 2.86 $W/m\,K$ [109]. When using high conductivity particles (called nano-particles), the discharge time with 0.1 and 0.6 % volume can be decreased respectively by 28% and 85% and the exergy efficiency increased by 12% and 40% [109].

Fukai et al. [127] experimentally and numerically investigated the effectiveness of carbon-fibre brushes (Figure 27) inserted in the shell side within a PCM shell-and-tube system. Carbon fibres brushes have typical thermal conductivities of 190 $W/m\,K$ while the PCM considered in this paper (paraffins) are characterised by low thermal conductivities (0.12-0.21 $W/m\,K$), melting temperatures in the range 43.8-50.6 °C, latent heat (180 kJ/kg) and

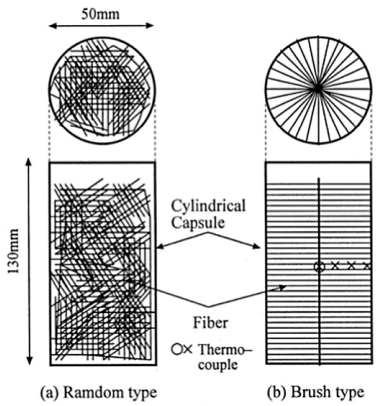

Figure 27: Arrangements of carbon fibres in cylindrical capsules [109]

energy density of 40 kWh/m^3. So, when adding the carbon brushes, the apparent thermal conductivity increases from 0.12-0.21 $W/m\,K$ to 0.4-0.51 $W/m\,K$ (+143-233%). The experimental results show that this effect is appreciable also in the case of very low carbon volume percentage. The authors claim that in the discharge stage the heat rate is increased by 30% when using just 1% in volume for the brushes. However, in the charge phase the brushes deplete the natural convection behaviour, leading to a lower rate improvement of 10-20% approximately. The authors report also that the typical packing ratio of the PCM is 75% in capsules and higher than 90% in shell-in-tube. This means that the shell-in-tube configuration have higher volume of PCM per volume of system. Therefore, the energy density is higher for shell-in-tube. However, this does not lead to higher heat transfer rates. In fact, capsules have typically higher exchange area per volume and therefore can reach higher heat transfer rate compared to shell-in-tube.

Tang et al. [126] examine the effectiveness of TCE of PCM composite by in-situ copper doping. The PCM in question is polyethylene glycol - SiO_2 hybrid PCM. Overall, there is enough statistical evidence to suggest that the thermal conductivity is linearly dependent on the weight percentage of Cu (R^2 equal to 94%). This is exemplified by a doping percentage of 2.1%wt of Cu, which leads to an effective thermal conductivity of 0.414 $W/m\,K$ (+38.1%) and the latent heat is preserved at 110 kJ/kg [126]. The discharging time is also reduced by 69.9% [126]. The material has also good thermal stability and consistency during operation.

4.5.3.3. PCM Slurries. The concept of micro-encapsulated PCMs is to create a pumpable heat transfer fluid with high specific energy density [150]. This is done with a mixture of PCM and HTF, the latter being typically water. There are several kinds of PCM slurries proposed in literature [150]:

- Ice slurry. i.e. ice crystals, water and additives
- PCM micro emulsions, i.e. PCM dispersed within a HTF
- Micro PCMs, i.e. dispersion of PCM micro-polymeric capsules inside a HTF
- Clathrate hydrate PCMs, where water is the hosting molecule
- Shape stabilized PCMs, where PCM is contained within an high density polyethylene structure.

The micro-encapsulation technique tends to solve typical PCM problems, such as corrosion, decomposition, sub cooling and leakage [150]. Typically, the average diameter of capsules is in the range of 1-1000 μm, but can be even

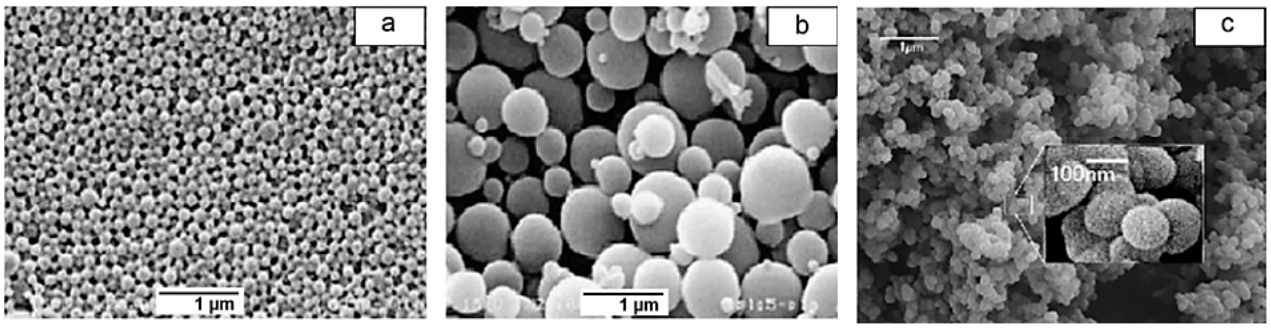

Figure 28: Microscope profiles of mPCM made by different methods. (a) Spray drying, (b) co-acervation and (c) in situ polymerization [150]

lower (Figure 28). This permits good control of volume change, high surface-to-volume ratio and possibility to use PCM for both storage medium and HTF. When using micro-PCMs, it is also important to consider the durability of the capsules. Therefore, it is suggested to [150]:

- Decrease the damage from the pumping system by keeping capsule diameters lower than 10 μm (durability 1200-5000 cycles). Moreover, centrifugal pumps are considered to be the best device for this aim.
- Keeping the core/shell ratio low, i.e. increase the thickness of the shell to decrease the probability of breakage. The best core/shell ratio is reported to be 3:1
- Increase the capsule fraction within the slurry.

Moreover, the issues reported above for the implementation of micro-PCMs leads to a trade-off between [150]:

- Increasing mass fraction of capsules, i.e. increasing energy storage density (the density of HTF also increase the bulk density up to 1.5-10 times)
- Decreasing mass fraction of capsules, i.e. decreasing the dynamic viscosity and the pressure drops
- Choosing a specific mass fraction so to keep the fluid Newtonian (typically levels are concentrations lower than 25-30% in volume).

As reported by Tay et al. [108], slurries are the traditional form of a transportable PCM system. HTF and PCM are a single entity, so there is no need for a heat exchanger. However, due to problems of pressure drop build-up and non-pumpability of the fluid, the volumetric percentage of the PCM needs to remain below a precautional limit of 30%. Even when in safe conditions, pumping slurries can lead to an increase of 150% of the parasitic consumptions. Moreover, the slurry need to be operated around the melting temperature of the PCM. Because of these limits, the slurry is not so convenient in terms of HTF energy density improvement when the concentration is constrained to be lower than 30%. Therefore, direct contact systems [108] are proposed because they don't need any additional material (Figure 29) between PCM and HTF (no tubes, no capsules). However, the PCM needs to be insoluble within the HTF. This leads to lower costs, due to no additional materials, and higher heat transfer coefficients, due to the absence of shells, i.e. no thermal resistance. In this case the PCM is 90% of the volume of the system, so the benefit of high energy density are more appreciable compared to slurries.

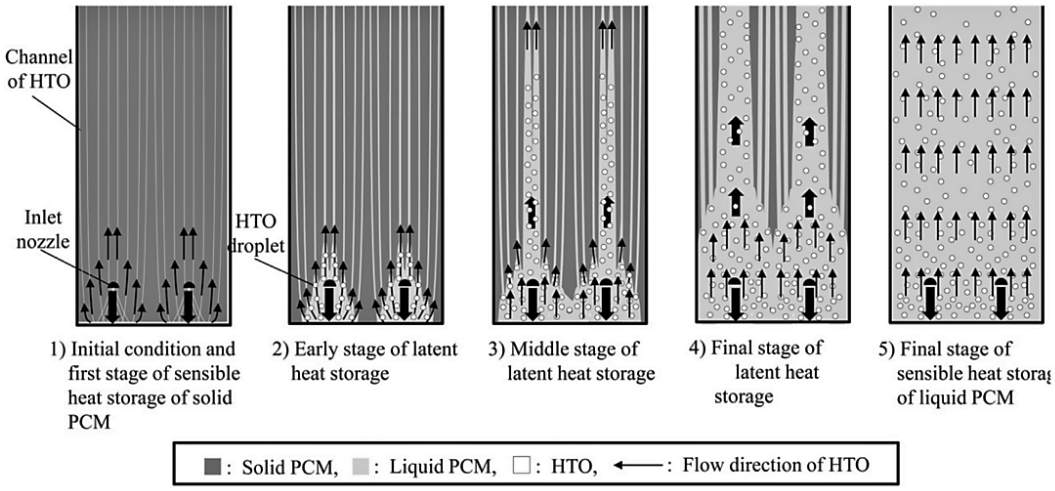

Figure 29: Flow pattern of heat transfer oil and melting process in direct contact PCM systems [108]

Huang et al. [107] analyse micro-encapsulated PCM slurries for thermal storage in a residential solar energy system. They claim that this method results in an increase of the average heat transfer coefficient and also simplifies the system, because the HTF is also the heat storage medium. Typically the diameter of the capsules are in the range of 2-8 μm. In this paper, a paraffin with melting temperature of around 65 °C is used as the PCM. From the results, one concern expressed is that using too much PCM can lead to higher concentration, increasing viscosity and lower thermal conductivity. Therefore, the heat transfer properties are not good enough to foster the system performance [107]. On the other hand, if the concentration of PCM inside the PCS is too low, the specific enthalpy improvement is negligible and therefore the energy density is not satisfactory [107]. Therefore, a typical trade-off problem exists on finding the best PCM concentration to maximise the performance of the thermal energy storage system [107].

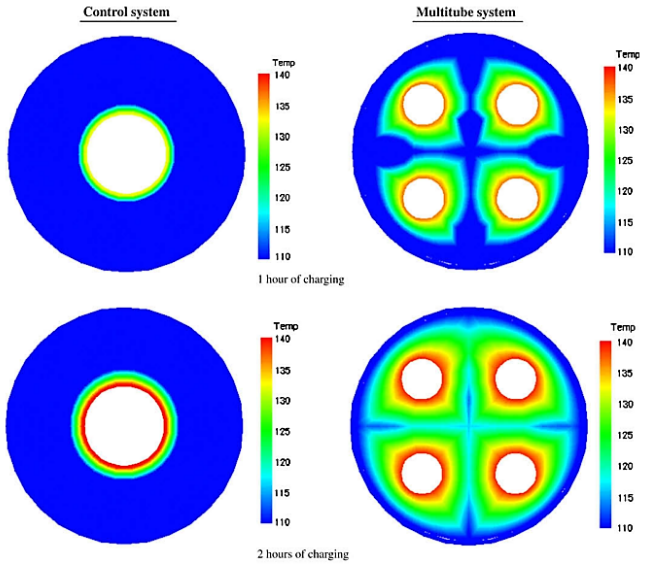

Figure 30: Measured temperatures within multi-tube and single tube systems [130]

4.5.3.4. Multi-tube Configurations. Agyenim at al. [130] investigated the implementation of multi-tubes configurations in S&T storage systems as a TCE technique. The effectiveness of this method is intuitive from a theoretical

point of view, considering that multi-tube systems have higher heat exchange areas at constant PCM volume, i.e. higher heat rate. To do so, the authors compare two configurations of S&T: single tube and 4 tubes in parallel. The PCM used is Erythritol, characterised by a melting temperature of 117 °C. What stands out from the results is that, in the case of the multi-tube, the heat transfer is characterised by high levels of convection, leading therefore to the creation of convective cells and higher heat transfer rates (Figure 30). The most striking result to emerge from the data is that the highest temperature gradients within the PCM is in the radial direction, while the axial gradients are just 2.5-3.5% of the radial one. Moreover, angular gradients are not null and must be considered. Therefore, the PCM heat transfer can be reduce to a 2D radial-angular problem. Finally, it is stated that the sub-cooling effect is present during solidification (discharging) of the heat storage system. This must be taken into consideration for the evaluation of the thermal performance of the system.

4.5.3.5. PCM and Heat Pipes. Utilization of Heat Pipes (HPS) has also been suggested [109, 151, 152], improving the heat transfer mechanism between PCM and HTF (Figure 31). The HPS spacing is a key parameter to be optimised because it can easily influence the performance of the system. Decreasing the spacing typically increases the exergy efficiency. HPS permit not only to improve the bulk conductivity of the PCM but also the heat exchange area of the system.

It seems that this topic demands further research in regards to the possible configurations of HPS and LH TESS. In addition, there is evidence [109] of possible good performance of hybrid-systems, such as HPS and fins with single or multiple PCMs. Overall, there is a general lack in the literature of second law/exergy analysis which must be included in performance evaluation to work out the best thermal energy storage system.

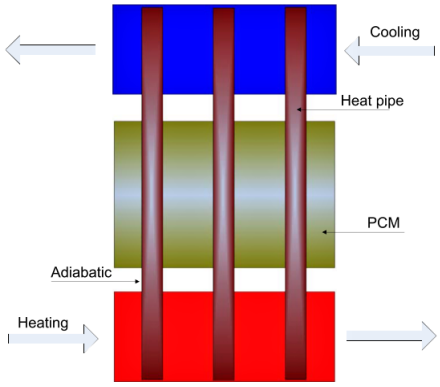

Figure 31: PCM-HP heat exchanger with two HTF flow channels [109]

4.5.3.6. Multiple or Cascaded PCM Systems. Multiple or Cascaded PCM (MPCM) systems can keep a quasi-uniform temperature difference between HTF and PCM [149, 148], leading to improved levels of heat transfer rate in each section of the HEX. In a single PCM this difference typically decreases along the HEX and therefore the overall heat transfer rate is quite low. The performance of the MPCM system depends also on the proportion of each PCM used and on the values of their melting temperatures. Several lines of evidence suggest that MPCM systems have higher storage energy potential and increase the exergy efficiency of the heat transfer system [109, 148], as reported in Table 22. However, 95% of the studies are just numerical [109]; therefore, there is a general need for

more experimental studies.

4.5.4. Li-Ion Cells Passive Cooling by PCMs

Among possible (TMS) for Li-Ion cells, PCM passive cooling is interesting because it is an effective but also low cost system; there is experimental evidence to suggest that just 12 mm of PCM material can reduce the battery temperature by up to 3 °C [153]. Moreover, a PCM passive TMS has the following advantages: cell temperature uniformity, moderate capital costs, low O&M costs, compactness, high efficiency, design simplicity, low parasitic power consumption (no moving fluid) and possible combination of PCM with downsized active cooling systems [153, 148, 6].

Ling et al. [148] report that PCMs are effective in increasing the temperature uniformity and balancing the battery system. This leads to lower capacity fading. For instance, considering a DR of 1C and 300 cycles, a system with PCM experiences a loss of capacity of 0.09 Wh/cycle instead of 0.20 Wh/cycle, therefore 55% lower.

Javani et al. [153] investigated a passive TMS for Li-Ion batteries using n-octadecane wax as the PCM material (chemical formula $CH_3(CH_2)_{16}CH_3$). Different DRs are considered and simulations are performed with/without PCM. The melting temperature of the PCM (i.e. its chemistry) must be in accordance with the temperature limit of the battery itself. The problem is also more important for applications of the battery in EVs. In this case, high DRs (high currents) are imposed to the cells and so high heat generation rates lead to high increases in operating temperatures. When high temperatures are experienced, an increase in Solid Electrolyte Interface (SEI) is triggered and this consequently leads to higher internal resistances and higher power losses by Joule effect. This leads finally to a reduction of operating life. All this motivates the necessity of strong and reliable TMS. It is clear from the results that the system which exploits PCM-soaked "wet foam" guarantees a maximum temperature that is 7.3 °C lower than a TMS without PCM; in addition, the temperature field is more uniform.

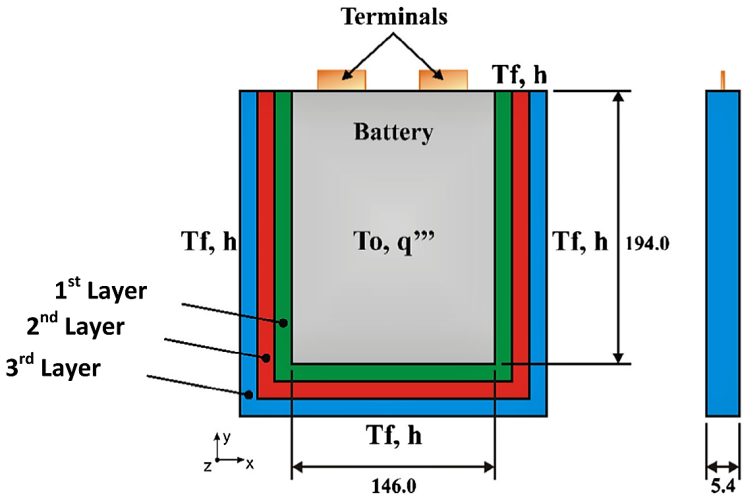

Figure 32: Lithium-ion polymer battery with three PCMs in layers (lengths in mm) [154].

Moraga et al. [154] introduced the application of multiple PCMs layers for the thermal regulation of Li-Ion batteries. The simulations are computed using an unsteady convection/conduction heat transfer model and considered a fixed

volumetric heat generation during the discharge phase. Moreover, the study looks at applying different 3-PCM combinations of 4 PCMs (Figure 32), with increasing melting temperatures of 123/234/341/412 °C. It is clear that the choice of melting temperature fitted to the interested device will specify the PCMs nature. The main outputs from this study are:

- Convection can be neglected for both solidification process (charge/rest battery, PCM discharge) and melting (discharge battery, charge of PCM)
- The best PCM configuration leads to a reduction of the cells maximum temperature up to 23 °C.
- The best PCM configuration is the one with a high-conductivity PCM close to the battery and low-conductivity PCM at the outer part.
- The best PCM is DSC=Decahydrate Sodium Carbonate, i.e. inorganic salt hydrate.

Moreover, the authors suggest that the main benefit of using PCMs for thermal management of Li-Ion batteries is the system simplification, reduced maintenance, reduced volume (depending on the energy density of PCM) and lower parasitic consumption (passive method). In addition, PCMs also manage to stabilise the cells' temperature when they are exposed to cold environments.

Pan et al. [155] analysed the performance in terms of heat transfer effectiveness of 4 different systems: natural convection, PCM pure paraffin, PCM with copper foam and PCM with copper fibres. The authors claim that, to guarantee a good performance of Li-Ion batteries, they must be operated within a temperature range of -20-60 °C and keep the temperature gradient within the cells lower than 5 °C. Soaked copper fibres (Figure 33) are a promising TCE method and the optimal porosity is demonstrated to be 90%. This system guarantees good heat transfer performance, temperature gradients within the cell lower than 2 °C and a maximum temperature lower than 60 °C (considered upper limit).

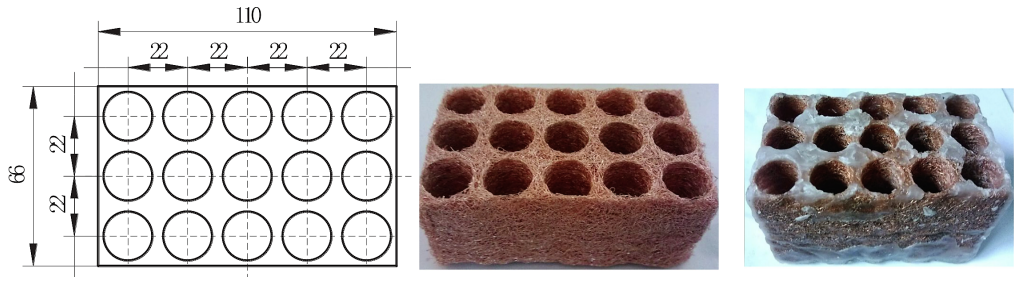

Figure 33: Scale size of battery pack, copper-fibres structure pure and filled with PCM (sizes in mm) [155].

Similarly, Li et al. [156] investigated the effectiveness of a passive PCM TMS for Li-Ion batteries with TCE such as porous copper foam. The authors compared a typical air cooling system, passive PCM and passive PCM-Metal Foam, the latter considering different levels of porosity and pore density. From the results, it appears that the PCM system guarantees a lower maximum temperature and improves the temperature uniformity. Moreover, the PCM-Metal Foam system improves the temperature uniformity due to an increase of the effective thermal conductivity. The air cooling system is not capable of maintaining the temperature below the safety limit. Moreover, the effectiveness of the foam is higher when the porosity is decreased (more metal) at a fixed pore density because the heat transfer

mechanism is dominated by conduction and therefore the natural convection depleting effect of the foam structure is more than counterbalanced by the increase of thermal conductivity. Pore density is also positive on the heat transfer because of the higher contact area between PCM and metal.

Kizilel et al. [18] analysed the effect of using PCMs for a TMS of Li-Ion batteries. The battery is tested in extreme conditions, such as ambient temperatures of 45 °C and DR of 2.08 C (10A). Four tests were performed [3]:

1) Pack 8S2P w/wo PCM ($T_{ambient}$, DR 1C) to test the average temperature and ΔT within the battery
2) Pack 4S4P w/wo PCM ($T_{ambient}$, DR 1C) to test the average temperature and the capacity degradation
3) Pack 7S2P w/wo PCM ($T_{ambient}$, DR 1C)
4) Pack 7S2P w/wo PCM (45 °C, DR 2.08C) to test the effect of extreme ambient temperature.

From test 1, it is clear that the PCM is capable of keeping the maximum battery centre temperature below 50 °C instead of 70 °C (Figure 34 **a**). While, with test number 2, it is clear that the capacity fading without PCM increase from 10.7 mAh/cycle to 12.2 mAh/cycle and is generally two times the value with the PCM (Figure 34 **b**).

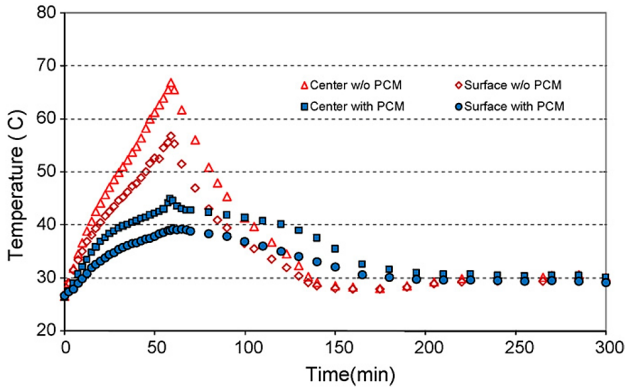

a) The effect of PCM on the thermal response of the 8S2P battery packs.

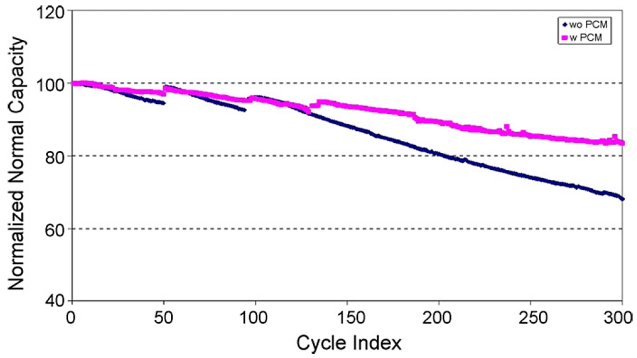

b) Capacity fading of 4S4P battery packs *with and w/o* PCM (Ah) (charge: 0.3C-rate/2.93 A, 1C-rate/8.8 A, T_{amb}: 25 °C, capacity: 8.8 Ah).

Figure 34: Effectiveness of PCM as TMS for Li-Ion Batteries [18].

Greco et al. [157] considered a TMS for a cylindrical battery with a PCM with compressed expanded natural graphite CENG. A simplified 1D model is used for the thermal simulation of both battery and PCM. The strong anisotropy of the thermal conductivity of the battery must be considered (axial value is much higher than the radial one, i.e. there is uniformity of temperature in the axial direction compared to the radial one). So, the thermal model can be easily considered 1D in the radial direction only. Results of CFD 3D models are in line with the simulated 1D models. Therefore, the assumption of a 1D model is considered to be appropriate (e.g. discrepancies are lower than 2% for natural convection). With PCMs the maximum temperature is kept below 40 °C for 2.9 h (Figure 35). Also, the maximum and internal temperatures are kept to values of 45.9 and 31.1 °C instead of 75 and 61 °C with forced convection.

Wang et al. [158] proposed a couple of new PCM composites for a TMS of Li-Ion batteries. The aim of the TMS

[3] Pack nSmP with n,m=number, S=Series, P=Parallel

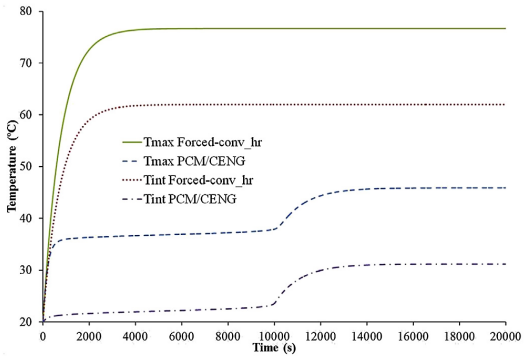

Figure 35: Comparison between the forced convection and the PCM/CENG cooling for $h_r = 20\,W/m^2\,K$ [157]

is to keep the temperature of the batteries as steady and uniform as possible. This must be guaranteed also in "abuse" conditions, i.e. DR 5C and high ambient temperature equal to 40 °C. The study investigated 3 kinds of PCM composites:

1) Pure paraffin
2) 20% EG - 80% paraffin
3) 3% EG - 47% epoxy - 50% paraffin.

The tests are conducted at different DRs (1C, 3C, 5C). The PCM_2 was demonstrated to be capable of decreasing the average temperature by (10, 12, 20) % and this was the only one capable of keeping the temperature gradient within the battery lower than 3 °C. The EG is used to increase the thermal conductivity of the PCM and therefore maximising the heat transfer rates. In terms of ageing effect (decrease of capacity with cycles), it can be seen from Figure 36 that the capacity decreases with cycles and this detrimental effect is more important for higher operating temperatures. In fact, with temperatures equal to (25,75) °C the capacity retention after 100 cycles is (94,77)%. Therefore, keeping the battery at a stable 25 °C is an important goal.

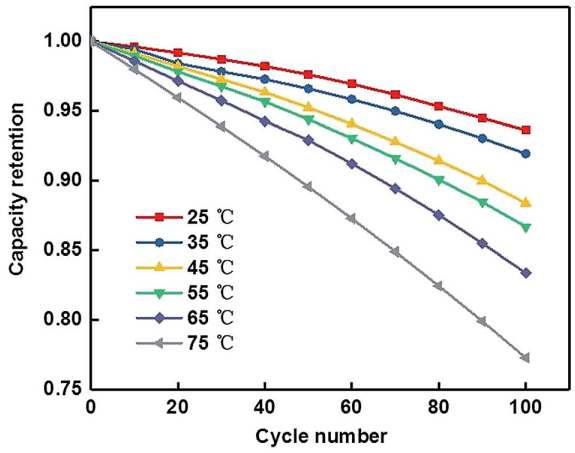

Figure 36: Battery charge–discharge cycle effect on capacity retention under different temperature conditions [158].

Babapoor et al. [159] investigated the TMS of Li-Ion batteries using a PCM with carbon fibres. The PCM is suggested because of its high heat storage capacity, low O&M costs and its retention of thermal properties during

operating life. Moreover, the authors claim that the PCM is capable of mitigating the maximum temperature of the battery during the discharge processes and also creating a uniform temperature within the battery pack. The study tackled the effect of different weight percentage of carbon fibres and length of fibres on the TMS performance. From the results, it can be claimed that the optimal value of fibre length is around 2 mm and the optimal weight fraction is 0.46%. This method guarantees a decrease of maximum operating temperature of 45% (considering a volumetric heat generation of 236.4 kW/m^3) and a maximum temperature difference decrease within the volume of up to 44%. It must be underlined that the carbon fibres results in an increase in the effective thermal conductivity of 100%.

Ling et al. [160] considered a passive PCM system as TMS. The PCM considered here is absorbed in a EG matrix to improve its thermal conductivity. The paraffin considered is a commercial RT42 (Rubitherm, T_m=42 °C, LH=187 kJ/kg). It is clear from the data reported by the authors that the higher the EG fraction, the lower the latent heat, the lower the specific heat but the higher the thermal conductivity. Also, the higher the packing density, the higher the thermal conductivity. The battery is tested with different simulated heat generation rates of 5, 10, 15 W (i.e. 196, 393, 589 W/m^3). The PCM model used for the simulation is the enthalpy formulation. The assumptions are no variation of density in PCM, constant thermal capacity and conductivity. A parametric study is proposed for the quantification of the effects of different thermal properties, type of paraffin used, mass fraction of PCM in the EG-PCM system and the packing density. From numerical solution, the best melting temperature appears to be 44 °C. A decrease in temperature rise is obtained by increasing the EG-PCM density. In addition, a more uniform temperature is guaranteed by increasing the mass fraction of the EG and by increasing the EG-PCM density. The optimum system is characterised by a paraffin mass fraction of 75% and a system density of 890 kg/m^3.

Finally, combinations of PCM and heat pipes have been experimentally evaluated [161, 162]. Specifically, Zao et al. [161] demonstrated that PCM HPS TMS can keep the Li-Ion cell maximum temperature below the safety limit (assumed equal to 50^oC) for longer than air-cooling or pure PCM TMS. Also, the temperature disuniformity is riduced by 28% by adding HPS to the pure PCM and kept lower than 5 K.

4.5.5. Li-Ion Cells Active Cooling by PCMs

Bai et al. [163] investigated the effectiveness of a TMS consisting of a PCM and water cooling plate for Li-Ion batteries (Figure 37). The idea is that water cooling is effective in keeping the average temperature low and the PCM is effective in making the temperature uniform throughout the system. The Li-Ion battery in this case is $LiFePO_4/graphite$. The cooling plate is positioned in the upper part and the PCM in the lower part. The study analysed the effect of different geometric, mechanical and thermal properties: the height of the water cooling plate (best is 5 cm, i.e. 20% of all battery), space between batteries (the higher, the more uniform the temperature in the system because of more PCM material per battery), mass flow rate of water (the higher, the better the heat transfer, the lower the temperature of the batteries but the pressure drop increases, together with the parasitic electric consumption), flow direction of water in adjacent batteries (better counter current because of the better temperature uniformity), thermal conductivity of PCM (in this study the thermal conductivity has very low effect in the performance of the system so there is no need to improve it with metal foam or matrix) and melting temperature of the PCM (better if higher).

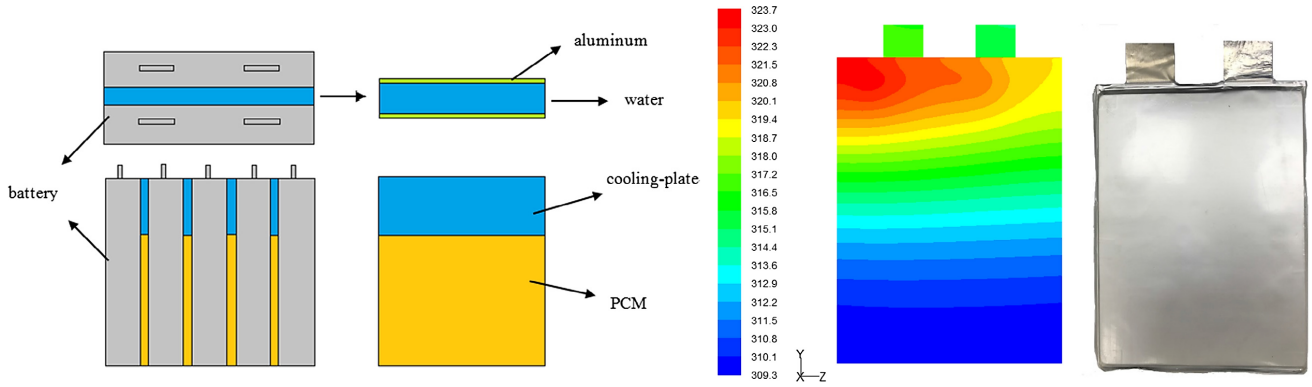

Figure 37: Left: Schematic of Li-Ion battery module with PCM/water cooling-plate. Right: Simulated temperature cloud of pouch battery at the end of 2 C discharge and actual picture of the battery cell [163].

Hemery et al. [164] analysed the effect of PCM and active liquid cooling on the TMS of Li-Ion batteries. This system is compared with traditional active air cooling. The authors highlight that the main problem of air cooling is the non-uniformity of cell temperatures, with upstream cells colder than downstream cells. Using a typical commercial PCM (RT28HC), the authors demonstrated that the effect of the PCM TMS is the same as forced air convection with air bulk velocity of 3 m/s but the temperature history is far more stable, underlining the PCM's superiority.

Finally, Ling et al. [72] analysed the possibility of applying hybrid TMS (PCM and air-cooling) for the thermal management of Li-Ion batteries. PCM alone (in this case a composite RT44HC/EG at 20%EG) can sometimes not be enough to keep the battery temperature below 60 °C, especially at high DRs (e.g. more than 1C). With the application of combined air cooling and passive PCMs, the temperature can successfully be kept lower than 50 °C. From the results, the maximum temperature in a 5S4P battery pack configuration increases every cycle, and goes above the safety limit of 60 °C after just 2 cycles, with a charge rate of 1C and DRs of 1.5-2C with a room temperature of 25 °C. Implementing air cooling can decrease the maximum temperature to levels below 50 °C, considering even conditions such as a DR of 2C and an increase of 7 °C in ambient temperature. In this case, the maximum temperature gradient is kept lower than 3 °C. Therefore, this hybrid system works well, where PCMs keep a maximum temperature and temperature gradient lower than the safety limits and air cooling cools down the PCM to restore all latent heat potential before the next battery discharge.

4.6. Summary

Overall, it seems clear from the literature that no TMS is holistically better than others and the choice between air cooling, liquid cooling, boiling and latent heat PCM systems is entirely linked to the specific combination of temperatures and heat rates for different operating conditions (i.e. DR, CR, ambient temperature) and dependent on capacity and geometry. Air cooling is effective for mild ambient temperatures and low CR, DR while liquid cooling is effective in keeping the maximum temperature below the limits in even extreme conditions but fails in reducing the in-cell thermal gradients. Improvements for both methods have been shown but these typically add mass (i.e. weight) and costs to the entire system, condition not ideal especially for automotive application. Boiling guarantees good temperature stability and uniformity but is intrinsically complex to operate. PCM passive systems

are promising to gain a proper isothermalisation of Li-Ion cells but, due to their low thermal conductivities and passive heat discharge, they can lead to thermal failures in case of repetitive extreme cycles, where the PCM doesn't have enough time to reject the cumulated heat and reach back its solid state. Active PCM systems, mainly a combination of liquid cooling and passive PCM, give promising results by reducing both maximum temperature and in-cell temperature gradients. Also, they introduce the potential to store the thermal energy and use it at need, converting a Li-Ion cell from simple EESS to a CHP system.

5. Conclusions

Li-Ion batteries will play an important role in reaching emission targets. Their performance however is quite sensitive to temperature. Therefore, the aims of an effective thermal management system TMS is to maintain a battery at an operating temperature within a certain optimal range and maximise temperature uniformity. This ideal condition to be guaranteed throughout either a Li-Ion cell or a Li-Ion battery pack operating life is defined as "isothermalisation".

Many studies have experimentally investigated the electrical performance of Li-Ion batteries under controlled environmental temperatures which do not impose a uniform temperature or a controlled rate of cooling, as a TMS would. The review also proposes that the ratio between the heat generation and the power production, i.e. quantifying the electro-chemical efficiency η, would help to advance research and development in this technological area. In this regard, a dataset for pouch and cylindrical cells has been created from data reported in literature and η has been computed. Overall, there is experimental evidence for a subset of chemistries and geometries that 20-30 ^oC is the best temperature range to minimise the ageing effect, leading to a potential decrease of the ageing rate from 0.12 to 0.04%/cycle. However, no specific temperature is indicated which can optimise the cycle electro-chemical efficiency and minimise the ageing effect.Therefore, a TMS should keep Li-Ion batteries at a specific temperature range according to the need for either higher electro-chemical efficiencies (i.e. lower heat generation rates) or higher operating life. More experimental data are necessary for high Charge-Discharge Rates CR-DR and high-low cell temperatures.

Four main approaches to the thermal management of Li-Ion batteries have been found in literature: air-cooling, liquid-cooling, boiling and Phase Change Materials (PCM). Air and liquid cooling can achieve good heat transfer performance but result in significant thermal gradients. Boiling is really effective in reaching an isothermal condition but is quite complex to operate and control. PCMs as a passive cooling approach are proposed as an effective and low-cost isothermalisation technique. However, under high ambient temperature and high discharge rates, PCM are not able to recover all latent energy potential during solidification, leading to possible thermal runaway. Overall, no TMS alone is holistically better than others and the choice is entirely linked to the specific combination of temperatures, heat rates, cells capacity and geometry. However, active PCM systems, mainly a combination of liquid cooling and passive PCM, show promising results towards an ideal isothermal condition. Also, they introduce the potential to store the thermal energy and use it as needed, converting a Li-Ion cell from a simple Electrical Energy Storage System (EESS) to a Combined Heat and Power (CHP) system.

In light of the literature reviewed, the authors suggest that future research should be focussed on the combination of PCM and active cooling TMS, to evaluate how to optimally combine the isothermalisation potential of the former with the cooling capability of the latter. Also, boiling TMS, both flow and pool typologies, need further experimental tests to fully evaluate their effectiveness. Heat flux, equivalent heat transfer coefficient and heat generation rate must be used as TMS assessment indices in addition to Li-Ion cell surface temperatures. Moreover, the electro-chemical efficiency should be introduced as additional TMS design metric together with the ageing effect rate to properly select the Li-Ion cells operating temperature and size the TMS.

Reference List

[1] REN21, "Renewables 2017 Global Status Report," tech. rep., 2017.

[2] REN21, "Renewables Global Futures Report: Great debates towards 100% renewable energy," tech. rep., 2017.

[3] International Energy Agency, "Technology Roadmap Energy storage," tech. rep., 2014.

[4] I. - International Energy Agency, "Tracking Clean Energy Progress 2017 Informing Energy Sector Transformations," tech. rep., 2017.

[5] B. Shabani and M. Biju, "Theoretical modelling methods for thermal management of batteries," *Energies*, vol. 8, no. 9, pp. 10153–10177, 2015.

[6] Z. Rao and S. Wang, "A review of power battery thermal energy management," *Renewable and Sustainable Energy Reviews*, vol. 15, pp. 4554–4571, 2011.

[7] S. Panchal, I. Dincer, M. Agelin-Chaab, R. Fraser, and M. Fowler, "Experimental and simulated temperature variations in a LiFePO4 - 20 Ah battery during discharge process," *Applied Energy*, vol. 180, pp. 504–515, 2016.

[8] S. Panchal, I. Dincer, M. Agelin-Chaab, R. Fraser, and M. Fowler, "Experimental and theoretical investigations of heat generation rates for a water cooled LiFePO 4 battery," *International Journal of Heat and Mass Transfer*, vol. 101, pp. 1093–1102, 2016.

[9] K. Chen, G. Unsworth, and X. Li, "Measurements of heat generation in prismatic Li-ion batteries," *Journal of Power Sources*, vol. 261, pp. 28–37, 2014.

[10] K. Chen and X. Li, "Accurate determination of battery discharge characteristics - A comparison between two battery temperature control methods," *Journal of Power Sources*, vol. 247, pp. 961–966, 2014.

[11] M. Malik, I. Dincer, M. A. Rosen, M. Mathew, and M. Fowler, "Thermal and electrical performance evaluations of series connected Li-ion batteries in a pack with liquid cooling," *Applied Thermal Engineering*, vol. 129, pp. 472–481, 2018.

[12] J. Cen, Z. Li, and F. Jiang, "Experimental investigation on using the electric vehicle air conditioning system for lithium-ion battery thermal management," *Energy for Sustainable Development*, vol. 45, pp. 88–95, 2018.

[13] F. He, H. Wang, and L. Ma, "Experimental demonstration of active thermal control of a battery module consisting of multiple Li-ion cells," *International Journal of Heat and Mass Transfer*, vol. 91, pp. 630–639, 2015.

[14] S. J. Drake, M. Martin, D. A. Wetz, J. K. Ostanek, S. P. Miller, J. M. Heinzel, and A. Jain, "Heat generation rate measurement in a Li-ion cell at large C-rates through temperature and heat flux measurements," *Journal of Power Sources*, vol. 285, pp. 266–273, 2015.

[15] C. Lin, S. Xu, Z. Li, B. Li, G. Chang, and J. Liu, "Thermal analysis of large-capacity LiFePO 4 power batteries for electric vehicles," *Journal of Power Sources*, vol. 294, pp. 633–642, 2015.

[16] M. R. Giuliano, A. K. Prasad, and S. G. Advani, "Experimental study of an air-cooled thermal management system for high capacity lithium-titanate batteries," *Journal of Power Sources*, vol. 216, pp. 345–352, 2012.

[17] C. Zhao, W. Cao, T. Dong, and F. Jiang, "Thermal behavior study of discharging/charging cylindrical lithium-ion battery module cooled by channeled liquid flow," *International Journal of Heat and Mass Transfer*, vol. 120, pp. 751–762, 2018.

[18] R. Kizilel, A. Lateef, R. Sabbah, M. M. Farid, J. R. Selman, and S. Al-Hallaj, "Passive control of temperature excursion and uniformity in high-energy Li-ion battery packs at high current and ambient temperature," *Journal of Power Sources*, vol. 183, pp. 370–375, 2008.

[19] S. Panchal, I. Dincer, M. Agelin-Chaab, M. Fowler, and R. Fraser, "Uneven temperature and voltage distributions due to rapid discharge rates and different boundary conditions for series-connected LiFePO4batteries," *International Communications in Heat and Mass Transfer*, vol. 81, pp. 210–217, 2017.

[20] S. Panchal, M. Haji Akhoundzadehr, K. Raahemifar, M. Fowler, and R. Fraser, "Heat and mass transfer modeling and investigation of multiple LiFePO 4 /graphite batteries in a pack at low C-rates with water-cooling," *International Journal of Heat and Mass Transfer*, vol. 135, pp. 368–377, 2019.

[21] G. Zubi, R. Dufo-López, M. Carvalho, and G. Pasaoglu, "The lithium-ion battery: State of the art and future perspectives," *Renewable and Sustainable Energy Reviews*, vol. 89, no. April, pp. 292–308, 2018.

[22] M. Meeus, "Overview of Battery Cell Technologies," in *European Battery Cell: R&I Workshop*, (Brussels), 2018.

[23] M. A. Hannan, M. M. Hoque, A. Hussain, Y. Yusof, and P. J. Ker, "State-of-the-Art and Energy Management System of Lithium-Ion Batteries in Electric Vehicle Applications: Issues and Recommendations," *IEEE Access*, vol. 6, pp. 19362–19378, 2018.

[24] M. Malik, I. Dincer, and M. A. Rosen, "Review on use of phase change materials in battery thermal management for electric and hybrid electric vehicles," *International Journal of Energy Research*, vol. 40, pp. 1011–1031, 2016.

[25] B. Nykvist and M. Nilsson, "Rapidly falling costs of battery packs for electric vehicles," *Nature Climate Change*, vol. 5, no. 4, pp. 329–332, 2015.

[26] Panasonic, "Lithium Ion Batteries," 2007.

[27] K. Yeow, H. Teng, M. Thelliez, and E. Tan, "3D Thermal Analysis of Li-ion Battery Cells with Various Geometries and Cooling Conditions Using Abaqus," in *2012 SIMULIA Community Conference*, no. Figure 1, pp. 1–17, 2012.

[28] P. Peng and F. Jiang, "Thermal safety of lithium-ion batteries with various cathode materials: A numerical study," *International Journal of Heat and Mass Transfer*, vol. 103, pp. 1008–1016, 2016.

[29] F. Lambert, "Elon Musk on Tesla/Panasonic's new 2170 battery cell: 'highest energy density cell in the world... that is also the cheapest'," 2017.

[30] J. B. Quinn, T. Waldmann, K. Richter, M. Kasper, and M. Wohlfahrt-Mehrens, "Energy Density of Cylindrical Li-Ion Cells: A Comparison of Commercial 18650 to the 21700 Cells," *Journal of The Electrochemical Society*, vol. 165, no. 14, pp. A3284–A3291, 2018.

[31] A123 Systems, "Battery Pack Design , Validation , and Assembly Guide using A123 Systems AMP20M1HD-A Nanophosphate Cells," tech. rep., 2014.

[32] H. Maleki, H. Wang, W. Porter, and J. Hallmark, "Li-Ion polymer cells thermal property changes as a function of cycle-life," *Journal of Power Sources*, vol. 263, pp. 223–230, 2014.

[33] International Organization for Standardization, "ISO/IEC PAS 16898:2012 - Electrically propelled road vehicles – Dimensions and designation of secondary lithium-ion cells," 2012.

[34] G. Zubi, R. Dufo-López, M. Carvalho, and G. Pasaoglu, "The lithium-ion battery: State of the art and future perspectives," *Renewable and Sustainable Energy Reviews*, vol. 89, no. October 2017, pp. 292–308, 2018.

[35] J. Cannarella and C. B. Arnold, "Stress evolution and capacity fade in constrained lithium-ion pouch cells," *Journal of Power Sources*, vol. 245, pp. 745–751, 2014.

[36] M. Wünsch, J. Kaufman, and D. U. Sauer, "Investigation of the influence of different bracing of automotive pouch cells on cyclic lifetime and impedance spectra," *Journal of Energy Storage*, vol. 21, no. October 2018, pp. 149–155, 2019.

[37] A. Samba, N. Omar, H. Gualous, O. Capron, P. Van Den Bossche, and J. Van Mierlo, "Impact of tab location on large format lithium-ion pouch cell based on fully coupled tree-dimensional electrochemical-thermal modeling," *Electrochimica Acta*, vol. 147, pp. 319–329, 2014.

[38] A. Samba, N. Omar, H. Gualous, O. Capron, P. Van Den Bossche, and J. Van Mierlo, "Impact of tab location on large format lithium-ion pouch cell based on fully coupled tree-dimensional electrochemical-thermal modeling," *Electrochimica Acta*, vol. 147, pp. 319–329, 2014.

[39] J. Warner, "Lithium-Ion and Other Cell Chemistries," *The Handbook of Lithium-Ion Battery Pack Design*, no. Cid, pp. 65–89, 2015.

[40] A. Burke and M. Miller, "Performance Characteristics of Lithium-ion Batteries of Various Chemistries for Plug-in Hybrid Vehicles," *EVS24 International Battery, Hybrid and Fuel Cell Electric Vehicle Symposium*, pp. 1–13, 2009.

[41] S. Panchal, S. Mathewson, R. Fraser, R. Culham, and M. Fowler, "Thermal Management of Lithium-Ion Pouch Cell with Indirect Liquid Cooling using Dual Cold Plates Approach," *SAE International Journal of Alternative Powertrains*, vol. 4, no. 2, 2015.

[42] S. Panchal, I. Dincer, M. Agelin-Chaab, R. Fraser, and M. Fowler, "Experimental investigation and simulation of temperature distributions in a 16Ah-LiMnNiCoO2battery during rapid discharge rates," *Heat and Mass Transfer/Waerme- und Stoffuebertragung*, vol. 53, no. 3, pp. 937–946, 2017.

[43] S. J. Drake, D. A. Wetz, J. K. Ostanek, S. P. Miller, J. M. Heinzel, and A. Jain, "Measurement of anisotropic thermophysical properties of cylindrical Li-ion cells," *Journal of Power Sources*, vol. 252, pp. 298–304, 2014.

[44] D. H. Jeon and S. M. Baek, "Thermal modeling of cylindrical lithium ion battery during discharge cycle," *Energy Conversion and Management*, vol. 52, no. 8-9, pp. 2973–2981, 2011.

[45] Y. Kim, S. Mohan, J. B. Siegel, A. G. Stefanopoulou, and Y. Ding, "The estimation of temperature distribution in cylindrical battery cells under unknown cooling conditions," *IEEE Transactions on Control Systems Technology*, vol. 22, no. 6, pp. 2277–2286, 2014.

[46] S. J. Bazinski and X. Wang, "Experimental study on the influence of temperature and state-of-charge on the thermophysical properties of an LFP pouch cell," *Journal of Power Sources*, vol. 293, pp. 283–291, 2015.

[47] S. J. Drake, *Thermal Conduction and Heat Generation Phenomena in Li-Ion Cells*. PhD thesis, 2014.

[48] J. Zhang, B. Wu, Z. Li, and J. Huang, "Simultaneous estimation of thermal parameters for large-format laminated lithium-ion batteries," *Journal of Power Sources*, vol. 259, pp. 106–116, 2014.

[49] H. Maleki, "Thermal Properties of Lithium-Ion Battery and Components," *Journal of The Electrochemical Society*, vol. 146, no. 3, p. 947, 1999.

[50] M. Fleckenstein, S. Fischer, O. Bohlen, and B. Bäker, "Thermal Impedance Spectroscopy - A method for the thermal characterization of high power battery cells," *Journal of Power Sources*, vol. 223, pp. 259–267, 2013.

[51] S. C. Chen, C. C. Wan, and Y. Y. Wang, "Thermal analysis of lithium-ion batteries," *Journal of Power Sources*, vol. 140, no. 1, pp. 111–124, 2005.

[52] A. Pesaran and M. Keyser, "Thermal characteristics of selected EV and HEV batteries," in *Sixteenth Annual Battery Conference on Applications and Advances. Proceedings of the Conference (Cat. No.01TH8533)*, pp. 219–225.

[53] R. Srinivasan, A. Carson Baisden, B. G. Carkhuff, and M. H. Butler, "The five modes of heat generation in a Li-ion cell under discharge," *Journal of Power Sources*, vol. 262, pp. 93–103, 2014.

[54] K. Somasundaram, E. Birgersson, and A. S. Mujumdar, "Thermal-electrochemical model for passive thermal management of a spiral-wound lithium-ion battery," *Journal of Power Sources*, vol. 203, pp. 84–96, 2012.

[55] E. Gümüşsu, Ö. Ekici, and M. Köksal, "3-D CFD modeling and experimental testing of thermal behavior of a Li-Ion battery," *Applied Thermal Engineering*, vol. 120, pp. 484–495, 2017.

[56] T. M. Bandhauer, S. Garimella, and T. F. Fuller, "Temperature-dependent electrochemical heat generation in a commercial lithium-ion battery," *Journal of Power Sources*, vol. 247, pp. 618–628, 2014.

[57] S. Panchal, R. Khasow, I. Dincer, M. Agelin-Chaab, R. Fraser, and M. Fowler, "Thermal design and simulation of mini-channel cold plate for water cooled large sized prismatic lithium-ion battery," *Applied Thermal Engineering*, vol. 122, pp. 80–90, 2017.

[58] S. Panchal, R. Khasow, I. Dincer, M. Agelin-Chaab, R. Fraser, and M. Fowler, "Numerical modeling and experimental investigation of a prismatic battery subjected to water cooling," *Numerical Heat Transfer; Part A: Applications*, vol. 71, no. 6, pp. 626–637, 2017.

[59] Y. Lai, S. Du, L. Ai, L. Ai, Y. Cheng, Y. Tang, and M. Jia, "Insight into heat generation of lithium ion batteries based on the electrochemical-thermal model at high discharge rates," *International Journal of Hydrogen Energy*, vol. 40, pp. 13039–13049, 2015.

[60] L. H. Saw, Y. Ye, and A. A. Tay, "Electro-thermal characterization of Lithium Iron Phosphate cell with equivalent circuit modeling," *Energy Conversion and Management*, vol. 87, pp. 367–377, 2014.

[61] B. Dawoud, E. Amer, and D. Gross, "Experimental investigation of an adsorptive thermal energy storage," *International journal of energy research*, vol. 31, no. August 2007, pp. 135–147, 2007.

[62] A. Maheshwari, M. A. Dumitrescu, M. Destro, and M. Santarelli, "a Modelling Approach To Understand Charge Discharge Differences in Thermal Behaviour in Lithium Iron Phosphate – Graphite Battery," *Electrochimica Acta*, vol. 243, pp. 129–141, 2017.

[63] T. Waldmann, M. Wilka, M. Kasper, M. Fleischhammer, and M. Wohlfahrt-Mehrens, "Temperature dependent ageing mechanisms in Lithium-ion batteries e A Post-Mortem study," *Journal of Power Sources*, vol. 262, pp. 129–135, 2014.

[64] J. Warner, *The Handbook of Lithium-Ion Battery Pack Design. Chemistry, Components, Types and Terminology.* Grand Blanc, MI, USA: Elsevier, 2015.

[65] A. Barai, R. Tangirala, K. Uddin, J. Chevalier, Y. Guo, A. McGordon, and P. Jennings, "The effect of external compressive loads on the cycle lifetime of lithium-ion pouch cells," *Journal of Energy Storage*, vol. 13, pp. 211–219, 2017.

[66] Q. Kellner, D. Worwood, A. Barai, W. D. Widanage, and J. Marco, "Duty-cycle characterisation of large-format automotive lithium ion pouch cells for high performance vehicle applications," *Journal of Energy Storage*, vol. 19, no. May, pp. 170–184, 2018.

[67] S. Al Hallaj, H. Maleki, J. Hong, and J. Selman, "Thermal modeling and design considerations of lithium-ion batteries," *Journal of Power Sources*, vol. 83, no. 1-2, pp. 1–8, 1999.

[68] M. Ghalkhani, F. Bahiraei, G.-A. Nazri, and M. Saif, "Electrochemical–Thermal Model of Pouch-type Lithium-ion Batteries," *Electrochimica Acta*, vol. 247, pp. 569–587, 2017.

[69] J. Jaguemont, N. Omar, M. Abdel-Monem, P. Van den Bossche, and J. Van Mierlo, "Fast-charging investigation on high-power and high-energy density pouch cells with 3D-thermal model development," *Applied Thermal Engineering*, vol. 128, pp. 1282–1296, 2018.

[70] T. L. Bergman, A. S. Lavine, F. P. Incropera, and D. P. Dewitt, *Fundamentals of Heat and Mass Transfer*. USA: John Wiley & Sons, Inc., 2011.

[71] E. Hosseinzadeh, R. Genieser, D. Worwood, A. Barai, J. Marco, and P. Jennings, "A systematic approach for electrochemical-thermal modelling of a large format lithium-ion battery for electric vehicle application," *Journal of Power Sources*, vol. 382, no. November 2017, pp. 77–94, 2018.

[72] Z. Ling, F. Wang, X. Fang, X. Gao, and Z. Zhang, "A hybrid thermal management system for lithium ion batteries combining phase change materials with forced-air cooling," *Applied Energy*, vol. 148, no. April, pp. 403–409, 2015.

[73] H. Liu, Z. Wei, W. He, and J. Zhao, "Thermal issues about Li-ion batteries and recent progress in battery thermal management systems: A review," *Energy Conversion and Management*, vol. 150, no. May, pp. 304–330, 2017.

[74] G. Xia, L. Cao, and G. Bi, "A review on battery thermal management in electric vehicle application," *Journal of Power Sources*, vol. 367, pp. 90–105, 2017.

[75] Y. Deng, C. Feng, J. E, H. Zhu, J. Chen, M. Wen, and H. Yin, "Effects of different coolants and cooling strategies on the cooling performance of the power lithium ion battery system: A review," *Applied Thermal Engineering*, vol. 142, no. April, pp. 10–29, 2018.

[76] R. W. Van Gils, D. Danilov, P. H. Notten, M. F. Speetjens, and H. Nijmeijer, "Battery thermal management by boiling heat-transfer," *Energy Conversion and Management*, vol. 79, pp. 9–17, 2014.

[77] R. Zhao, S. Zhang, J. Liu, and J. Gu, "A review of thermal performance improving methods of lithium ion battery: Electrode modification and thermal management system," *Journal of Power Sources*, vol. 299, pp. 557–577, 2015.

[78] X. Li, F. He, and L. Ma, "Thermal management of cylindrical batteries investigated using wind tunnel testing and computational fluid dynamics simulation," *Journal of Power Sources*, vol. 238, pp. 395–402, 2013.

[79] D. Chen, J. Jiang, G. H. Kim, C. Yang, and A. Pesaran, "Comparison of different cooling methods for lithium ion battery cells," *Applied Thermal Engineering*, vol. 94, pp. 846–854, 2016.

[80] L. H. Saw, Y. Ye, M. C. Yew, W. T. Chong, M. K. Yew, and T. C. Ng, "Computational fluid dynamics simulation on open cell aluminium foams for Li-ion battery cooling system," *Applied Energy*, vol. 204, pp. 1489–1499, 2017.

[81] L. H. Saw, H. M. Poon, H. S. Thiam, Z. Cai, W. T. Chong, N. A. Pambudi, and Y. J. King, "Novel thermal management system using mist cooling for lithium-ion battery packs," *Applied Energy*, vol. 223, no. December 2017, pp. 146–158, 2018.

[82] K.-h. Chen, T. Han, B. Khalighi, and P. Klaus, "Air cooling concept for Li-ion battey pack in cell level," in *Proceedings of the ASME 2017 Heat Transfer Summer Conference*, pp. 1–12, 2017.

[83] S. Shahid and M. Agelin-Chaab, "Analysis of cooling effectiveness and temperature uniformity in a battery pack for cylindrical batteries," *Energies*, vol. 10, no. 8, 2017.

[84] K. Yu, X. Yang, Y. Cheng, and C. Li, "Thermal analysis and two-directional air flow thermal management for lithium-ion battery pack," *Journal of Power Sources*, vol. 270, pp. 193–200, 2014.

[85] Y. S. Choi and D. M. Kang, "Prediction of thermal behaviors of an air-cooled lithium-ion battery system for hybrid electric vehicles," *Journal of Power Sources*, vol. 270, pp. 273–280, 2014.

[86] Y. Huo, Z. Rao, X. Liu, and J. Zhao, "Investigation of power battery thermal management by using mini-channel cold plate," *Energy Conversion and Management*, vol. 89, pp. 387–395, 2015.

[87] D. Worwood, Q. Kellner, M. Wojtala, W. D. Widanage, R. McGlen, D. Greenwood, and J. Marco, "A new approach to the internal thermal management of cylindrical battery cells for automotive applications," *Journal of Power Sources*, vol. 346, pp. 151–166, 2017.

[88] K. Shah, C. McKee, D. Chalise, and A. Jain, "Experimental and numerical investigation of core cooling of Li-ion cells using heat pipes," *Energy*, vol. 113, pp. 852–860, 2016.

[89] W. Yuan, Z. Yan, Z. Tan, W. Chen, and Y. Tang, "Heat-pipe-based thermal management and temperature characteristics of Li-ion batteries," *Canadian Journal of Chemical Engineering*, vol. 94, no. 10, pp. 1901–1908, 2016.

[90] A. Jarrett and I. Y. Kim, "Design optimization of electric vehicle battery cooling plates for thermal performance," *Journal of Power Sources*, vol. 196, no. 23, pp. 10359–10368, 2011.

[91] A. Jarrett and I. Y. Kim, "Influence of operating conditions on the optimum design of electric vehicle battery cooling plates," *Journal of Power Sources*, vol. 245, pp. 644–655, 2014.

[92] W. Tong, K. Somasundaram, E. Birgersson, A. S. Mujumdar, and C. Yap, "Numerical investigation of water cooling for a lithium-ion bipolar battery pack," *International Journal of Thermal Sciences*, vol. 94, pp. 259–269, 2015.

[93] T. Deng, G. Zhang, and Y. Ran, "Study on thermal management of rectangular Li-ion battery with serpentine-channel cold plate," *International Journal of Heat and Mass Transfer*, vol. 125, pp. 143–152, 2018.

[94] S. Panchal, R. Khasow, I. Dincer, M. Agelin-Chaab, R. Fraser, and M. Fowler, "Thermal design and simulation of mini-channel cold plate for water cooled large sized prismatic lithium-ion battery," *Applied Thermal Engineering*, vol. 122, pp. 80–90, 2017.

[95] X. H. Yang, S. C. Tan, and J. Liu, "Thermal management of Li-ion battery with liquid metal," *Energy Conversion and Management*, vol. 117, pp. 577–585, 2016.

[96] C. Lan, J. Xu, Y. Qiao, and Y. Ma, "Thermal management for high power lithium-ion battery by minichannel aluminum tubes," *Applied Thermal Engineering*, vol. 101, pp. 284–292, 2016.

[97] X. Du, Z. Qian, Z. Chen, and Z. Rao, "Experimental investigation on mini - channel cooling – based thermal management for Li - ion battery module under different cooling schemes," *Int J Energy Res.*, vol. 42, no. December 2017, pp. 2781–2788, 2018.

[98] T. Zhang, Q. Gao, G. Wang, Y. Gu, Y. Wang, W. Bao, and D. Zhang, "Investigation on the promotion of temperature uniformity for the designed battery pack with liquid flow in cooling process," *Applied Thermal Engineering*, vol. 116, pp. 655–662, 2017.

[99] H. Hirano, T. Tajima, T. Hasegawa, T. Sekiguchi, and M. Uchino, "Boiling liquid battery cooling for electric vehicle," *IEEE Transportation Electrification Conference and Expo, ITEC Asia-Pacific 2014 - Conference Proceedings*, pp. 1–4, 2014.

[100] T. M. Bandhauer and S. Garimella, "Passive, internal thermal management system for batteries using microscale liquid-vapor phase change," *Applied Thermal Engineering*, vol. 61, no. 2, pp. 756–769, 2013.

[101] Z. An, L. Jia, X. Li, and Y. Ding, "Experimental investigation on lithium-ion battery thermal management based on flow boiling in mini-channel," *Applied Thermal Engineering*, vol. 117, pp. 534–543, 2017.

[102] Z. An, J. . Li, X. Li, and Y. Ding, "Experimental investigation on lithium-ion battery thermal management based on flow boiling in mini-channel," *Applied Thermal Engineering*, vol. 117, pp. 534–543, 2017.

[103] A. Sharma, V. V. Tyagi, C. R. Chen, and D. Buddhi, "Review on thermal energy storage with phase change materials and applications," *Renewable and Sustainable Energy Reviews*, vol. 13, no. 2, pp. 318–345, 2009.

[104] L. F. Cabeza, *Advances in thermal energy storage systems*. Cambridge, UK: Elsevier Ltd, 2015.

[105] J. Pereira da Cunha and P. Eames, "Thermal energy storage for low and medium temperature applications using phase change materials - A review," *Applied Energy*, vol. 177, pp. 227–238, 2016.

[106] C. R. Abujas, A. Jové, C. Prieto, M. Gallas, and L. F. Cabeza, "Performance comparison of a group of thermal conductivity enhancement methodology in phase change material for thermal storage application," *Renewable Energy*, vol. 97, pp. 434–443, 2016.

[107] M. J. Huang, P. C. Eames, S. McCormack, P. Griffiths, and N. J. Hewitt, "Microencapsulated phase change slurries for thermal energy storage in a residential solar energy system," *Renewable Energy*, vol. 36, no. 11, pp. 2932–2939, 2011.

[108] N. Tay, M. Liu, M. Belusko, and F. Bruno, "Review on transportable phase change material in thermal energy storage systems," *Renewable and Sustainable Energy Reviews*, vol. 75, no. October 2015, pp. 0–1, 2016.

[109] N. I. Ibrahim, F. A. Al-Sulaiman, S. Rahman, B. S. Yilbas, and A. Z. Sahin, "Heat transfer enhancement of phase change materials for thermal energy storage applications: A critical review," *Renewable and Sustainable Energy Reviews*, vol. 74, no. October 2015, pp. 26–50, 2017.

[110] L. Liu, D. Su, Y. Tang, and G. Fang, "Thermal conductivity enhancement of phase change materials for thermal energy storage: A review," *Renewable and Sustainable Energy Reviews*, vol. 62, pp. 305–317, 2016.

[111] L. Fan and J. M. Khodadadi, "Thermal conductivity enhancement of phase change materials for thermal energy storage: A review," *Renewable and Sustainable Energy Reviews*, vol. 15, no. 1, pp. 24–46, 2011.

[112] M. M. Kenisarin, "High-temperature phase change materials for thermal energy storage," *Renewable and Sustainable Energy Reviews*, vol. 14, pp. 955–970, 2010.

[113] A. Caron-Soupart, J.-F. Fourmigu?, P. Marty, and R. Couturier, "Performance analysis of thermal energy storage systems using phase change material," *Applied Thermal Engineering*, vol. 98, no. 1, pp. 85–97, 2016.

[114] X. Yang, Y. Li, Z. Lu, L. Zhang, Q. Zhang, and L. Jin, "Thermal and Fluid Characteristics of a Latent Heat Thermal Energy Storage Unit," *Energy Procedia*, vol. 104, pp. 425–430, 2016.

[115] B. Zalba, J. M. Marın, L. F. Cabeza, and H. Mehling, "Review on thermal energy storage with phase change: materials, heat transfer analysis and applications," *Applied thermal engineering*, vol. 23, no. 3, pp. 251–283, 2003.

[116] L. A. Tse, A. S. Lavine, R. B. Lakeh, and R. E. Wirz, "Exergetic optimization and performance evaluation of multi-phase thermal energy storage systems," *Solar Energy*, vol. 122, pp. 396–408, 2015.

[117] H. Zhang, J. Baeyens, G. Cáceres, J. Degrève, and Y. Lv, "Thermal energy storage: Recent developments and practical aspects," *Progress in Energy and Combustion Science*, vol. 53, pp. 1–40, 2016.

[118] F. Agyenim, N. Hewitt, P. Eames, and M. Smyth, "A review of materials, heat transfer and phase change problem formulation for latent heat thermal energy storage systems (LHTESS)," *Renewable and Sustainable Energy Reviews*, vol. 14, no. 2, pp. 615–628, 2010.

[119] H. Zhang, J. Baeyens, G. Cáceres, J. Degrève, and Y. Lv, "Thermal energy storage: Recent developments and practical aspects," *Progress in Energy and Combustion Science*, vol. 53, pp. 1–40, 2016.

[120] M. M. Islam, A. K. Pandey, M. Hasanuzzaman, and N. A. Rahim, "Recent progresses and achievements in photovoltaic-phase change material technology: A review with special treatment on photovoltaic thermal-phase change material systems," *Energy Conversion and Management journal*, vol. 126, pp. 177–204, 2016.

[121] N. R. Jankowski and F. P. Mccluskey, "A review of phase change materials for vehicle component thermal buffering," *Applied Energy*, vol. 113, pp. 1525–1561, 2014.

[122] A. Sharma, L. D. Won, D. Buddhi, and J. U. Park, "Numerical heat transfer studies of the fatty acids for different heat exchanger materials on the performance of a latent heat storage system," *Renewable Energy*, vol. 30, pp. 2179–2187, 2005.

[123] M. Dannemand, J. M. Schultz, J. B. Johansen, and S. Furbo, "Long term thermal energy storage with stable supercooled sodium acetate trihydrate," *Applied Thermal Engineering*, vol. 91, pp. 671–678, 2015.

[124] A. Sciacovelli, F. Gagliardi, and V. Verda, "Maximization of performance of a PCM latent heat storage system with innovative fins," *Applied Energy*, vol. 137, pp. 707–715, 2015.

[125] T. Oya, T. Nomura, M. Tsubota, N. Okinaka, and T. Akiyama, "Thermal conductivity enhancement of erythritol as PCM by using graphite and nickel particles," *Applied Thermal Engineering*, vol. 61, no. 2, pp. 825–828, 2013.

[126] B. Tang, M. Qiu, and S. Zhang, "Thermal conductivity enhancement of PEG/SiO 2 composite PCM by in situ Cu doping," *Solar Energy Materials and Solar Cells*, vol. 105, pp. 242–248, 2012.

[127] J. Fukai, Y. Hamada, Y. Morozumi, and O. Miyatake, "Improvement of thermal characteristics of latent heat thermal energy storage units using carbon-fiber brushes: experiments and modeling," *International Journal of Heat and Mass Transfer*, vol. 46, pp. 4513–4525, 2003.

[128] B. Tang, H. Wei, D. Zhao, and S. Zhang, "Light-heat conversion and thermal conductivity enhancement of PEG/SiO 2 composite PCM by in situ Ti 4 O 7 doping," *Solar Energy Materials & Solar Cells*, vol. 161, pp. 183–189, 2016.

[129] B. Tang, H. Wei, D. Zhao, and S. Zhang, "Light-heat conversion and thermal conductivity enhancement of PEG/SiO2 composite PCM by in situ Ti4O7 doping," *Solar Energy Materials and Solar Cells*, vol. 161, no. October 2016, pp. 183–189, 2017.

[130] F. Agyenim, P. Eames, and M. Smyth, "Heat transfer enhancement in medium temperature thermal energy storage system using a multitube heat transfer array," *Renewable Energy*, vol. 35, no. 1, pp. 198–207, 2010.

[131] B. Kanimozhi, A. Prabhu, M. Anish, and P. K. Harish Kumar, "Review On Heat Transfer Enhancement Techniques in Thermal Energy Storage Systems," *Journal of Engineering Research and Applications www.ijera.com ISSN*, vol. 4, no. 1, pp. 144–149, 2014.

[132] P. F. De Castro, A. Ahmed, and D. G. Shchukin, "Confined-Volume Effect on the Thermal Properties of Encapsulated Phase Change Materials for Thermal Energy Storage," *Chemistry - A European Journal*, vol. 22, no. 13, pp. 4389–4394, 2016.

[133] G. Peiro, J. Gasia, L. Mir, and L. F. Cabeza, "Experimental evaluation at pilot plant scale of multiple PCMs (cascaded) vs. single PCM configuration for thermal energy storage," *Renewable Energy*, vol. 83, pp. 729–736, 2015.

[134] M. M. Farid and A. Kanzawa, "Thermal Performance of a Heat Storage Module Using PCM's With Different Melting Temperatures: Mathematical Modelling," *Transactions of the ASME*, vol. 111, pp. 152–157, 1989.

[135] M. M. Farid, Y. Kim, and A. Kansawa, "Thermal Performance of a Heat Storage Module Using PCM's With Different Melting Temperature: Experimental," *Solar Energy Engineering*, vol. 112, pp. 125–131, 1990.

[136] T. Watanabe and A. Kanzawa, "Second law optimization of a latent heat storage system with PCMS having different melting points," *Heat Recovery Systems and CHP*, vol. 15, no. 7, pp. 641–653, 1995.

[137] Z. X. Gong and A. S. Mujumdar, "Enhancement of energy charge-discharge rates in composite slabs of different phase change materials," *International Journal of Heat and Mass Transfer*, vol. 39, no. 4, pp. 725–733, 1996.

[138] R. Domanski and G. Fellah, "Exergy analysis for the evaluation of a thermal storage system exmploying PCMs with different melting temperatures," ˜ *Pergamon Applied Thermal Engineering*, vol. 16, no. 11, pp. 907–919, 1996.

[139] Z.-X. Gong and A. S. Mujumdar, "Thermodynamic optimisation of the thermal process in energy storage using mutiple phase change materials," *Applied Thermal Engineering*, vol. 17, no. 11, pp. 1067–1083, 1997.

[140] J. Wang, G. Chen, and F. Zheng, "Study on phase change temperature distributions of composite PCMs in thermal energy storage systems," *International Journal of Energy Research Int. J. Energy Res*, vol. 23, pp. 277–285, 1999.

[141] S. Shaikh and K. Lafdi, "Effect of multiple phase change materials (PCMs) slab configurations on thermal energy storage," *Energy Conversion and Management*, vol. 47, pp. 2103–2117, 2006.

[142] Y. Tian and C. Y. Zhao, "Thermal and exergetic analysis of Metal Foam-enhanced Cascaded Thermal Energy Storage (MF-CTES)," *International Journal of Heat and Mass Transfer*, vol. 58, pp. 86–96, 2013.

[143] A. H. Mosaffa, L. G. Farshi, C. A. I. Ferreira, and M. A. Rosen, "Energy and exergy evaluation of a multiple-PCM thermal storage unit for free cooling applications," *Renewable Energy*, vol. 68, pp. 452–458, 2014.

[144] M. Ezra, Y. Kozak, V. Dubovsky, and G. Ziskind, "Analysis and optimization of melting temperature span for a multiple-PCM latent heat thermal energy storage unit," *Applied Thermal Engineering*, vol. 93, pp. 315–329, 2015.

[145] H. J. Xu and C. Y. Zhao, "Thermal performance of cascaded thermal storage with phase-change materials (PCMs). Part I: Steady cases," *International Journal of Heat and Mass Transfer*, vol. 106, pp. 932–944, 2017.

[146] H. J. Xu and C. Y. Zhao, "Thermal performance of cascaded thermal storage with phase-change materials (PCMs). Part II: Unsteady cases," *International Journal of Heat and Mass Transfer*, vol. 106, pp. 945–957, 2017.

[147] N. H. S. Tay, M. Liu, M. Belusko, and F. Bruno, "Review on transportable phase change material in thermal energy storage systems," *Renewable and Sustainable Energy Reviews*, vol. 75, pp. 264–277, 2017.

[148] Z. Ling, Z. Zhang, G. Shi, X. Fang, L. Wang, X. Gao, Y. Fang, T. Xu, S. Wang, and X. Liu, "Review on thermal management systems using phase change materials for electronic components, Li-ion batteries and photovoltaic modules," *Renewable and Sustainable Energy Reviews*, vol. 31, pp. 427–438, 2014.

[149] R. V. Seeniraj and N. Lakshmi Narasimhan, "Performance enhancement of a solar dynamic LHTS module having both fins and multiple PCMs," *Solar Energy*, vol. 82, pp. 535–542, 2008.

[150] M. Jurkowska and I. Szczygieł, "Review on properties of microencapsulated phase change materials slurries (mPCMS)," *Applied Thermal Engineering*, vol. 98, pp. 365–373, 2015.

[151] J. Zhao, Z. Rao, C. Liu, and Y. Li, "Experiment study of oscillating heat pipe and phase change materials coupled for thermal energy storage and thermal management," *International Journal of Heat and Mass Transfer*, vol. 99, pp. 252–260, 2016.

[152] J. Zhao, J. Qu, and Z. Rao, "Thermal characteristic and analysis of closed loop oscillation heat pipe/phase change material (CLOHP/PCM) coupling module with different working media," *International Journal of Heat and Mass Transfer*, vol. 126, pp. 257–266, 2018.

[153] N. Javani, I. Dincer, G. F. Naterer, and G. L. Rohrauer, "Modeling of passive thermal management for electric vehicle battery packs with PCM between cells," *Applied Thermal Engineering*, vol. 73, pp. 307–316, 2014.

[154] N. O. Moraga, J. P. Xamán, and R. H. Araya, "Cooling Li-ion batteries of racing solar car by using multiple phase change materials," *Applied Thermal Engineering*, vol. 108, pp. 1041–1054, 2016.

[155] M. Pan and W. Lai, "Cutting copper fiber/paraffin composite phase change material discharging experimental study based on heat dissipation capability of Li-ion battery," *Renewable Energy*, vol. 114, pp. 408–422, 2017.

[156] W. Q. Li, Z. G. Qu, Y. L. He, and Y. B. Tao, "Experimental study of a passive thermal management system for high-powered lithium ion batteries using porous metal foam saturated with phase change materials," *Journal of Power Sources*, vol. 255, pp. 9–15, 2014.

[157] A. Greco, X. Jiang, and D. Cao, "An investigation of lithium-ion battery thermal management using paraffin/porous-graphite-matrix composite," *Journal of Power Sources*, vol. 278, pp. 50–68, 2015.

[158] Z. Wang, X. Li, G. Zhang, Y. Lv, C. Wang, F. He, C. Yang, and C. Yang, "Thermal management investigation for lithium-ion battery module with different phase change materials," *The Royal Society of Chemistry*, vol. 7, pp. 42909–42918, 2017.

[159] A. Babapoor, M. Azizi, and G. Karimi, "Thermal management of a Li-ion battery using carbon fiber-PCM composites," *Applied Thermal Engineering*, vol. 82, pp. 281–290, 2015.

[160] Z. Ling, J. Chen, X. Fang, Z. Zhang, T. Xu, X. Gao, and S. Wang, "Experimental and numerical investigation of the application of phase change materials in a simulative power batteries thermal management system," *Applied Energy*, vol. 121, pp. 104–113, 2014.

[161] J. Zhao, P. Lv, and Z. Rao, "Experimental study on the thermal management performance of phase change material coupled with heat pipe for cylindrical power battery pack," *Experimental Thermal and Fluid Science*, vol. 82, pp. 182–188, 2017.

[162] Q. Wang, Z. Rao, Y. Huo, and S. Wang, "Thermal performance of phase change material/oscillating heat pipe-based battery thermal management system," *International Journal of Thermal Sciences*, vol. 102, pp. 9–16, 2016.

[163] F. Bai, M. Chen, W. Song, Z. Feng, Y. Li, and Y. Ding, "Thermal management performances of PCM/water cooling-plate using for lithium-ion battery module based on non-uniform internal heat source," *Applied Thermal Engineering journal*, vol. 126, pp. 17–27, 2017.

[164] C.-V. H. Hemery, F. Pra, J.-F. Robin, and P. Marty, "Experimental performances of a battery thermal management system using a phase change material," *Journal of Power Sources*, vol. 270, pp. 349–358, 2014.

Appendix A. Efficiency and Heat Ratio

Appendix A.1. Pouch Cells

Appendix A.1.1. Instant Performance

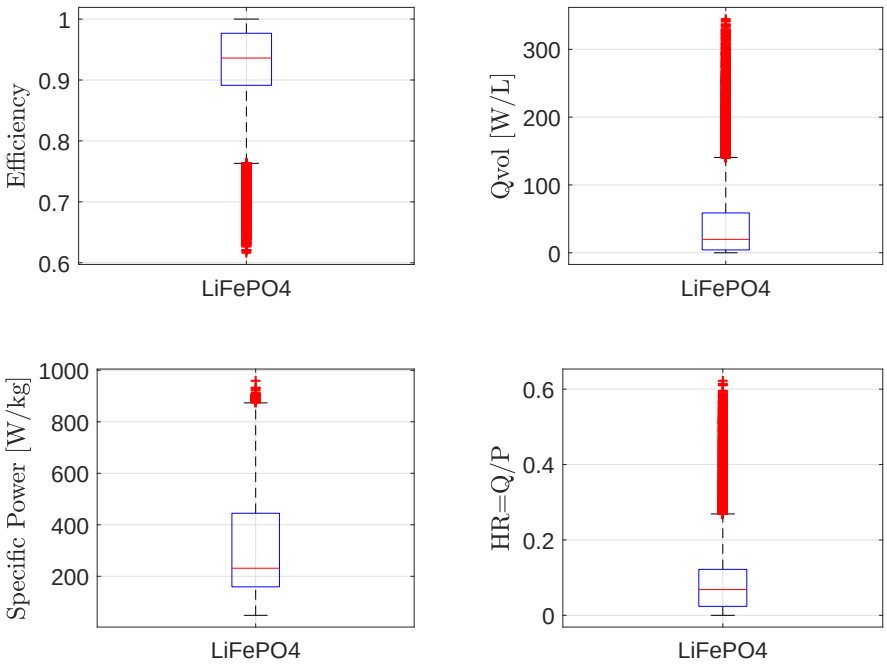

Figure Appendix A.1: $LiFePO_4$ Pouch Cell: Instant Performance Overview [7, 8, 57, 58, 9, 59, 60, 61, 62]

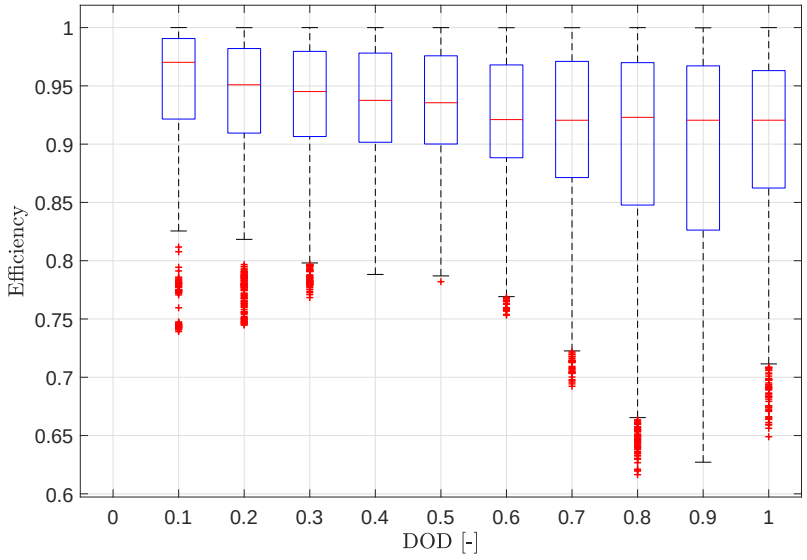

Figure Appendix A.2: Pouch Cell: Efficiency vs. DOD [7, 8, 57, 58, 9, 59, 60, 61, 62]

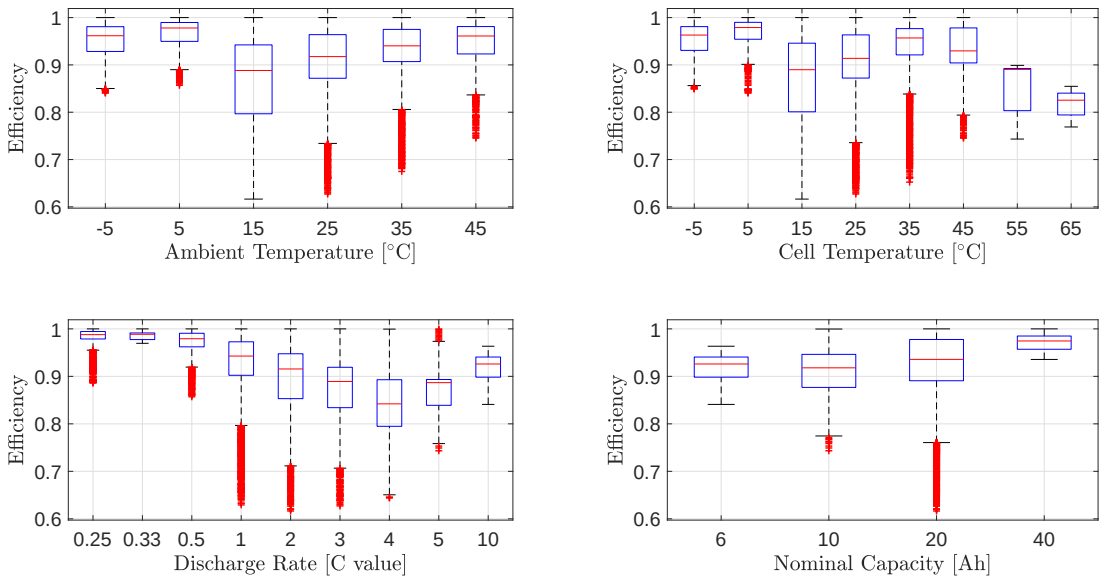

Figure Appendix A.3: Pouch Cell: Efficiency parametric sensitivity [7, 8, 57, 58, 9, 59, 60, 61, 62].

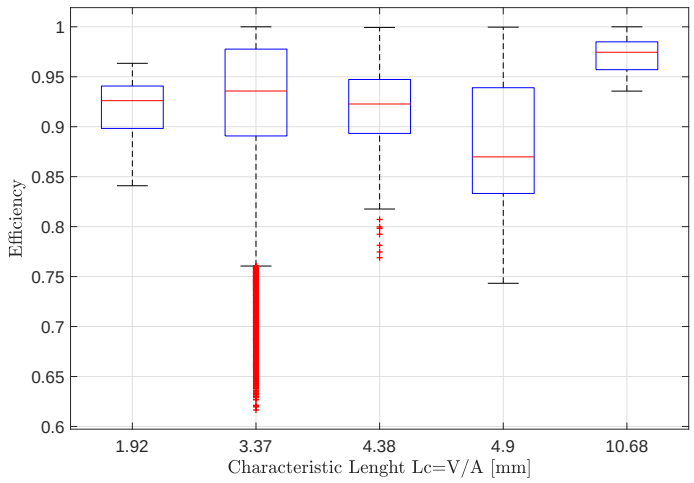

Figure Appendix A.4: Pouch Cell: Efficiency vs Characteristic Length L_c [7, 8, 57, 58, 9, 59, 60, 61, 62].

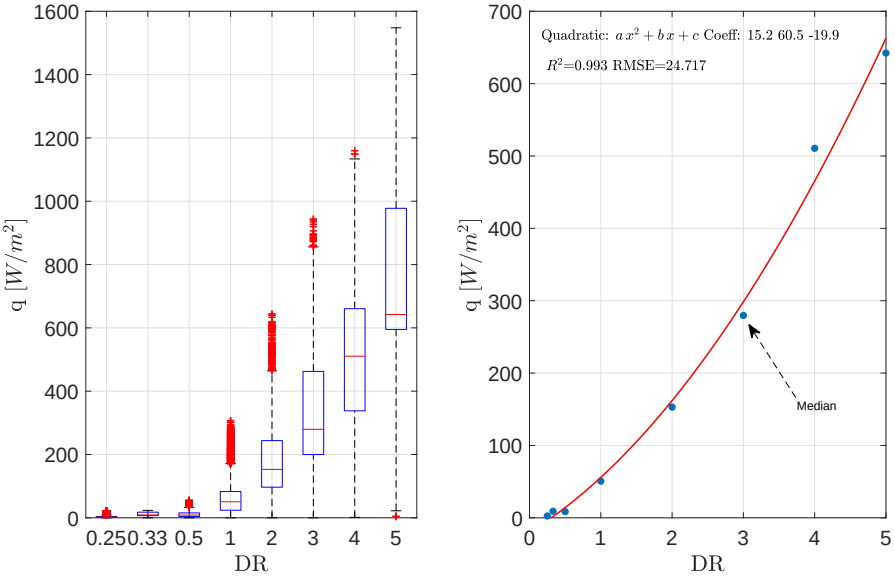

Figure Appendix A.5: Pouch Cell: Heat flux vs DR [7, 8, 57, 58, 9, 59, 60, 61, 62].

Appendix A.1.2. Overall Performance

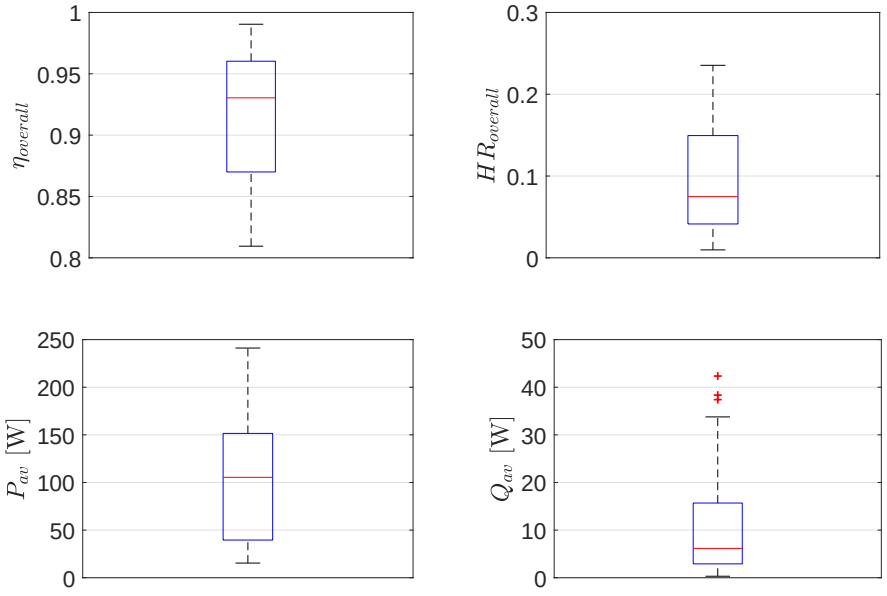

Figure Appendix A.6: $LiFePO_4$ Pouch Cell: Overall Performance Overview [7, 8, 57, 58, 9, 59, 60, 61, 62].

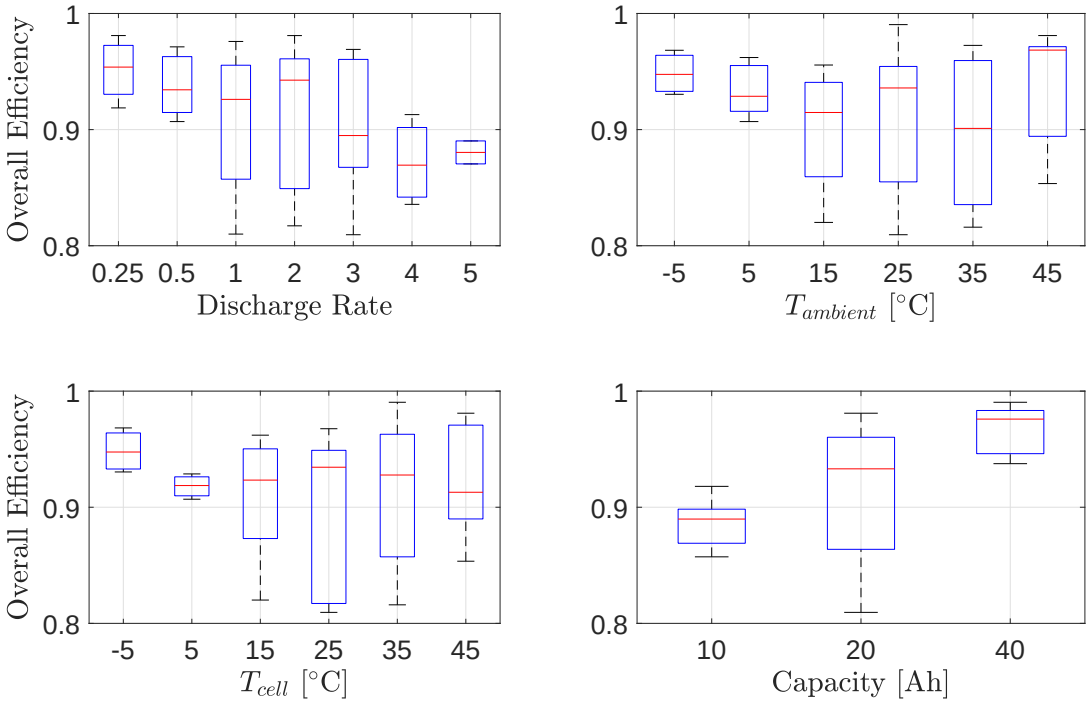

Figure Appendix A.7: Pouch Cell: Overall Efficiency parametric sensitivity [7, 8, 57, 58, 9, 59, 60, 61, 62].

Table Appendix A.1: Overall Discharge Performance of Pouch Cells [7, 8, 57, 58, 9, 59, 60, 61, 62]

Ref.	DR	T_{amb}	Cap_{nom}	Δt	DOD_{end}	T_{min}	T_{max}	ΔT	T_{ml}	Vol	A	m	P_{av}	$\dot{Q}_{av}$	E_{tot}	E	Q	$\eta_{overall}$	$HR_{overall}$
[9]	0.25	-10	20	3.99	100%	-10.50	-9.21	1.30	-9.86	263	783	496	15.38	1.15	65.96	61.37	4.59	93.04%	7.48%
[9]	0.25	0	20	4.00	100%	1.30	2.36	1.06	1.83	263	783	496	15.86	1.40	68.97	63.36	5.61	91.87%	8.85%
[9]	0.25	10	20	3.98	100%	10.56	11.26	0.70	10.91	263	783	496	16.09	1.03	68.18	64.09	4.09	94.00%	6.38%
[9]	0.25	20	20	3.99	100%	20.07	20.49	0.43	20.28	263	783	496	16.21	0.54	66.75	64.59	2.16	96.76%	3.35%
[9]	0.25	30	20	3.97	99%	29.13	29.52	0.39	29.32	263	783	496	16.25	0.46	66.32	64.50	1.82	97.25%	2.83%
[9]	0.25	40	20	3.99	100%	38.97	39.29	0.32	39.13	263	783	496	16.27	0.32	66.22	64.96	1.26	98.10%	1.94%
[15]	0.33	23	40	3.02	100%	23.18	28.84	5.66	26.00	576	539	1138	41.95	0.41	127.72	126.50	1.23	99.04%	0.97%
[9]	0.5	-10	20	1.99	99%	-10.57	-7.63	2.93	-9.10	263	783	496	29.65	2.05	62.95	58.89	4.06	93.55%	6.90%
[9]	0.5	0	20	2.00	100%	1.33	3.69	2.36	2.51	263	783	496	30.99	3.18	68.26	61.90	6.35	90.69%	10.26%
[9]	0.5	10	20	1.99	100%	10.57	12.34	1.77	11.45	263	783	496	31.66	2.95	68.99	63.11	5.88	91.47%	9.32%
[9]	.5	20	20	1.99	100%	20.03	21.33	1.30	20.68	263	783	496	32.07	2.30	68.54	63.95	4.59	93.31%	7.17%
[9]	0.5	30	20	1.99	100%	29.12	29.91	0.80	29.52	263	783	496	32.25	1.24	66.69	64.21	2.48	96.28%	3.86%
[9]	0.5	40	20	2.00	100%	38.96	39.67	0.71	39.31	263	783	496	32.36	0.96	66.51	64.60	1.91	97.13%	2.96%
[9]	1	-10	20	0.99	99%	-10.60	-5.35	5.24	-7.98	263	783	496	57.07	2.40	58.63	56.26	2.37	95.97%	4.20%
[9]	1	0	20	0.99	99%	1.32	5.51	4.18	3.41	263	783	496	60.33	4.63	64.62	60.01	4.61	92.87%	7.68%
[8]	1	6	20	0.86	86%	5.88	9.22	3.33	7.55	263	783	496	57.67	12.65	60.48	49.60	10.88	82.01%	21.94%
[9]	1	10	20	1.00	100%	10.55	13.83	3.28	12.19	263	783	496	62.07	5.15	67.22	62.07	5.15	92.34%	8.30%
[8]	1	16	20	0.92	92%	15.39	19.01	3.62	17.20	263	783	496	58.68	13.76	66.40	53.78	12.61	81.00%	23.45%
[9]	1	20	20	0.99	99%	20.05	22.40	2.35	21.22	263	783	496	63.31	4.34	67.09	62.79	4.30	93.59%	6.85%
[61]	1	22	40	1.00	100%	23.00	26.10	3.10	24.55	506	1039	990	114.53	6.15	120.68	114.53	6.15	94.90%	5.37%
[15]	1	24	40	1.00	100%	27.10	37.18	10.08	32.11	576	539	1138	124.41	3.07	126.85	123.79	3.06	97.59%	2.47%
[59]	1	25	10	0.96	96%	23.43	33.87	10.44	28.62	138	282	260	22.68	3.78	25.27	21.66	3.61	85.73%	16.65%
[60]	1	25	10	1.00	100%	25.19	30.86	5.67	28.02	127	290	261	31.35	2.80	33.98	31.19	2.79	91.80%	8.93%
[8]	1	25	20	0.96	96%	24.86	27.09	2.23	25.97	263	783	496	61.07	13.77	71.49	58.33	13.16	81.60%	22.55%
[9]	1	30	20	1.00	100%	28.94	30.49	1.55	29.71	263	783	496	63.83	2.98	66.56	63.59	2.97	95.54%	4.66%
[8]	1	35	20	0.97	97%	34.24	35.41	1.18	34.82	263	783	496	61.86	7.47	66.91	59.70	7.21	89.22%	12.08%
[9]	1	40	20	1.00	100%	38.94	40.24	1.31	39.59	263	783	496	64.23	2.09	66.06	63.98	2.08	96.85%	3.26%

Units: $T_{amb}\,[^\circ C], Cap_{nom}\,[Ah], \Delta t\,[h], T_{min}\,[^\circ C], T_{max}\,[^\circ C], \Delta T\,[^\circ C], T_{ml}\,[^\circ C], Vol\,[mL], A\,[cm^2], m\,[gr]$

$P_{av}\,[W], \dot{Q}_{av}[W], E_{tot}\,[Wh], E\,[Wh], Q\,[Wh]$

Table Appendix A.2: Overall Discharge Performance of Pouch Cells [7, 8, 57, 58, 9, 59, 60, 61, 62]

Ref.	DR	T_{amb}	Cap_{nom}	Δt	DOD_{end}	T_{min}	T_{max}	ΔT	T_{ml}	Vol	A	m	P_{av}	$\dot{Q}_{av}$	E_{tot}	E	Q	$\eta_{overall}$	$HR_{overall}$
[9]	2	-10	20	0.50	99%	-10.43	-2.20	8.23	-6.34	263	783	496	108.68	3.56	55.77	54.00	1.77	96.83%	3.27%
[9]	2	0	20	0.50	100%	1.55	8.58	7.03	5.05	263	783	496	116.27	5.75	61.01	58.14	2.88	95.29%	4.95%
[8]	2	7	20	0.40	80%	6.04	12.67	6.62	9.34	263	783	496	105.41	20.66	50.22	41.99	8.23	83.61%	19.60%
[9]	2	10	20	0.50	100%	10.83	16.31	5.49	13.56	263	783	496	120.61	7.35	63.98	60.30	3.67	94.26%	6.09%
[8]	2	16	20	0.44	88%	15.29	20.80	5.51	18.04	263	783	496	112.96	25.28	61.09	49.92	11.17	81.71%	22.38%
[9]	2	20	20	0.50	99%	20.22	24.47	4.25	22.34	263	783	496	123.91	6.97	64.87	61.42	3.46	94.67%	5.63%
[61]	2	22	40	0.50	100%	25.39	32.90	7.51	29.13	506	1039	990	225.50	15.03	120.27	112.75	7.51	93.75%	6.66%
[15]	2	24	40	0.50	100%	24.10	40.05	15.95	32.01	576	539	1138	241.13	4.68	122.29	119.96	2.33	98.10%	1.94%
[60]	2	25	10	0.50	100%	25.28	38.70	13.41	31.94	127	290	261	60.76	6.67	33.55	30.23	3.32	90.10%	10.98%
[8]	2	26	20	0.47	93%	25.01	28.93	3.92	26.96	263	783	496	116.56	23.07	65.14	54.37	10.76	83.48%	19.80%
[9]	2	30	20	0.50	100%	29.47	32.54	3.08	31.00	263	783	496	125.39	5.43	65.41	62.70	2.72	95.85%	4.33%
[8]	2	35	20	0.48	96%	34.27	37.71	3.44	35.98	263	783	496	115.42	19.81	64.60	55.14	9.46	85.35%	17.16%
[9]	2	40	20	0.50	100%	39.11	41.54	2.43	40.32	263	783	496	126.44	3.66	65.05	63.22	1.83	97.19%	2.89%
[9]	3	0	20	0.33	100%	1.35	10.61	9.27	5.95	263	783	496	168.74	6.65	58.46	56.25	2.22	96.21%	3.94%
[8]	3	7	20	0.25	75%	5.91	14.75	8.84	10.31	263	783	496	147.73	22.63	42.79	37.11	5.68	86.72%	15.32%
[9]	3	10	20	0.33	100%	10.56	18.07	7.51	14.30	263	783	496	176.06	8.18	61.41	58.69	2.73	95.56%	4.65%
[8]	3	17	20	0.29	86%	15.36	24.70	9.34	20.00	263	783	496	162.88	38.34	57.62	46.64	10.98	80.95%	23.54%
[9]	3	20	20	0.33	100%	20.03	26.26	6.23	23.13	263	783	496	181.49	9.56	63.68	60.50	3.19	95.00%	5.27%
[59]	3	25	10	0.32	96%	24.10	44.14	20.04	34.01	138	282	260	79.36	12.02	29.09	25.26	3.82	86.85%	15.14%
[60]	3	25	10	0.33	100%	25.38	45.78	20.40	35.46	127	290	261	89.37	11.07	33.31	29.64	3.67	88.98%	12.38%
[8]	3	27	20	0.30	90%	24.95	31.26	6.31	28.09	263	783	496	163.06	33.77	59.28	49.11	10.17	82.84%	20.71%
[9]	3	30	20	0.33	99%	29.11	33.77	4.66	31.44	263	783	496	184.51	7.21	63.10	60.72	2.37	96.24%	3.91%
[8]	3	36	20	0.31	94%	34.33	39.34	5.01	36.83	263	783	496	165.68	19.46	58.07	51.97	6.10	89.49%	11.75%
[9]	3	40	20	0.33	100%	38.95	42.81	3.86	40.87	263	783	496	186.10	5.94	64.01	62.03	1.98	96.91%	3.19%
[8]	4	8	20	0.19	77%	5.50	17.39	11.88	11.40	263	783	496	194.41	23.86	42.07	37.47	4.60	89.07%	12.27%
[8]	4	17	20	0.21	85%	15.31	26.16	10.85	20.70	263	783	496	208.76	37.40	52.35	44.40	7.95	84.81%	17.91%
[8]	4	27	20	0.22	90%	25.02	33.85	8.83	29.41	263	783	496	215.27	42.35	57.89	48.38	9.52	83.56%	19.67%
[8]	4	36	20	0.23	93%	34.23	41.11	6.88	37.66	263	783	496	219.12	20.90	56.09	51.20	4.88	91.29%	9.54%
[59]	5	25	10	0.19	96%	24.43	52.61	28.18	38.31	138	282	260	143.32	21.33	31.45	27.37	4.07	87.05%	14.88%
[60]	5	25	10	0.20	100%	25.19	57.70	32.51	41.16	127	290	261	143.16	17.65	32.00	28.49	3.51	89.03%	12.33%
[62]	10	25	6	0.09	88%	27.72	33.90	6.18	30.80	164	853	270	166.68	13.91	15.89	14.67	1.22	92.30%	8.35%

Units: $T_{amb}\,[^{\circ}C], Cap_{nom}\,[Ah], \Delta t\,[h], T_{min}\,[^{\circ}C], T_{max}\,[^{\circ}C], \Delta T\,[^{\circ}C], T_{ml}\,[^{\circ}C], Vol\,[mL], A\,[cm^2], m\,[gr]$

$P_{av}\,[W], \dot{Q}_{av}[W], E_{tot}\,[Wh], E\,[Wh], Q\,[Wh]$

Appendix A.2. Cylindrical Cells

Appendix A.2.1. Instant Performance

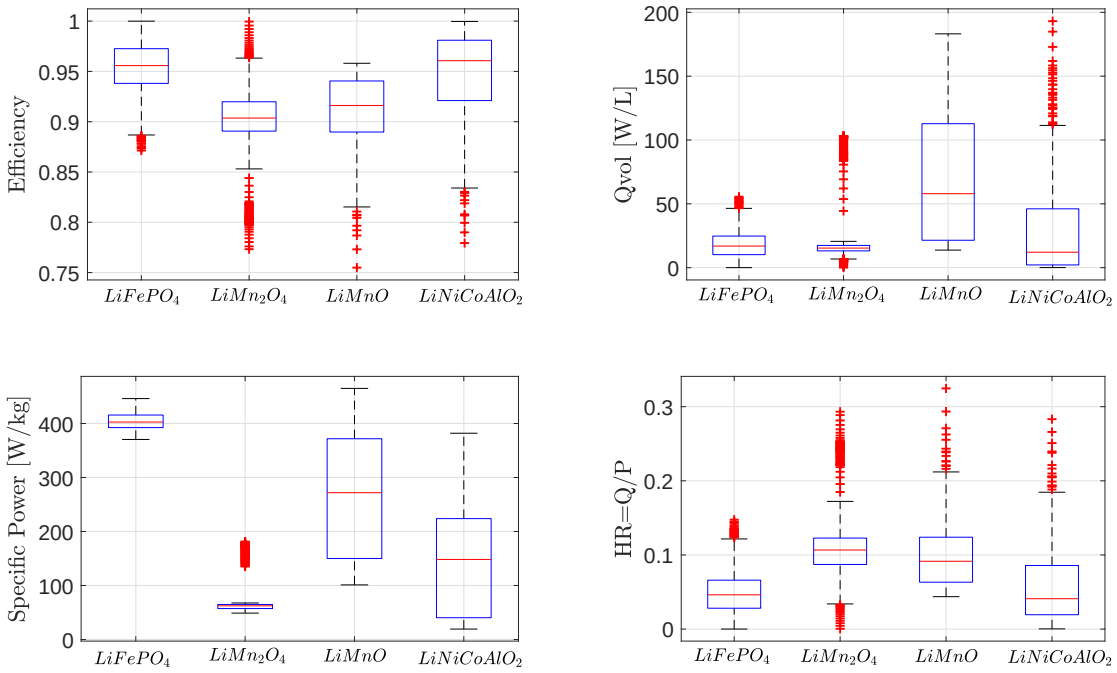

Figure Appendix A.8: Cylindrical Cells: Instant Performance Overview [53, 54, 55, 56].

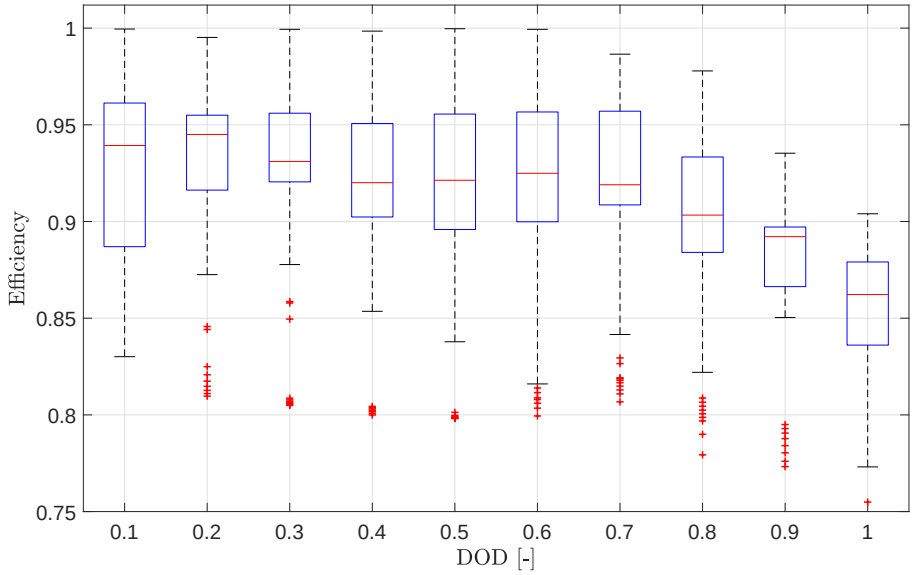

Figure Appendix A.9: Cylindrical Cell: Efficiency vs. DOD [53, 54, 55, 56].

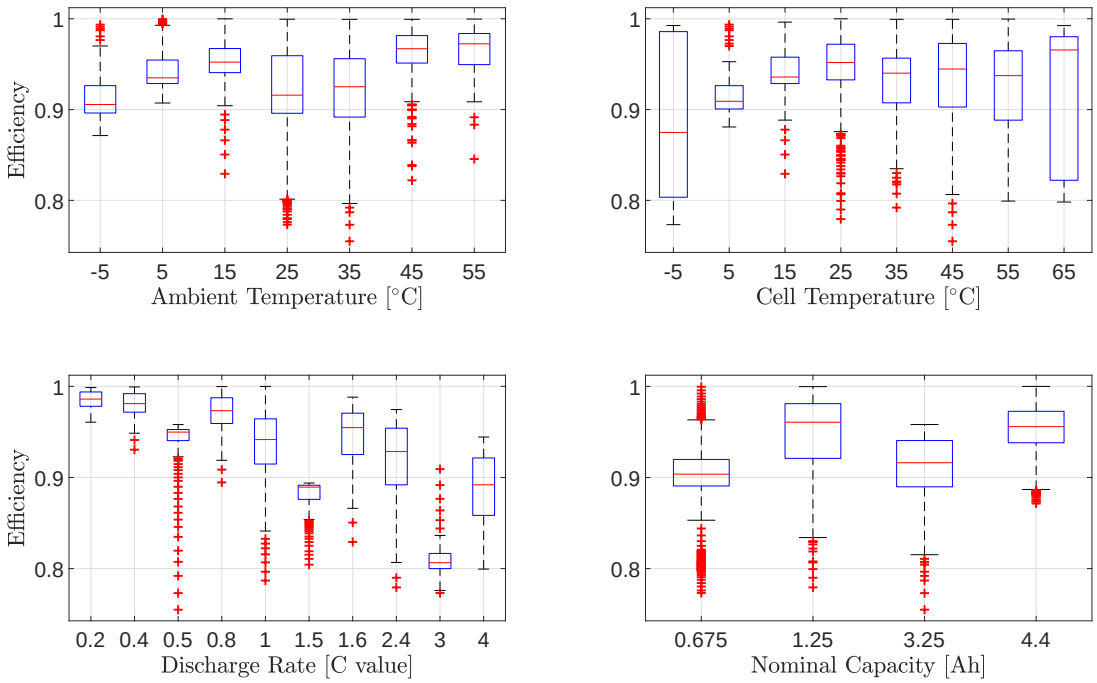

Figure Appendix A.10: Cylindrical Cell: Efficiency parametric sensitivity [53, 54, 55, 56].

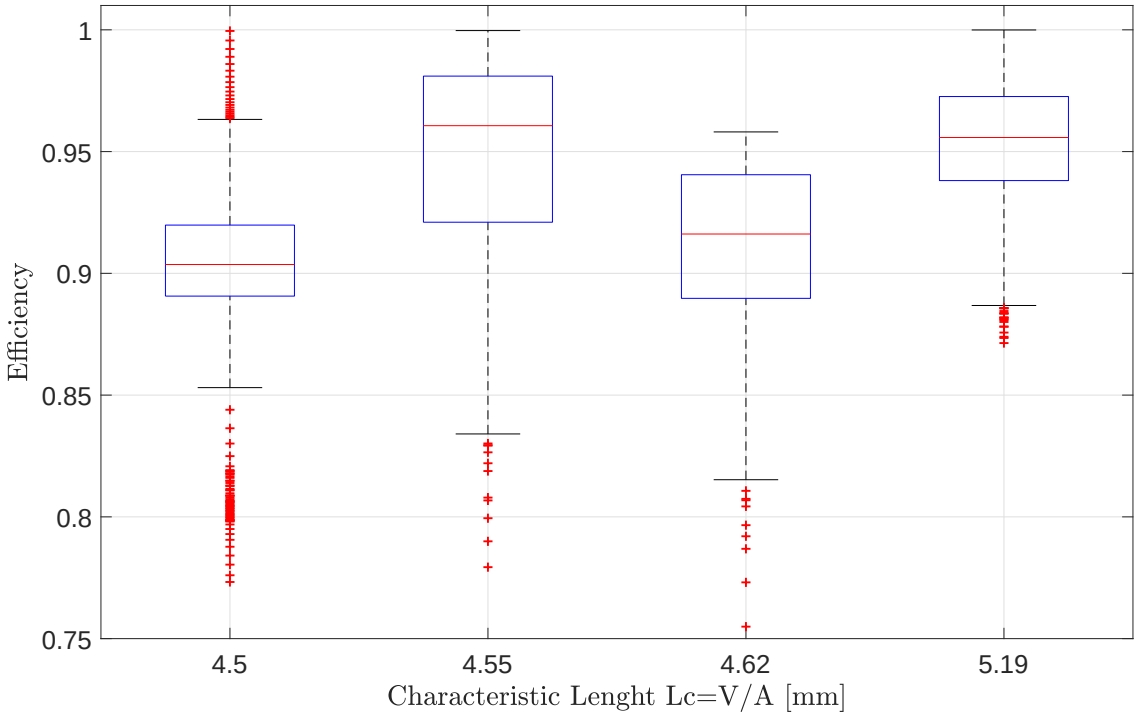

Figure Appendix A.11: Cylindrical Cell: Efficiency vs Characteristic Length L_c [53, 54, 55, 56].

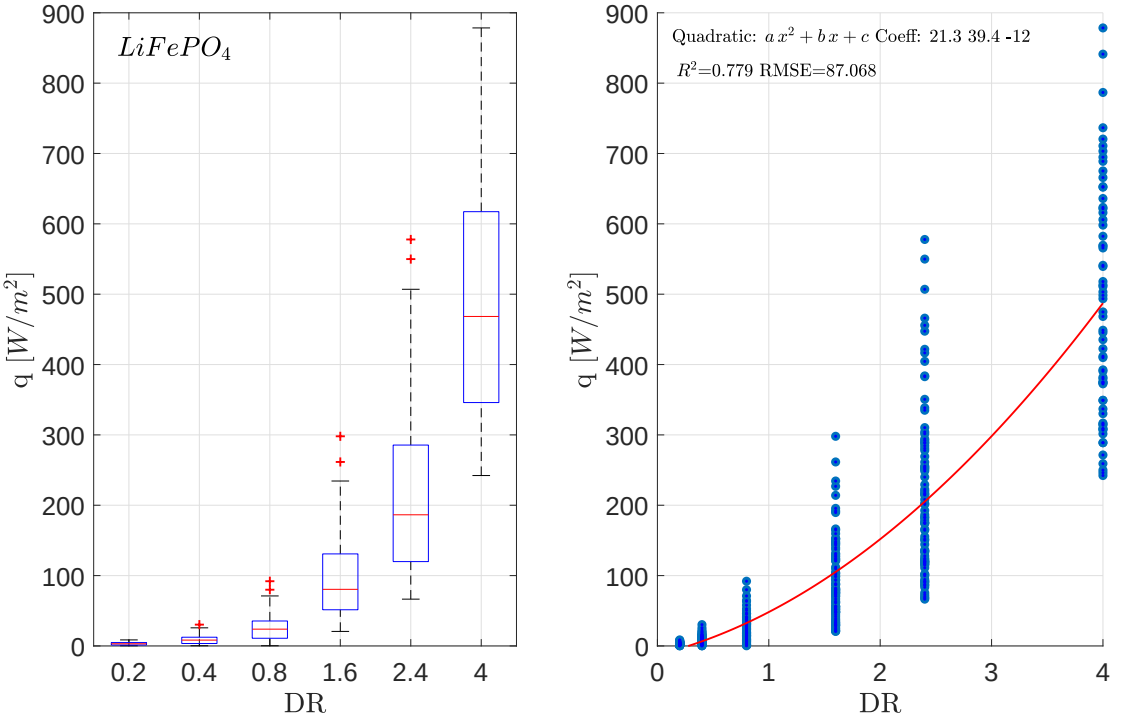

Figure Appendix A.12: Cylindrical $LiFePO_4$ Cell: Heat flux vs DR [56].

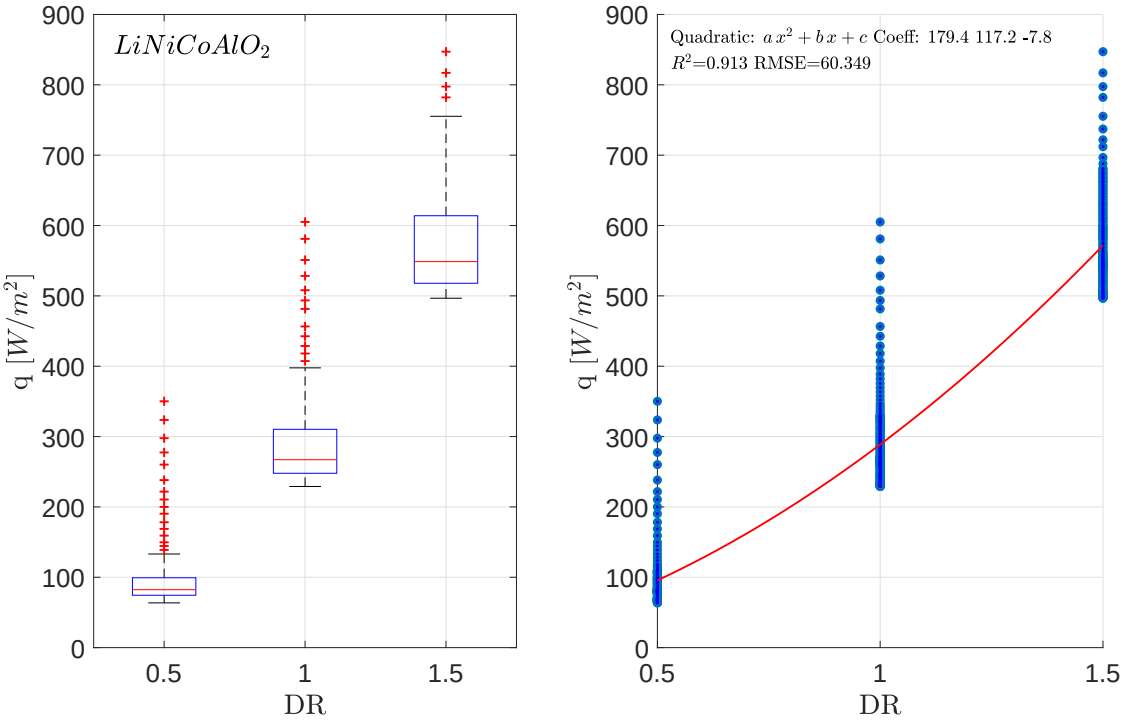

Figure Appendix A.13: Cylindrical $LiNiCoAlO_2$ Cell: Heat flux vs DR [55].

Appendix A.2.2. Overall Performance

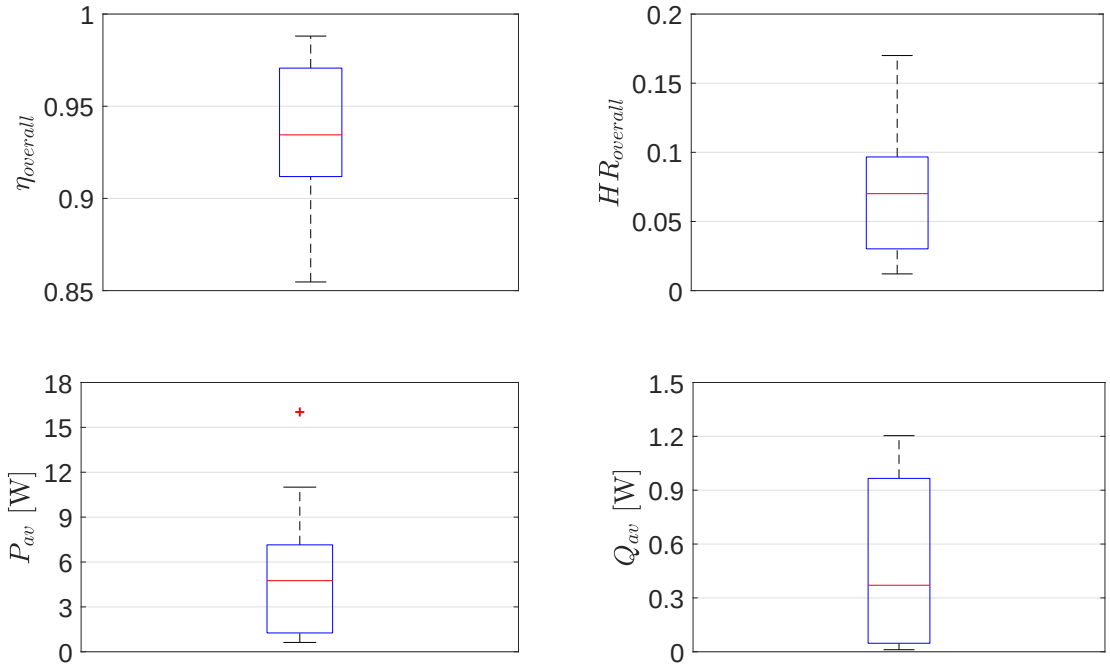

Figure Appendix A.14: Cylindrical Cells: Overall Performance Overview

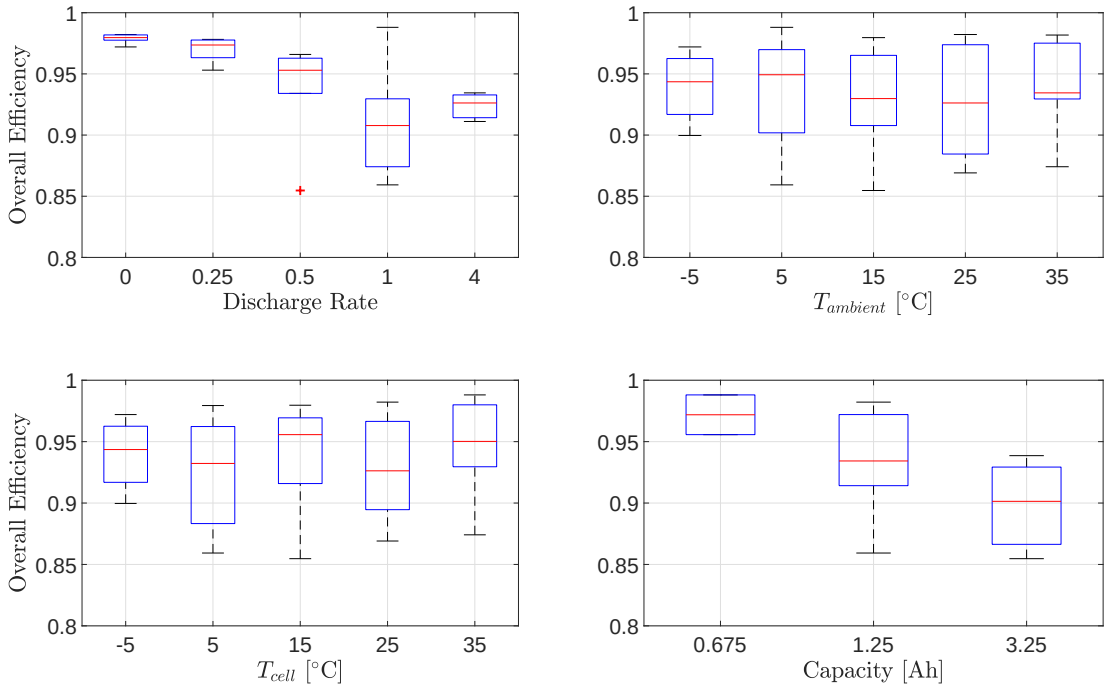

Figure Appendix A.15: Cylindrical Cell: Overall Efficiency parametric sensitivity

Table Appendix A.3: Overall Discharge Performance of Cylindrical Cells [53, 54, 55, 56]

Ref.	DR	T_{amb}	Cap_{nom}	Δt	DOD_{end}	T_{min}	T_{max}	ΔT	T_{ml}	Vol	A	m	P_{av}	$\dot{Q}_{av}$	E_{tot}	E	Q	$\eta_{overall}$	$HR_{overall}$
[56]	0.2	44.7	3.60	1.25	72%	44.7	44.7	0.0	44.7	16.96	37.28	40.5	0.63	0.01	2.32	2.28	0.04	98.2%	1.8%
[56]	0.2	54.8	3.60	1.25	72%	54.8	54.8	0.0	54.8	16.96	37.28	40.5	0.63	0.01	2.32	2.28	0.04	98.2%	1.9%
[56]	0.2	34.9	3.60	1.25	72%	34.9	34.9	0.0	34.9	16.96	37.28	40.5	0.63	0.01	2.32	2.27	0.05	98.0%	2.1%
[56]	0.2	24.9	3.60	1.25	72%	24.9	24.9	0.0	24.9	16.96	37.28	40.5	0.63	0.01	2.31	2.26	0.05	97.9%	2.1%
[56]	0.2	14.9	3.60	1.25	72%	14.9	14.9	0.0	14.9	16.96	37.28	40.5	0.62	0.02	2.31	2.24	0.06	97.2%	2.9%
[56]	0.4	54.9	1.80	1.25	72%	54.9	54.9	0.0	54.9	16.96	37.28	40.5	1.26	0.03	2.32	2.27	0.05	97.8%	2.2%
[56]	0.4	45.0	1.80	1.25	72%	45.0	45.0	0.0	45.0	16.96	37.28	40.5	1.26	0.03	2.32	2.26	0.05	97.7%	2.3%
[56]	0.4	34.9	1.80	1.25	72%	34.9	34.9	0.0	34.9	16.96	37.28	40.5	1.25	0.03	2.32	2.26	0.06	97.4%	2.7%
[56]	0.4	24.9	1.80	1.25	72%	24.9	24.9	0.0	24.9	16.96	37.28	40.5	1.25	0.04	2.32	2.24	0.08	96.7%	3.5%
[56]	0.4	14.9	1.80	1.25	72%	14.9	14.9	0.0	14.9	16.96	37.28	40.5	1.23	0.06	2.32	2.21	0.11	95.3%	4.9%
[55]	0.5	25.0	1.95	3.25	98%	25.1	35.3	10.2	30.2	17.55	37.95	48.5	5.70	0.97	13.00	11.11	1.89	85.5%	17.0%
[56]	0.8	54.9	0.90	1.25	72%	54.9	54.9	0.0	54.9	16.96	37.28	40.5	2.50	0.09	2.33	2.25	0.08	96.6%	3.5%
[56]	0.8	44.9	0.90	1.25	72%	44.9	44.9	0.0	44.9	16.96	37.28	40.5	2.49	0.10	2.33	2.25	0.09	96.3%	3.9%
[56]	0.8	34.9	0.90	1.25	72%	34.9	34.9	0.0	34.9	16.96	37.28	40.5	2.48	0.11	2.33	2.23	0.10	95.7%	4.5%
[56]	0.8	25.0	0.90	1.25	72%	25.0	25.0	0.0	25.0	16.96	37.28	40.5	2.45	0.13	2.33	2.21	0.12	94.9%	5.3%
[56]	0.8	14.9	0.90	1.25	72%	14.9	14.9	0.0	14.9	16.96	37.28	40.5	2.40	0.17	2.31	2.16	0.15	93.4%	7.1%
[54]	1	24.0	1.00	0.675	100%	24.8	32.9	8.2	28.8	16.54	36.76	48.5	2.43	0.11	2.54	2.43	0.11	95.6%	4.6%
[55]	1	25.0	0.98	3.25	98%	25.6	44.8	19.2	35.1	17.55	37.95	48.5	11.01	1.20	11.90	10.73	1.17	90.1%	10.9%
[55]	1.5	25.0	0.65	3.25	97%	25.1	55.7	30.6	40.1	17.55	37.95	48.5	16.03	1.05	11.04	10.37	0.68	93.9%	6.5%
[56]	1.6	45.0	0.45	1.25	72%	45.0	45.0	0.0	45.0	16.96	37.28	40.5	4.90	0.37	2.37	2.20	0.17	93.0%	7.6%
[56]	1.6	55.0	0.45	1.25	72%	55.0	55.0	0.0	55.0	16.96	37.28	40.5	4.92	0.37	2.38	2.21	0.17	92.9%	7.6%
[56]	1.6	35.0	0.45	1.25	72%	35.0	35.0	0.0	35.0	16.96	37.28	40.5	4.83	0.41	2.36	2.18	0.19	92.1%	8.6%
[56]	1.6	25.0	0.45	1.25	72%	25.0	25.0	0.0	25.0	16.96	37.28	40.5	4.75	0.45	2.34	2.14	0.20	91.4%	9.4%
[56]	1.6	14.7	0.45	1.25	72%	14.7	14.7	0.0	14.7	16.96	37.28	40.5	4.59	0.51	2.30	2.07	0.23	90.0%	11.2%
[56]	2.4	15.0	0.30	1.25	72%	15.0	15.0	0.0	15.0	16.96	37.28	40.5	6.65	0.96	2.28	1.99	0.29	87.4%	14.4%
[56]	2.4	45.0	0.30	1.25	72%	45.0	45.0	0.0	45.0	16.96	37.28	40.5	7.17	1.03	2.46	2.15	0.31	87.4%	14.4%
[56]	2.4	55.0	0.30	1.25	72%	55.0	55.0	0.0	55.0	16.96	37.28	40.5	7.23	1.04	2.48	2.17	0.31	87.4%	14.4%
[56]	2.4	35.0	0.30	1.25	72%	35.0	35.0	0.0	35.0	16.96	37.28	40.5	7.07	1.06	2.44	2.12	0.32	86.9%	15.1%
[56]	2.4	25.0	0.30	1.25	72%	25.0	25.0	0.0	25.0	16.96	37.28	40.5	6.86	1.12	2.39	2.06	0.34	85.9%	16.4%
[54]	3	24.0	0.30	0.675	90%	24.8	73.2	48.5	48.4	16.54	36.76	48.5	6.58	0.08	2.00	1.97	0.02	98.8%	1.2%
[56]	4	15.0	0.15	1.25	58%	15.0	15.0	0.0	15.0	16.96	37.28	40.5	9.95	0.72	1.55	1.44	0.10	93.2%	7.3%
[56]	4	54.8	0.15	1.25	58%	54.8	54.8	0.0	54.8	16.96	37.28	40.5	10.98	0.77	1.70	1.59	0.11	93.4%	7.0%
[56]	4	44.9	0.15	1.25	58%	44.9	44.9	0.0	44.9	16.96	37.28	40.5	10.81	0.86	1.69	1.57	0.12	92.6%	8.0%
[56]	4	35.0	0.15	1.25	58%	35.0	35.0	0.0	35.0	16.96	37.28	40.5	10.58	0.98	1.68	1.53	0.14	91.5%	9.3%
[56]	4	24.9	0.15	1.25	58%	24.9	24.9	0.0	24.9	16.96	37.28	40.5	10.24	1.00	1.63	1.48	0.14	91.1%	9.8%

Units: $T_{amb}\,[^\circ C], Cap_{nom}\,[Ah], \Delta t\,[h], T_{min}\,[^\circ C], T_{max}\,[^\circ C], \Delta T\,[^\circ C], T_{ml}\,[^\circ C], Vol\,[mL], A\,[cm^2], m\,[gr]$

$P_{av}\,[W], \dot{Q}_{av}[W], E_{tot}\,[Wh], E\,[Wh], Q\,[Wh]$